N°d'ordre :

Université de Saida- Dr. Moulay Tahar
Faculté des Sciences

Thèse

Présentée pour obtenir le diplôme de

Doctorat 3ème Cycle

Filière : Physique
Spécialité : Physique des matériaux

Par :
Toufik NOURI

Thème :

Conception théorique de nouveaux oxydes ternaires demi-métalliques

Thèse soutenue le 21/11/2022 devant le jury composé de :

N°	Nom et prénom	Grade	Etablissement	Qualité
01	ELKEURTI Mohammed	Pr.	Université de Saida – Dr. Moulay Tahar	Président
02	AMARA Kadda	Pr.	Université de Saida – Dr. Moulay Tahar	Rapporteur
03	KHELFAOUI Friha	MCA	Université de Saida – Dr. Moulay Tahar	Co-rapporteur
04	BOUTALEB Miloud	MCA	Université de Saida – Dr. Moulay Tahar	Examinateur
05	MOKADDEM Allel	Pr.	Centre Universitaire Nour Bachir El Bayadh	Examinateur
06	BENSAID Djillali	Pr.	Université de Ain Temouchent	Examinateur

Ordre number:

University of Saida- Dr. Moulay Tahar
Faculty of Science

Thesis

Presented to obtain:

3rd Cycle Doctoral degree

Option: Physics
Specialty: Materials science

By:
Toufik NOURI

Theme:

Theoretical design of new half-metallic ternary oxides

Thesis defended on 21/11/2022 in front of the board of examiners:

N°	Full name	Grade	Establishment	Quality
01	ELKEURTI Mohammed	Pr.	University of Saida – Dr. Moulay Tahar	President
02	AMARA Kadda	Pr.	University of Saida – Dr. Moulay Tahar	Supervisor
03	KHELFAOUI Friha	MCA	University of Saida – Dr. Moulay Tahar	Co-supervisor
04	BOUTALEB Miloud	MCA	University of Saida – Dr. Moulay Tahar	Examiner
05	MOKADDEM Allel	Pr.	University Center of Nour Bachir El Bayadh	Examiner
06	BENSAID Djillali	Pr.	University of Ain Temouchent	Examiner

Dedication:

This Thesis is proudly dedicated to my parents

for their endless support

My brother boubaker and his sons

All my professors at Saida University

Friends and colleagues, and everyone

who encouraged me.

Toufik Nouri

Acknowledgements

First of all, I thank Allah for blessing me with strength, patience and will to complete this work.

I would like to express my deepest gratitude to my supervisor Professor Kadda Amara, for the continuous support of my doctoral research, for his patience, motivation and enthusiasm, His guidance helped me all the time. My sincere thanks also go to Dr. Friha Khelfaoui (my co-supervisor), for her constant support and guidance.

I would like to extend my sincere thanks to the members of the physico-chemical studies laboratory doctoral committee and particularly to Professor ELKEURTI Mohammed, director of the physico-chemical studies laboratory at University of Saida – Dr. Moulay Tahar for their generous support and encouragement during the preparation this manuscript.

Special thank goes to the board of examiners: the president ELKEURTI Mohammed, Professor at university of Saida, BOUTALEB Miloud, Professor at university of Saida, MOKADDEM Allel, Professor at Nour El-Bachir university center of El-Bayadh and BENSAID Djillali Professor at university of Ain Temouchent, for kindly agreed to be part of the jury and spending their valuable time reading and correcting my thesis.

I extend my gratitude to my colleagues and all my Physics professors at department of Physics,

Besides research, I am grateful to my parents for their endless support over the years and I would like to express my thanks to all my friends.

Toufik Nouri

Table of contents:

List of tables:

List of figures:

List of commonly used abbreviations :

AFM	Antiferromagnetic
APW	Augmented Plane Wave
APW+lo	Augmented Plane Waves + local orbitals.
CBM	Conduction band minimum
DOS	Density of states.
DFT	Density Functional Theory.
FM	Ferromagnetic
FP-LAPW	Full Potential Linearized Augmented Plane Wave.
GMR	Giant Magnetoresistance
TMR	Tunneling Magnetoresistance
GGA	Generalised Gradient Approximation.
HF	Hartree-Fock
HMF	Half-Metallic Ferromagnets.
HM gap	Half-Metallic gap
KS	Kohn-Sham.
LAPW	Linearized Augmented Plane Wave.
LAPW+LO	Linearized Augmented Plane Waves + local orbitals.
LDA	Local Density Approximation.
LDA+U	Local Density Approximation + Hubbard term U.
LSDA	Local Spin Density Approximation.
mBJ	Modified Becke-Jonshon
MRAM	Magnetic random-access memory
MT	Muffin-Tin
NM	Non-magnetic
PBE	Pedrew, Burke et Ernzerhof
VBM	Valence band maximum
XC	Exchange-Correlation potentiel.

General introduction

General introduction:

Materials were historically linked to technological development, and there has always been research driven by the need of novel materials with specific properties. In the recent past, extensive theoretical and experimental research has been carried out to investigate a new class of magnetic materials called half-metallic (HM) ferromagnets, the fundamental characteristic of these materials lie in the electronic properties: one spin channel possesses metallic conduction while the other spin channel is insulating or semiconducting. Therefore, due to the presence of the gap at fermi level in one spin channel, the spin polarization can reach 100%. Initially, the HM character was predicted by De Groot et al. in 1983 in half-Heusler NiMnSb compound [1]. Later, much effort has been spent to explore half metallicity experimentally as well as theoretically in variety of materials such as: CrO_2[2] and Fe_3O_4[3] transition-metal oxides, the half-metallicity in these oxides remained unknown until it was revealed by first-principles calculations. Heusler compounds have been intensively studied and they provide a fertile soil for exploring HMFs including the Half Heusler alloys NiYSb and CoYSb[4], full Heusler alloys Co_2MnX (X = Al, Ga, Si, Ge, Sn)[5] and inverse Heusler alloys Sc_2CrAl, Ti_2NiAl, Mn_2ZnSi[6]. Mavropoulos and Galanakis found that zinc blende phase of VAs, VSb, CrAs, CrSb, VTe, CrSe, and CrTe[7] are good candidates for HMFs, Bouadjemi et al. [8]also found that perovskite $PrMnO_3$ is a HM ferromagnet, double perovskites Sr_2CrReO_6 [9] and Sr_2FeReO_6[10] also potential HMFs.

Recently, HM ferromagnets are attracting more attention due to their applications in spintronics which is a new type of electronics that exploits not only the charge of the electrons but also their fundamental quantum property named the spin. The beginning of this technological revolution was the discovery of the giant magnetoresistance (GMR) in 1988 independently by Albert Fert and Peter Grünberg[11], who were honoured with the Nobel Prize in Physics 2007 for their discovery. High spin polarization HM ferromagnets with high Curie temperature are very required in spintronics devices such as MRAM and hard discs.

To investigate HM ferromagnets and other materials, first-principles calculations represent a powerful computational method (simulation) that have been intensively used in research besides doing experiments, they are used to confirm experimental findings and design materials with desired features, estimate material properties when experiments are hard to perform (expensive experiments), or even design materials that have not been synthesized yet

(prior to experiments), first principles calculations start directly from quantum mechanical equations and do not often require any experimental parameters aside from fundamental constants and they are based on Density Functional Theory DFT which was founded by Hohenberg and Kohn (1964)[12] and developed by Kohn-Kham (1965)[13], Walter Kohn was awarded Nobel Prize (1998) for developing DFT. Thanks to the development of computers and DFT theory, the speed and accuracy of performing calculations have both been significantly improved. Today, first principles calculations are implemented in many codes such as: Wien2k[14], Quantum Espresso[15], Vasp…

HM ferromagnets are characterized by the half metallicity that is usually originated from d or f orbitals of the transition metals for many compounds, but recent research shows that it is possible to obtain HM ferromagnets from compounds that don't contain any transition metal, it is the case of $LiBeO_3$[16], $KBeO_3$[17] and $KMgO_3$ [18]perovskites with elements containing only s and p orbitals, this motivates us to investigates XMg_3O_4 (X=Li, Na, K, Rb) compounds.

This thesis is organized as follows: In **chapter 1**, an overview of the basic concepts of first principles calculations. In **chapter 2**, we give introduction to magnetic materials and their classification, then we introduce the concept of half metallic ferromagnets (HMFs) and their characteristics, next we talk about spintronics, Discussion of the results obtained in the present work will be presented in **chapter 3**. Finally, we end this study with a general conclusion and perspectives.

References:

[1] R. A. de Groot, F. M. Mueller, P. G. van Engen, and K. H. J. Buschow, "New class of materials: half-metallic ferromagnets," *Phys Rev Lett*, vol. 50, no. 25, p. 2024, 1983.

[2] K. Schwarz, "CrO2 predicted as a half-metallic ferromagnet," *Journal of Physics F: Metal Physics*, vol. 16, no. 9, p. L211, 1986.

[3] Z. Zhang and S. Satpathy, "Electron states, magnetism, and the Verwey transition in magnetite," *Phys Rev B*, vol. 44, no. 24, p. 13319, 1991.

[4] I. Galanakis, P. H. Dederichs, and N. Papanikolaou, "Origin and properties of the gap in the half-ferromagnetic Heusler alloys," *Phys Rev B*, vol. 66, no. 13, p. 134428, 2002.

[5] I. Galanakis, P. H. Dederichs, and N. Papanikolaou, "Slater-Pauling behavior and origin of the half-metallicity of the full-Heusler alloys," *Phys Rev B*, vol. 66, no. 17, p. 174429, 2002.

[6] S. Skaftouros, K. Özdoğan, E. Şaşıoğlu, and I. Galanakis, "Generalized Slater-Pauling rule for the inverse Heusler compounds," *Phys Rev B*, vol. 87, no. 2, p. 024420, 2013.

[7] X. Li and J. Yang, "First-principles design of spintronics materials," *Natl Sci Rev*, vol. 3, no. 3, pp. 365–381, 2016.

[8] B. Bouadjemi, S. Bentata, A. Abbad, W. Benstaali, and B. Bouhafs, "Half-metallic ferromagnetism in PrMnO3 perovskite from first principles calculations," *Solid State Commun*, vol. 168, pp. 6–10, 2013.

[9] H. Kato *et al.*, "Metallic ordered double-perovskite Sr 2 CrReO 6 with maximal Curie temperature of 635 K," *Appl Phys Lett*, vol. 81, no. 2, pp. 328–330, 2002.

[10] K.-I. Kobayashi, T. Kimura, Y. Tomioka, H. Sawada, K. Terakura, and Y. Tokura, "Intergrain tunneling magnetoresistance in polycrystals of the ordered double perovskite Sr 2 FeReO 6," *Phys Rev B*, vol. 59, no. 17, p. 11159, 1999.

[11] C. Day, "Discoverers of giant magnetoresistance win this year's physics Nobel," *Phys Today*, vol. 60, no. 12, p. 12, 2007.

[12] P. Hohenberg and W. Kohn, "Inhomogeneous electron gas," *Physical review*, vol. 136, no. 3B, p. B864, 1964.

[13] W. Kohn, "Nobel Lecture: Electronic structure of matter—wave functions and density functionals," *Rev Mod Phys*, vol. 71, no. 5, p. 1253, 1999.

[14] P. Blaha, K. Schwarz, G. K. H. Madsen, D. Kvasnicka, and J. Luitz, "wien2k," *An augmented plane wave+ local orbitals program for calculating crystal properties*, vol. 60, 2001.

[15] P. Giannozzi *et al.*, "QUANTUM ESPRESSO: a modular and open-source software project for quantum simulations of materials," *Journal of physics: Condensed matter*, vol. 21, no. 39, p. 395502, 2009.

[16] F. Khelfaoui *et al.*, "First-principles study on structural, mechanical, and magneto-electronic properties in new half-metallic perovskite LiBeO3," *Computational Condensed Matter*, vol. 21, p. e00399, 2019.

[17] V. Ashwin, M. B. Ahamed, and S. B. Elavarasi, "Structural, electronic, magnetic and half-metallic properties of cubic perovskites NaBeO3 and KBeO3 using PBE-GGA

and TB-mBJ approach: A DFT perspective," *Applied Physics A*, vol. 126, no. 11, pp. 1–11, 2020.

[18] M. Hamlat, K. Boudia, K. Amara, F. Khelfaoui, and N. Marbouh, "Half-metallic stability of the cubic perovskite KMgO3," *Computational Condensed Matter*, vol. 23, p. e00456, 2020.

Chapter 1

Theoretical background

1.1. Introduction:

The properties of materials are ultimately determined by the interactions of electrons and nuclei. The fundamental description of these interactions requires quantum mechanics, which was founded and developed at the beginning of the 20th century by great minds such as Bohr, De Broglie, Schrödinger, Dirac and others. At present, a lot of theoretical schemes have been proposed to interpret experimental measurements, to predict new effects and to design new materials from first principles (or ab initio). A calculation is said to be ab initio if it starts from basic equations without the use of any empirical parameters. The resolution the Schrödinger equation, which is a central equation to all quantum mechanical calculations, is needed to explain the material's properties. Unfortunately, it is impossible to solve this equation analytically for a system with many particles. This chapter gives a description about the methods used to solve the Schrodinger equation. In particular, we describe how to solve the Schrödinger equation using approximations such as the Born-Oppenheimer approximation (Born and Oppenheimer, 1927) and Hartree-Fock formalism (Hartree, 1928, Fock, 1930), then, we describe Density functional theory (DFT), which was founded by Hohenberg and Kohn (1964) and developed by Kohn-Sham (1965). In 1998 Walter Kohn was awarded Nobel Prize for his development of DFT, which has become very successful and very popular, particularly in the recent years and that is evident from the histogram of Fig I.1, which report an estimation of the number of publications using density functional theory. In recent past, it is clear that in the last decade, the DFT has grown exponentially in several computational areas because of its versatility and reliability to calculate the properties of materials from electronic density. Scientists has developed codes focused to simulate molecular and material properties such as Wien2k (used in this work), Quantum Espresso, VASP and CASTEP…

In this chapter, an overview of the basic concepts of first principles calculations is given, we explain the approximations used Schrödinger equation for materials, the density functional theory (DFT) and the Kohn-Sham equations. Then, we discuss in more detail the issue of exchange and correlation in DFT and how to solve Kohn Sham equations. In addition, we introduce FP-LAPW method and Wien2k code (which is the main code used here).

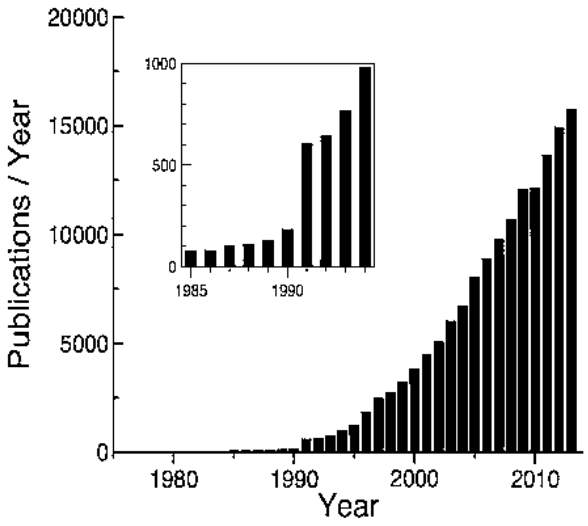

Fig. 1. 1 Numbers of papers that mention DFT (data obtained from Web of Knowledge) [1]

1.2. Many body problem:

The basis to study a quantum mechanical system, is to solve the Schrödinger equation, which was first proposed by Erwin Schrödinger[19] in 1926.The challenge of materials science is the solution of the time independent many-body Schrodinger equation in the non-relativistic case.

Let us consider a material of M nuclei, with spatial coordinates that are represented collectively as $\vec{R} = \{\vec{R}_1, \vec{R}_2, \dots, \vec{R}_M\}$ and N electrons, with coordinates $\vec{r} = \{\vec{r}_1, \sigma_1, \dots \vec{r}_N, \sigma_N\}$, where the i^{th} electron has three spatial coordinates, and its spin σ_i , all information about this system is contained in the wave function, which explicitly depends on the coordinates of all particles in the system. For simplicity, we denote the wave function as $\psi(\vec{r}, \vec{R})$ and the time-independent Schrodinger equation has the form:

$$\hat{H}\psi(\vec{r}, \vec{R}) = E\psi(\vec{r}, \vec{R}) \qquad 1.1$$

Where E is the total energy of the system and $\hat{H}$ is the Hamiltonian, which has the form

$$\hat{H} = \hat{T}_n + \hat{T}_e + \hat{V}_{nn} + \hat{V}_{ne} + \hat{V}_{ee} \qquad 1.2$$

Here $\hat{T}_N$ and $\hat{T}_e$ represent nuclear and electronic kinetic operators, respectively:

$$\hat{T}_N = -\frac{\hbar^2}{2}\sum_{I=1}^{M}\frac{\nabla_I{}^2}{M_I} \ , \quad \hat{T}_e = -\frac{\hbar^2}{2m}\sum_{i=1}^{N}\nabla_i{}^2 \qquad 1.3$$

$\hat{V}_{nn}$, $\hat{V}_{ne}$ and $\hat{V}_{ee}$ are the potential energy operators for nuclear-nuclear, nuclear-electron and electron-electron interactions accordingly:

$$\hat{V}_{nn} = \frac{ke^2}{2}\sum_{I\neq J}\frac{Z_I Z_J}{r_{IJ}} \quad , \qquad \hat{V}_{ne} = -ke^2\sum_{i,J}\frac{Z_I}{r_{iJ}} \quad , \quad \hat{V}_{ee} = \frac{ke^2}{2}\sum_{i\neq j}\frac{1}{r_{ij}} \qquad 1.4$$

In this case $r_{IJ} = \left|\vec{R}_I - \vec{R}_J\right|$, $r_{iJ} = \left|\vec{r}_i - \vec{R}_J\right|$, $r_{ij} = \left|\vec{r}_i - \vec{r}_j\right|$ 1.5

Where M and Z refers to the mass and the charge of the nucleus, m and e to the mass and the charge of the electron, r to distance, k the Coulomb's constant $(k = 1/4\pi\varepsilon_0)$ and the subscripts I, J and i, j refer to nuclei and electrons respectively, ∇^2 is the Laplacian operator, which in cartesian coordinates has the form:

$$\nabla^2 = \frac{\partial^2}{\partial x^2} + \frac{\partial^2}{\partial y^2} + \frac{\partial^2}{\partial z^2} \qquad 1.6$$

To simplify this equation, atomic units will be used in which $4\pi\varepsilon_0 = \hbar = m_e = e = 1$ so they can be omitted from the Schrödinger equation

$$\hat{H} = -\frac{1}{2}\sum_{I=1}^{M}\frac{\nabla_I{}^2}{M_I} - \frac{1}{2}\sum_{i=1}^{N}\nabla_i{}^2 + \frac{1}{2}\sum_{I\neq J}\frac{Z_I Z_J}{r_{IJ}} - \sum_{i,J}\frac{Z_I}{r_{iJ}} + \frac{1}{2}\sum_{i\neq j}\frac{1}{r_{ij}} \qquad 1.7$$

In principle, everything about the system is known if one can solve the above Schrödinger equation. However, it is impossible to solve it in practice because of the large number of variables, so we have to go through approximations.

1.3. Born Oppenheimer approximation:

The first basic approximation to solve the many body problem was proposed by Born and Oppenheimer[20] in 1927. Since the nuclei are much heavier and massive than electrons (the mass of a proton is about 1800 times the mass of an electron), the nuclei move much more slowly compared to electrons. Therefore, we can treat them as motionless particles and separate the movement of nuclei and electrons. As a result, it is reasonable to consider electrons moving in an external field of fixed nuclei.

The so-called Born Oppenheimer approximation means that the kinetic energy term for the nuclei is approximated to zero and the nucleus-nucleus Coulomb term is a constant, which can be cancelled for a suitable choice of the origin of potential energy. Under the Born-Oppenheimer approximation the electronic Hamiltonian, $\widehat{H}_e$ takes the form:

$$\widehat{H}_e = \hat{T}_e + \hat{V}_{ne} + \hat{V}_{ee} \qquad 1.8$$

In this approximation the wave function is written as a product of the electronic wave function ψ_e and the nuclear one ψ_n

$$\psi(\vec{r}, \vec{R}) = \psi_e(\vec{r}; \vec{R})\psi_n(\vec{R}) \qquad 1.9$$

Where ψ_n is the nuclear wave function and ψ_e is the electronic wave function, which depends explicitly on the electronic coordinates and parametrically on the nuclear coordinates. $\psi_e(\vec{r}; \vec{R})$ is the solution fot the electronic motion (we can use ψ_e for short):

$$\widehat{H}_e\psi_e = E_e(R)\psi_e \qquad 1.10$$

The total energy E is then the sum of the electronic energy $E_e(R)$ and the constant of nuclear repulsion term :

$$E = E_e + \frac{1}{2}\sum_{I \neq J} \frac{Z_I Z_J}{r_{IJ}} \qquad 1.11$$

If the electronic problem is solved, we can solve for the motion of the nuclei. The Born-Oppenheimer approximation separates the movement of nuclei and electrons, but the resulting electronic Schrödinger equation I-10 is still extremely complex, due to the electron-electron interactions.

1.4. Hartree approximation:

Although the Born-Oppenheimer approximation considerably reduces the complexity of the Schrödinger equation, the resulting electronic Schrödinger equation is still extremely complex. To solve this problem, new approach was developed by Douglas Hartree [21]–[23] in 1928. In this method, we consider the electrons as independent particles, in which each electron is assumed to move in an effective potential created by the fixed nuclei and the remaining electrons. The electronic wave function of this Hamiltonian is a product of mono-electronic functions:

$$\psi_e(\vec{r}_1, \vec{r}_2, \dots\dots\dots, \overrightarrow{r_N}) = \phi_1(\vec{r}_1) \dots\dots \phi_N(\vec{r}_N) = \prod_i \phi_i(\vec{r}_i) \qquad 1.12$$

The Hamiltonian of the system $\widehat{H}_e$ will now be equal to a sum of Hamiltonians h_i, everyone of which depends only on the coordinates of a single electron :

$$\widehat{H}_e = \sum_i (-\frac{1}{2}\nabla_i^2 + V_H(\vec{r}_i) + V_{ext}(\vec{r}_i)) = \sum_i h_i \qquad 1.13$$

Where V_{ext} the external potential which is generated by the nuclei given by:

$$V_{ext}(r) = -\sum_J \frac{Z_I}{|r - R_J|} \qquad 1.14$$

The total energy E_e^H, which is the expectation value of the Hamiltonian operator given by $E_e^H = \langle \psi_e | \widehat{H}_e | \psi_e \rangle$

$$E_e^H = \underbrace{-\frac{1}{2}\sum_i \int \phi_i^*(r)\nabla^2\phi_i(r)d^3r}_{T_e} + \underbrace{\frac{1}{2}\sum_{i,j\neq i} \iint \frac{|\phi_i(\vec{r})|^2 |\phi_j(\vec{r}')|^2}{|\vec{r} - \vec{r}'|} d^3r d^3r'}_{E_H}$$
$$+ \underbrace{\sum_i \int \phi_i^*(r) V_{ext}(\vec{r})\phi_i(r)d^3r}_{E_{ext}} \qquad 1.15$$

With T_e is the kinetic energy of the electrons, E_H is the Hartree energy of electron-electron interactions and E_{ext} is the electron-nuclei energy interactions.
Using a variational principle, we obtain from this the single-particle Hartree equations:

$$(-\frac{1}{2}\nabla^2 + V_H(\vec{r}_i) + V_{ext}(\vec{r}_i))\phi_i(\vec{r}) = \varepsilon_i\phi_i(\vec{r}) \qquad 1.16$$

V_H is the classical Coulomb interaction generated by the charge density $\rho(\vec{r}') = \sum_j |\phi_j(\vec{r}')|^2$:

$$V_H = \sum_j \int \frac{|\phi_j(\vec{r}')|^2}{|\vec{r} - \vec{r}'|} d^3r' = \sum_i \int \frac{\rho(\vec{r}')}{|\vec{r} - \vec{r}'|} d^3r' \qquad 1.17$$

The Hartree approximation does not satisfy the important criteria for wavefunctions, because electrons are fermions, the wave function must change sign if two electrons change places with each other. This is known as the Pauli Exclusion Principle (antisymmetric). Exchanging two electrons does not change the sign of the Hartree product, which is a serious drawback. Antisymmetric wave function must verify Eq 1-18:

$$\psi_e(\vec{r}_1, \vec{r}_2 \dots \vec{r}_i, \vec{r}_j \dots \vec{r}_N) = -\psi_e(\vec{r}_1, \vec{r}_2 \dots \vec{r}_j, \vec{r}_i \dots \vec{r}_N) \quad 1.18$$

1.5. Hartree-Fock approximation:

In 1930, Fock pointed out that the Hartree wave function was invalid as it did not satisfy the Pauli Exclusion Principle, The Hartree-Fock[24]–[27]theory incorporates the exclusion principle, they write the total ground state wave function as a Slater determinant that has the form:

$$\psi_{HF}(\vec{r}, \sigma) = \frac{1}{\sqrt{N!}} \begin{vmatrix} \phi_1(\vec{r}_1, \sigma_1) & \phi_1(\vec{r}_2, \sigma_2) & \dots & \phi_1(\vec{r}_N, \sigma_N) \\ \phi_2(\vec{r}_1, \sigma_1) & \phi_2(\vec{r}_2, \sigma_2) & \dots & \phi_2(\vec{r}_N, \sigma_N) \\ . & . & & . \\ . & . & & . \\ \phi_N(\vec{r}_N, \sigma_N) & \phi_N(\vec{r}_N, \sigma_N) & \dots & \phi_N(\vec{r}_N, \sigma_N) \end{vmatrix} \quad 1.19$$

The total energy E_e^H, which is the expectation value of the Hamiltonian operator given by $E_e^H = \langle \psi_{HF} | \hat{H}_e | \psi_{HF} \rangle$

$$E_e^{HF} = \underbrace{-\frac{1}{2}\sum_i \int \phi_i^*(\vec{r}) \nabla^2 \phi_i(\vec{r}) d^3\vec{r}}_{T_e} + \underbrace{\frac{1}{2}\sum_{i,j} \iint \frac{|\phi_i(\vec{r})|^2 |\phi_j(\vec{r}')|^2}{|\vec{r} - \vec{r}'|} d^3r d^3r'}_{E_H}$$
$$+ \underbrace{\sum_i \int \phi_i^*(\vec{r}) V_{ext}(\vec{r}) \phi_i(\vec{r}) d^3\vec{r}}_{E_{ext}} + E_x \quad 1.20$$

The last term in Eq 1-20 is called the HF exchange energy, it has the form:

$$E_x = -\frac{1}{2}\sum_{i,j} \delta_{\sigma_i,\sigma_j} \int \frac{\phi_i^*(\vec{r}) \phi_j(\vec{r}) \phi_j^*(\vec{r}') \phi_i(\vec{r}')}{|\vec{r} - \vec{r}'|} d^3r d^3r' \quad 1.21$$

The single-particle Hartree-Fock equations, obtained using a variational calculation, are:

$$\left[-\frac{1}{2}\nabla^2 + V_H(\vec{r}) + V_{ext}(\vec{r})\right] \phi_i(\vec{r}) - \sum_j \delta_{\sigma_i,\sigma_j} \phi_j(\vec{r}) \int \frac{\phi_j^*(\vec{r}') \phi_i(\vec{r}')}{|\vec{r} - \vec{r}'|} d^3r' = \varepsilon_i \phi_i(\vec{r}) \quad 1.22$$

When we compare these equations with the Hartree equation Eq, we realize that here we now have an additional term. It is called the non-local exchange potential, which describes the effects of exchange between electrons. It corrects the defect of the Hartree approximation, but it considerably complicates the calculations. It is given by:

$$V_x^{HF} = -\sum_j \delta_{\sigma_i,\sigma_j} \frac{\phi_j(\vec{r})}{\phi_i(\vec{r})} \int \frac{\phi_j^*(\vec{r}')\phi_i(\vec{r}')}{|\vec{r}-\vec{r}'|} d^3r' \qquad 1.23$$

HF describes exchange correctly, but correlation is totally missed, this approximation remains an indispensable benchmark in molecular physics, although extended systems such as solids remain a challenge. It is extremely expensive since the number of configurations increases very rapidly with the number of electrons. The Hartree-Fock approach can be relatively suitable for systems with small number of localised electrons but fails in case of perfect metals.

1.6. Density Functional Theory DFT:

Density Functional Theory (DFT) is presently the most widely used theory to compute the total energy and electronic structure of matter...). It is based on Hohenberg and Kohn theorems[12], the basic concept in this theory is to use the ground state electron density $\rho(r)$ as the fundamental variable, rather than the electronic wave-function, which depends on 3N variables. An important advantage of using the electron density over the wave-function is the much-reduced dimensionality, regardless of how many electrons one has in the system, the electron density is a function of only 3 variables (x, y, z). This enables DFT to be applied to much large systems, hundreds or even thousands of atoms, and the computational cost for a many-body system is thus saved in this theory.

1.6.1. Electron density and Thomas Fermi model:

The basic variable in DFT is the electron density[28] .It determines the probability of finding any of the N electrons within element volume. It can be expressed as measurable observable only dependent on spatial coordinates:

$$\rho(\vec{r}) = \sum_{i=1}^{N} |\phi_i(\vec{r})|^2 \qquad 1.24$$

The electron density contains all necessary information about the system. In detail that means it contain information about the electron number *N* as well as the external potential. The total number of electrons can be obtained by integration of the electron density over the whole space:

$$\int \rho(\vec{r}) d\vec{r} = \mathrm{N} \qquad 1.25$$

The function $\rho(\vec{r})$ is a non-negative function $\rho(\vec{r}) \geq 0$ that vanishes at infinity: $\rho(\mathrm{r} = \infty) = 0$

The concept of using the electron density rather than the wave function can be traced back to the work of Thomas and Fermi in 1927, almost forty years before the Hohenberg-Kohn theorems were published. Thomas and Fermi[29], [30] treated the kinetic energy based on a homogeneous gas system of free electrons (the wave functions used are plane wave functions). The kinetic energy of electrons is expressed as:

$$T(\rho) = C_F \int \rho^{5/3}(\vec{r})\, d^3\vec{r} \qquad 1.26$$

With:

$$C_F = \frac{3\hbar^2}{10m}(3\pi)^{2/3} \qquad 1.27$$

The total energy of a system in an external potential V_{ext} is written as a functional of the electron density $\rho(\vec{r})$ as:

$$E_{TF} = C_F \int \rho^{5/3}(\vec{r})\, d^3\vec{r} + \frac{1}{2}\iint \frac{\rho(\vec{r})\rho(\vec{r}')}{|\vec{r}-\vec{r}'|} d^3r d^3r' + \int \rho(\vec{r}) V_{ext}(\vec{r})\, d^3\vec{r} \qquad 1.28$$

Where the first term is the kinetic energy of the non-interacting electrons in a homogeneous electron gas (HEG), the second term is the classical electrostatic Hartree energy approximated by the classical Coulomb repulsion between electrons and the third term is the classical electrostatic energy of the nucleus-electron coulomb interaction.

Although it is an important first step, the TF model remains not good approximation, not only because of the poor description of the uniform gas in the representation of the kinetic energy, but also the complete neglect of exchange and correlation terms in the electron-electron interaction. In the original TF method, the exchange and correlation among electrons was neglected. Then, ameliorations have been made to this model by adding other effects, such as:

-The local exchange term introduced by Dirac[31] in 1930:

$$E_{TFD}[\rho] = E_{TF}[\rho] - C_x \int \rho^{4/3}(\vec{r})\, d^3\vec{r} \qquad 1.29$$

-The correlation effect proposed by Wigner:

$$T(\rho) = -a \int \frac{\rho^{4/3}(\vec{r})}{b + \rho^{1/3}(\vec{r})}\, d^3\vec{r} \qquad 1.30$$

Despite these improvements, this model is insufficient and give inaccurate results.

1.6.2. Hohenberg and Kohn theorems:

The formalism of the density functional theory (DFT) is based on the two theorems of Hohenberg and Kohn[12], published in1964.

Theorem 1 (Uniqueness): « the external potential $\hat{V}_{ext}$ is (to within a constant) a unique functional of $\rho(\vec{r})$ ».

An immediate consequence is that the ground-state expectation value of any observable $\hat{O}$ is a unique functional of the exact ground-state electron density: $\langle\psi|\hat{O}|\psi\rangle = O[\rho]$

Proof: Suppose the opposite, where for the density $\rho(\vec{r})$ corresponds two different external potentials $\hat{V}_{ext}^{(1)}$ and $\hat{V}_{ext}^{(2)}$. For simplicity, assume the ground state is non-degenerate as in the origin paper of Hohenberg and Kohn. Now clearly $\hat{V}_{ext}^{(1)} - \hat{V}_{ext}^{(2)} = const$, the two potentials are associated with two different Hamiltonians, $\hat{H}$ and $\hat{H}'$, and two different wave-function $\psi^{(1)}$ and $\psi^{(2)}$, with

$\hat{H}\psi^{(1)} = E_1\psi^{(1)}$ and $\hat{H}'\psi^{(2)} = E_2\psi^{(2)}$. Since $\psi^{(2)}$ is not the ground state of $\hat{H}$, we have by the minimal property of the ground state:

$$\begin{aligned} E_1 = \langle\psi^{(1)}|\hat{H}|\psi^{(1)}\rangle &< \langle\psi^{(2)}|\hat{H}|\psi^{(2)}\rangle \\ &< \langle\psi^{(2)}|\,\hat{H}'|\psi^{(2)}\rangle + \langle\psi^{(2)}|\hat{H} - \hat{H}'|\psi^{(2)}\rangle \\ &< E_2 + \int \rho(\vec{r})\left[\hat{V}_{ext}^{(1)} - \hat{V}_{ext}^{(2)}\right]d\vec{r} \end{aligned} \qquad 1.31$$

Similarly

$$\begin{aligned} E_2 = \langle\psi^{(2)}|\,\hat{H}'|\psi^{(2)}\rangle &< \langle\psi^{(1)}|\,\hat{H}'|\psi^{(1)}\rangle \\ &< \langle\psi^{(1)}|\hat{H}|\psi^{(1)}\rangle + \langle\psi^{(1)}|\,\hat{H}' - \hat{H}|\psi^{(1)}\rangle \\ &< E_1 - \int \rho(\vec{r})\left[\hat{V}_{ext}^{(1)} - \hat{V}_{ext}^{(2)}\right]d\vec{r} \end{aligned} \qquad 1.32$$

Adding Eq-1-31 and Eq-1-32 gives the contradiction:

$$E_1 + E_2 < E_2 + E_1 \qquad 1.33$$

Hence, no two different external potentials can give rise to the same density $\rho(\vec{r})$, there is a one-to-one mapping between the density and the external potential $\hat{V}_{ext}$, and the wave- function as $\psi \leftrightarrow \hat{V}_{ext} \leftrightarrow \rho(\vec{r})$, then, the total energy of interacting electrons in an external potential is given exactly as a functional of the ground state electronic density $\rho(\vec{r})$.

$$E = E[\rho(\vec{r})] \qquad 1.34$$

Separating the interaction with the external potential from kinetic energy and electron -electron interaction, it is possible to write the total energy as:

$$E[\rho(\vec{r})] = F[\rho(\vec{r})] + \int \rho(\vec{r})\hat{V}_{ext}(\vec{r})\, d\vec{r} \qquad 1.35$$

Where the term F is called a universal functional, because it does not depend on external potential V_{ext} , the exchange and correlation effects are contained in this functional.

Theorem 2 (Variational principle): « For a given external potential, the true density $\rho_0(\vec{r})$ minimizes the total energy functional».

$$E[\rho_0(\vec{r})] = minE[\rho(\vec{r})] \qquad 1.36$$

To prove the second HK theorem, we need to show that the density that minimises the functional $E[\rho(\vec{r})]$ is the ground state density. We can express $E[\rho(\vec{r})]$ in terms of the wave function ψ

$$E[\psi] = \langle\psi|\hat{H}|\psi\rangle = F[\rho(\vec{r})] + \int \rho(\vec{r})\hat{V}_{ext}(\vec{r})\, d\vec{r} = E[\rho(\vec{r})] \qquad 1.37$$

Where $\hat{H}$ is the general Hamiltonian defined in equation 1-37 .By the variational principle, this is minimised when the wavefunction is the ground state wave function of the Hamiltonian corresponding to V_{ext} , ψ_0. In particular, we can consider the ground state associated with a different external potential $V_{ext}^{'}$, ψ'. Taking the ground state densities corresponding to V_{ext} and V'_{ext} as ρ' and ρ_0 we can use the variational principle to write:

$$E[\rho'(\vec{r})] = E[\psi'] > E[\psi_0] = E[\rho_0(\vec{r})] \qquad 1.38$$

This shows that the functional $E[\rho(\vec{r})]$ is minimised by the true ground state density, as required. Although HK theorems put particle density $\rho(\vec{r})$ as the basic variable, it is still impossible to calculate any property of a system because the universal functional is unknown. This difficulty was overcome by Kohn and Sham in 1965, who proposed the well-known Kohn-Sham equations.

1.7. Kohn-Sham equations:

Hohenberg-Kohn theorems proved the existence of an exact solution for the ground state of the system, but they do not offer a practical approach for its calculation. However, in 1965, Kohn and Sham[13], [32] proposed a concept that allowed to turn DFT into a real computational tool.

Since the expression for the Hartree energy as a functional of the density is known, the unknown universal functional $F[\rho]$ in equation 1-35 can be decomposed into a classical part $E_H[\rho]$ and another functional $G[\rho(\vec{r})]$:

$$F[\rho] = E_H[\rho] + G[\rho(\vec{r})] \qquad 1.39$$

Where the expression of the Hartree energy $E_H[\rho]$is already given in equation 1-15. Like $F[\rho]$, $G[\rho(\vec{r})]$ is an unknown universal functional of the density. The total energy can then be written as:

$$E_e = \int \rho(\vec{r})\hat{V}_{ext}(\vec{r})\, d^3\vec{r} + \frac{1}{2}\iint \frac{\rho(\vec{r})\rho(\vec{r}')}{|\vec{r}-\vec{r}'|} d^3r d^3r' + G[\rho(\vec{r})] \qquad 1.40$$

The Kohn and Sham proposed a scheme to evaluate $G[\rho(\vec{r})]$ that is analogous to the Hartree's method (independent particles), In this scheme, one can decompose this G[ρ(r)] into two parts:

$$G[\rho(\vec{r})] = T_s[\rho(\vec{r})] + E_{xc}[\rho(\vec{r})] \qquad 1.41$$

The first term is the kinetic energy of a non-interacting system with the same density. The second term is the exchange–correlation energy. One can rewrite the total energy as:

$$E_e[\rho(\vec{r})] = \underbrace{T_s[\rho(\vec{r})] + E_{xc}[\rho(\vec{r})]}_{G[\rho(\vec{r})]} + E_H[\rho(\vec{r})] + \int \rho(\vec{r})V_{ext}(\vec{r})d\vec{r} \qquad 1.42$$

The term E_{xc} contains the difference between the exact and non-interacting kinetic energies and also the non-classical contribution to the electron-electron interactions, It takes care of all the non-classical exchange-correlation effects and can be written as.

$$E_{xc}[\rho(\vec{r})] = E_x[\rho(\vec{r})] + E_c[\rho(\vec{r})] \qquad 1.43$$

Where E_c is due to electron correlation and E_x is the exchange energy.

Minimizing the total energy in Eq. (1. 42) under the constraint of particle number conservation, one obtain:

$$\int \delta\rho(\vec{r})\left\{V_{\text{eff}}^{KS}(\vec{r}) + \frac{\delta T_s[\rho(\vec{r})]}{\delta\rho(\vec{r})} - \mu\right\} d^3r = 0 \qquad 1.44$$

where μ is the chemical potential and:

$$V_{\text{eff}}^{KS}(\vec{r}) = V_H(\vec{r}) + V_{ext}(\vec{r}) + V_{xc}(\vec{r}) \qquad 1.45$$

Where V_{eff}^{KS} is the Kohn-Sham effective potential and V_{xc} is the exchange-correlation potential, which is due to non-classical effects:

$$V_{xc}[\rho(\vec{r})] = \frac{\delta E_{xc}[\rho(\vec{r})]}{\delta\rho(\vec{r})} \qquad 1.46$$

Equation 1-44 equivalent to:

$$\underbrace{\left(-\frac{1}{2}\nabla^2 + V_{\text{eff}}^{KS}(\vec{r})\right)}_{\hat{H}^{KS}}\varphi_i(\vec{r}) = \epsilon_i\varphi_i(\vec{r}) \qquad 1.47$$

The KS scheme basic idea is to map the complex, interacting electronic systems into a set of fictitious non-interacting particles ($V_{ee} = 0$) in an external effective potential V_{eff}^{KS} , In this method, the ground state density of the real interacting system is assumed to be equivalent to that of the fictitious non-interacting (auxiliary system). Fig. I.2.

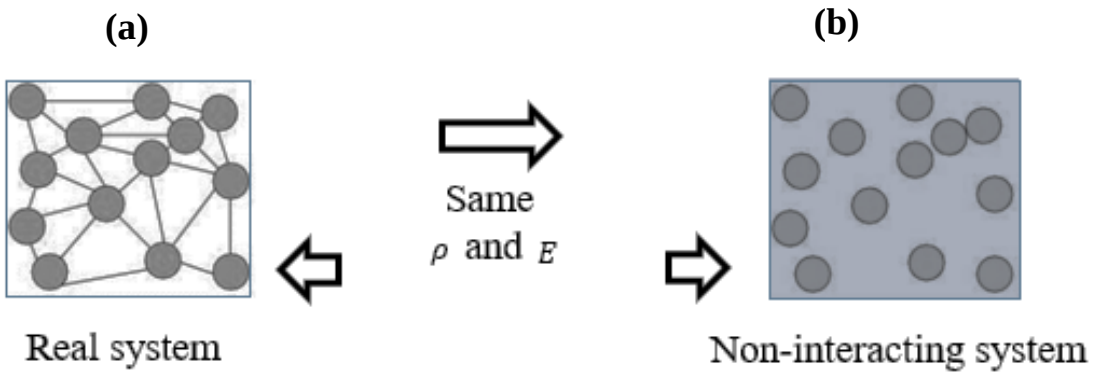

Fig. 1. 2 Representation of relationship between the real many body system (left hand side) and the non-interacting system of Kohn-Sham density functional theory (right hand side).

The Kohn-Sham equations are gathered in 1-48, they represent a self-consistent problem, and describe the ground-state of a non-interacting system of particles in an external potential V_{KS} .These equations are typically solved by an iterative procedure (see section I.9.2). Nevertheless, the exact ground state electron density can be calculated only, if the exact expression for the exchange-correlation potential V_{xc} can be found.

$$\begin{cases} \left(-\frac{1}{2}\nabla^2 + V_{\text{eff}}^{KS}(\vec{r})\right)\varphi_i(\vec{r}) = \epsilon_i\varphi_i(\vec{r}) \\ V_{\text{eff}}^{KS}(\vec{r}) = V_H(\vec{r}) + V_{ext}(\vec{r}) + V_{xc}(\vec{r}) \\ \rho(\vec{r}) = \sum_{occ} |\phi_i(\vec{r})|^2 \end{cases} \quad 1.48$$

In case of spin-polarized system:

The charge density consists of a spin-up density $\rho^{\uparrow}$ and spin-down density $\rho^{\downarrow}$:

$$\rho(\vec{r}) = \rho^{\uparrow}(\vec{r}) + \rho^{\downarrow}(\vec{r}) \quad 1.49$$

The ground-state energy is then a functional of both spin directions:

$$E = E\left[\rho^{\uparrow}, \rho^{\downarrow}\right] \quad 1.50$$

The Kohn-Sham equation for spin-polarized case is written as:

$$\left(-\frac{\hbar^2}{2m}\nabla^2 + V_H(\vec{r}) + V_{ext}(\vec{r}) + V_{xc,\sigma}(\vec{r})\right)\varphi_{i,\sigma}(\vec{r}) = \epsilon_{i,\sigma}\varphi_{i,\sigma}(\vec{r}) \quad 1.51$$

With σ the spin index. The spin density has the form:

$$\rho_\sigma(\vec{r}) = \sum_{i=1}^{N} \varphi_{i,\sigma}^*(\vec{r})\varphi_{i,\sigma}(\vec{r}) \quad 1.52$$

with the highest occupied orbital defined by the electron count. The exchange correlation potential becomes:

$$V_{xc,\sigma}(\vec{r}) = \frac{\delta E_{xc}[\rho^{\uparrow}, \rho^{\downarrow}]}{\delta\rho_\sigma(\vec{r})} \quad 1.53$$

Now there are two sets of equations to be solved, one for each spin-direction, and the exchange-correlation potential is the only spin-dependent operator in the Kohn-Sham equation.

1.8. Exchange and correlation energy:

One of the great challenges in electronic structure calculations is determining the exchange correlation energy E_{xc} because it needs to be approximated. As noted earlier, the E_{xc} functional contains the non-classical contributions to the potential energy due to the electron-electron interaction and the difference between the kinetic energy of the real system and the kinetic energy related to the non-interacting system, it is possible to find reasonable approximations which are local or at least semi-local in the density. Here, we will give a short overview of the most important and widely used approximations for E_{xc}.

The Exchange and correlation approximations can be categorized according to the variables used in the construction of the functional as presented in table which represents some approximations for E_{xc} energy. By adding more variables, the energy becomes more accurate and complex. However, it does not necessarily guarantee higher accuracy for specific systems, as some approximation can perform very well for certain systems.

Approximation	**dependence**
LDA	$\rho(\vec{r})$
GGA	$\rho(\vec{r}), \lvert\vec{\nabla}\rho(\vec{r})\rvert$
meta-GGA	$\rho(\vec{r}), \nabla^2\rho(\vec{r}), \tau(\vec{r})$
Hydrid functional	Exact exchange $\rho(\vec{r}), \lvert\vec{\nabla}\rho(\vec{r})\rvert$

Table. 1. 1 Various forms of Exchange and correlation energy E_{xc} for different approximations used in solid-state DFT.

1.8.1. Local Density Approximation LDA:

The simplest approximation for the exchange and correlation energy in DFT is known as the Local Density Approximation (LDA). It was firstly proposed by Kohn and Sham[32] and it holds for systems with slowly varying densities. The main idea about this approximation is that a real system of interacting-electrons can be treated as a Uniform Electron Gas (UEG), in which

electrons are uniformly distributed all over the space with positive background of nuclei, within this approximation the exchange and correlation energy can be written as:

$$E_{xc}^{LDA} = \int \rho(\vec{r}) \varepsilon_{xc}^{LDA}(\rho(\vec{r}))\, d\vec{r} \qquad 1.54$$

Where ε_{xc}^{LDA} is the exchange and correlation energy per electron of an electron gas with uniform density, this function can be divided into exchange and correlation energy contributions $\varepsilon_{xc}^{LDA}(\rho) = \varepsilon_x(\rho) + \varepsilon_c(\rho)$, of which the exchange part is known, derived by Dirac[33]:

$$\varepsilon_x(\rho) = -\frac{4}{3}\left(\frac{3}{\pi}\right)^{1/3} \rho^{1/3} = -\frac{4}{3}\left(\frac{9}{4\pi^2}\right)^{1/3} \frac{1}{r_s} \qquad 1.55$$

r_s is known as the Wigner-Seitz[34] radius is related to the density as:

$$r_s = \frac{4}{3}\, \pi {r_s}^3 = \frac{1}{\rho} \qquad 1.56$$

The correlation energy. ε_c is not known exactly, but it has been numerically evaluated with great accuracy with Quantum Monte Carlo calculations by Ceperley and Alder[35]. Many functionals for the correlation energy density have been developed by Perdew-Zunger[36], Perdew & Wang[37], 1992 and Vosko, Wilk, & Nusair[38], 1980.

The LDA is expected to be a good approximation for systems with densities that vary slowly, even if this condition is hardly met for real system. According to many previous works, LDA has proved to be accurate for a wide variety of systems. One of its great advantages is the prediction of geometries and elastic properties. In many cases, LDA gives good results elastic moduli, and it is considered satisfactory in materials science. However, LDA yields significant errors for the bonding, the dissociation energy and the cohesive energy. Therefore, it remains an important challenge to solid state physicists and chemists to seek further for ways to improve the local-density results.

For spin polarized systems, the local spin-density approximation (LSDA) is an improvement for systems where the spin of electrons is important, the exchange and correlation energy has the form:

$$E^{LSDA}{}_{xc}[\rho^{\uparrow}, \rho^{\downarrow}] = \int \rho(\vec{r}) \varepsilon_{xc}^{LDA}(\rho^{\uparrow}, \rho^{\downarrow}) d\vec{r} \qquad 1.57$$

Where $\varepsilon_{xc}(\rho^{\uparrow}, \rho^{\downarrow})$ is the exchange and correlation energy per particle of' a homogeneous, spin-polarized electronic system. Parametrizations of $\varepsilon_{xc}(\rho^{\uparrow}, \rho^{\downarrow})$ have been given by von Barth and Hedin[39] (1972), Gunnarsson and Lundqvist[25], [26] (1976), Vosko et al[23]. (1980), and Perdew and Zunger[21] (1981).

1.8.2. Generalized Gradient Approximation (GGA):

Another approach to approximate the exchange and correlation energy is the Generalized Gradient Approximations (GGA), Kohn and Sham already noticed that the charge density gradient, $\vec{\nabla}\rho(\vec{r})$, is necessary to obtain a better estimate of the exchange and correlation energy. GGA was introduced by Perdew and co-workers to improve LDA for inhomogeneous systems, where the density is rapidly varying. The exchange and correlation energy is given by:

$$E_{xc}^{GGA} = \int \rho(\vec{r})\varepsilon_{xc}^{GGA}(\rho(\vec{r}), \vec{\nabla}\rho(\vec{r}))d\vec{r} \qquad 1.58$$

The local exchange-correlation energy of the GGA approximation ε_{xc}^{GGA} depends not only on the local charge density but also on the local charge density gradient.

Many forms of GGA functionals have been suggested. Two of the most popular functionals which are widely used in calculations involving solids are the Perdew-Wang functional (PW91)[27] and the Perdew-Burke-Ernzerhof functional (PBE)[28], [29]. The latter is one of the most commonly used in condensed-matter studies today, due to its accuracy for a range of properties. It has demonstrated to be accurate over a variety of systems. In addition, there exist two variants of the original PBE functional: the revised PBE (RevPBE)[30] functional, which is intended to produce more accurate surface binding (adsorption) energies, and the PBE for solids (PBEsol)[31] functional, which is designed to produce a more accurate description of equilibrium bond lengths and lattice parameters in solids. PBE often gives results of the lattice constants in better agreement with experiment, but for the bulk moduli is not good compared to experiments.

Since GGA allows for a larger fluctuation than LDA, GGA generally gives better results than LDA, such as total energies, atomization energies, energy barriers and structural energy differences. Despite the improvements, GGA has some shortcomings, it is unable to describe the electrons highly localized *d*- and *f*-shells.

1.8.3. Meta-GGA methods:

Meta-GGA is essentially an extension of the GGA in which the non-interacting kinetic energy density $\tau(\vec{r})$ is used as input to the functional as well as the electron density and its gradient

$$E_{xc}^{MGGA} = \int \rho(\vec{r})\varepsilon_{xc}(\rho(\vec{r}), \vec{\nabla}\rho(\vec{r}), \tau(\vec{r}))d\vec{r} \qquad 1.59$$

$\tau(\mathbf{r})$ is defined as the sum of the squares of the gradients of the KS orbitals:

$$\tau(\vec{r}) = \frac{1}{2}\sum_{i=1}^{N} \nabla^2 \left|\phi_i^{KS}(\vec{r})\right|^2 \qquad 1.60$$

For LDA and GGA, the construction of ε_{xc} is straight forward, as it only involves the density, whereas for meta-GGAs, a rather complicated process involving the orbitals is necessary to construct the second derivative of the density.

The widely used meta-GGA functional is The TPSS (Tao-Perdew-Staroverov-Scuseria)[32] functional which does not contain empirical parameters. Generally, meta-GGAs improves the performance in predicting lattice parameters in solids, but bond lengths in molecules can be worse.

1.8.4. Hybrid functionals:

In hybrid functionals, the HF exact exchange is fractionally added to LDA or GGA. The Heyd-Scuseria-Ernzerhof (HSE)[33], [34] is the most popular hybrid functional which uses a screened-exchange potential. The screened functional make use of long-range HF exact exchange to describe the Coulomb potential. Therefore, the use of HF exact exchange is highly demanding for calculations on large systems. The short range (SR) of exchange is taken from HF exact exchange while long range of the exchange is obtained from PBE functional. The HSE hybrid functional is written as:

$$E_{xc}^{HSE} = \alpha E_x^{HF,SR} + (1-\alpha)E_x^{PBE,SR} + \alpha E_x^{PBE,LR} + \alpha E_c^{PBE} \qquad 1.61$$

Due to the inclusion of exact exchange energy, the performance of hybrid functionals is better for many molecular properties, such as binding energies, bond lengths, vibrational frequencies,

and electronic structure (band gap) of insulators, semiconductor, which tend to be poorly described by LDA/GGA functionals.

There are many hybrid functionals used such as: B3LYP[35], [36], PBE0[36], HSE, and HSE06[33], [34].

1.9. Solving Kohn and Sham equations:

1.9.1. Basis Sets:

For practical implementation of DFT, it is important to express the Kohn-Sham orbitals, $\varphi_i(r)$in Eq. (1.48), in a reasonable basis, $\{\varphi_P^{basis}(r)\}$,

$$\varphi_i(r) = \sum_{p=1}^{P} c_p^i \, \varphi_p^{basis}(r) \qquad 1.62$$

where c_p^i are constant coefficients. Consequently, the Kohn-Sham equations are equivalent to the system of linear equations:

$$\begin{bmatrix} & \cdots & \\ \vdots & \langle\varphi_m|\hat{H}^{KS}|\varphi_n\rangle - \mathcal{E}_i\langle\varphi_m|\varphi_n\rangle & \vdots \\ & \cdots & \end{bmatrix} \begin{bmatrix} c_1^i \\ \vdots \\ \\ \vdots \\ c_P^i \end{bmatrix} = \begin{bmatrix} 0 \\ \vdots \\ \\ \vdots \\ 0 \end{bmatrix} \qquad 1.63$$

Diagonalisation of the matrix H yields P eigenvalues and P sets of coefficients c_p^i . In principle, the function space where the eigenfunctions φ_i belong to is infinite-dimensional, hence P is infinite. For practical reason, P needs to be truncated, while keeping in mind that the actual size of the basis set directly influences accuracy of the solution. Suitable basis wave functions can decrease the value of P needed for the prescribed accuracy. One of the most popular basis sets are plane wave sets, that are particularly effective for describing periodic systems such as crystals.

1.9.2. Self-Consistency in DFT calculations:

In order to solve the Kohn-Sham equations, an iterative procedure is needed to solve the problem. This approach is called the self-consistent field cycle (*SCF cycle*) and is shown in Fig

I.3. We start with an initial value of the input density ρ^{in} , which is typically a superposition of the atomic densities of the system:

$$\rho^{in} = \sum_{atom} \rho^{atom} \qquad 1.64$$

Then we construct the effective potential V_{KS} and set up the Kohn-Sham equations. What follows is the computationally most expensive step of solving the Kohn-Sham equations for a given basis set to obtain the Kohn-Sham orbitals and energies.

A new output density can then be calculated from those orbitals according to the relation:

$$\rho^{out} = \sum_{i=1}^{N} |\varphi_i^{out}(\vec{r})|^2 \qquad 1.65$$

Self-consistency is reached if $\rho^{out} = \rho^{in}$. If this is not the case, the procedure is iterated with a new guess density constructed from ρ^{out}[37]. In practice, the self-consistency cycle is stopped when some convergence criterion is reached. The two most common criteria are based on the difference of total energies or densities from iteration:

$$\rho^{i} - \rho^{(i-1)} < \epsilon_{\rho} \quad , \quad E^{i} - E^{(i-1)} < \epsilon_{E} \qquad 1.66$$

Where ρ^{i} and E^{i} are the density and total energy at the iteration i similarly, $\rho^{(i-1)}$ and $E^{(i-1)}$ are the density and total energy at the iteration $(i-1)$, ϵ_E and ϵ_ρ are user defined tolerances. Using the output density ρ^{out} as the new input density fails badly in many ways. For real systems it is impossible to find the exact self-consistent density with numerical methods, but we can come arbitrarily close.

The idea to reaching self-consistency is to mix the output density ρ^{out} with the input density $\rho^{in}$of the same iteration, it's is a clever way to generate the input density for the next iteration and to accelerate the convergence. The simplest mixing scheme is linear such as[38]:

$$\rho_{i+1}^{in} = (1-\alpha)\rho_i^{in} + \alpha\rho_i^{out} \qquad 1.67$$

Where i is the iteration index and α is the mixing parameter $0 \leq \alpha \leq 1$. Other methods involving the Jacobian or Hessian matrix prove to be more efficient than linear mixing. The family of Broyden mixing methods take not only numerical details, but also algorithmic

complexity into account, and update the inverse Jacobian successively with each iteration. Their efficiency has led to the widespread use of Broyden-type mixing in contemporary Kohn-Sham solvers.

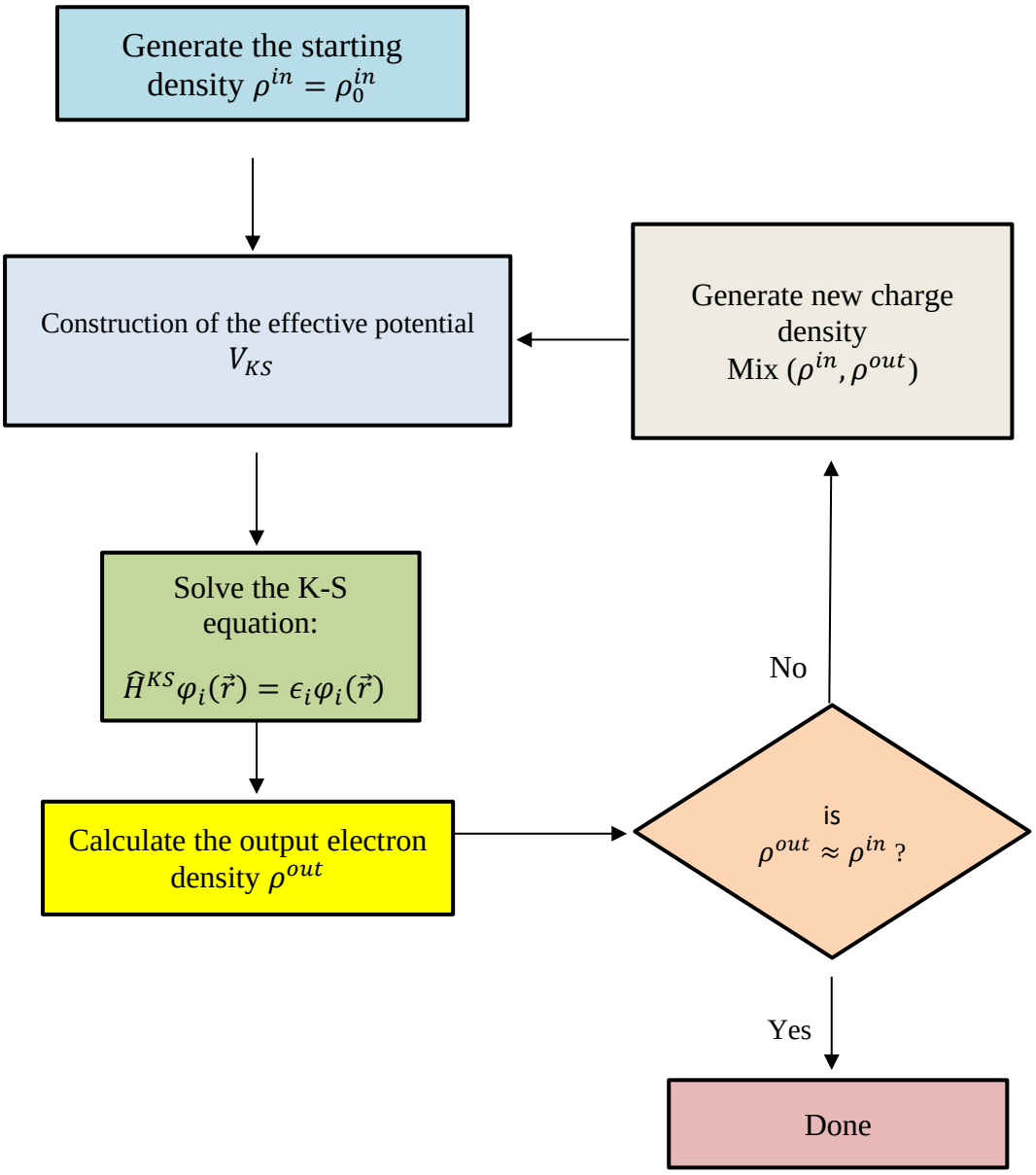

Fig. 1. 3 Schematic representation of the iterative, self-consistent solution of the Kohn-Sham equations.

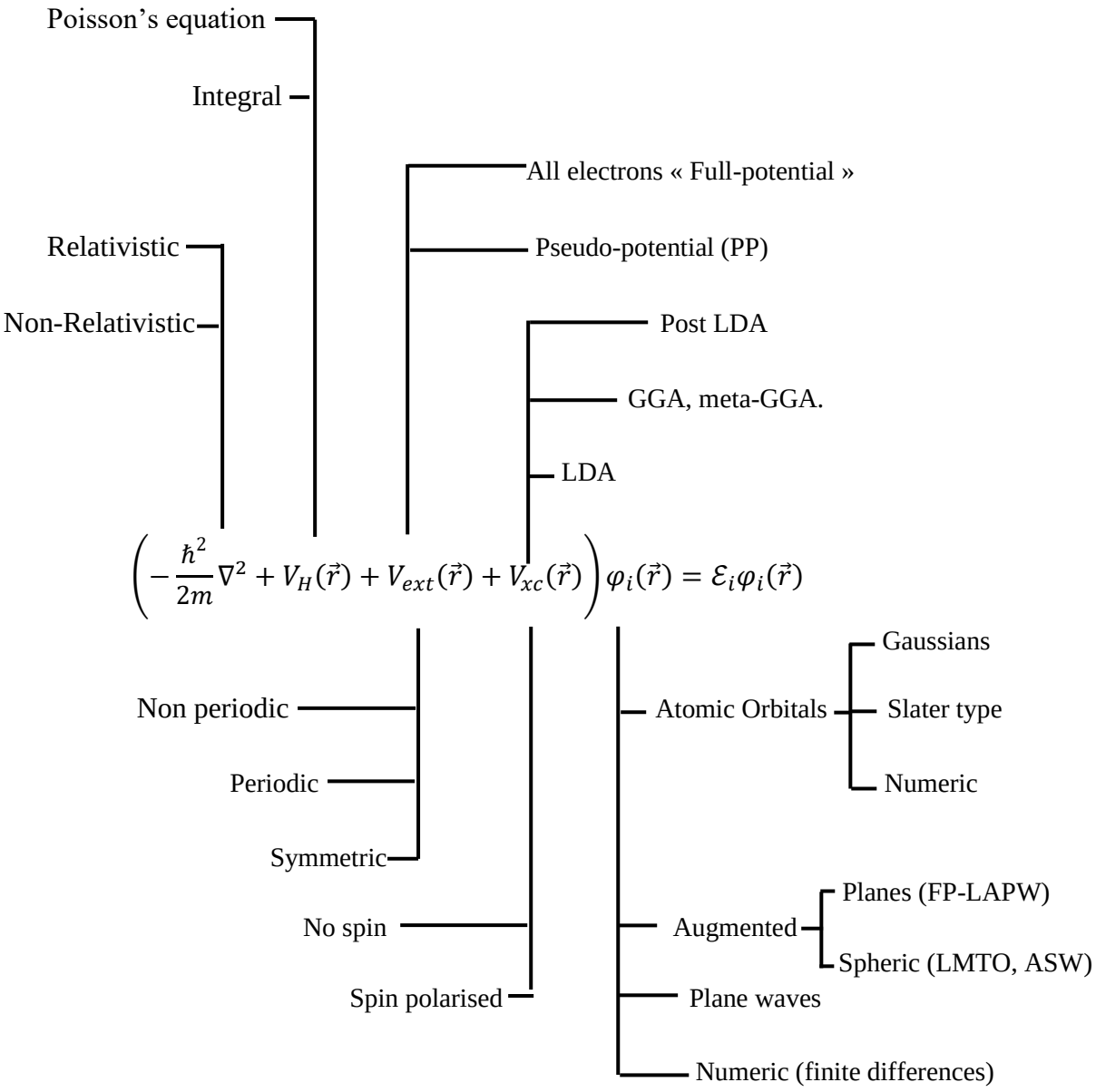

Fig. 1. 4 Schematic representation of various DFT-based methods of calculation.

1.10. Plane waves:

In order to perform an electron structure calculation for atomic or molecular systems one needs to expand the Kohn-Sham wave functions in some suitable basis set. The property of periodicity, which is inherent for solid state systems, restrains the form of one-particle basis sets to a linear combination of Bloch functions:

$$\psi_{\vec{k}}(\vec{r}) = u_{\vec{k}}(\vec{r})e^{i\vec{k}\vec{r}} \qquad 1.68$$

Within this equation the Bloch factor $e^{i\vec{k}\vec{r}}$ is known but the undetermined part $u_{\vec{k}}(\vec{r})$ has the periodicity of the lattice. Therefore, the wave function $u_{\vec{k}}(\vec{r})$ can be written (according to a Fourier series) as the sum over plane waves of the same periodicity, which includes a sum of (all) reciprocal lattice vectors $\vec{G}$.

$$\psi_{\vec{k}}(\vec{r}) = \sum_{\vec{G}} c_{\vec{k},\vec{G}} e^{i(\vec{k}+\vec{G})\vec{r}} \qquad 1.69$$

A plane-wave basis set possesses some advantages - it has a simple form; thus, the construction of the Hamiltonian matrix is generally much faster than its diagonalization; it is unbiased; thus, the resulted wave function is independent of atom location and does not suffer from the basis set superposition error; its set of expansion coefficients can be easily transformed from reciprocal space to real space and back via the Fast Fourier- Transform (FFT) algorithm. Nevertheless, the size of a plane-wave basis set, which is required for adequate description of a given system, is much bigger than in the case of using of localized orbitals and may comprise several ten thousand single plane-waves.

The use of plane waves to describe the valence electron wavefunctions is a natural one since the valence electrons behave almost like free particles away form the core. However, around the core the wavefunctions oscillate rapidly due to the tightly bound core electrons. This means that to accurately describe the wavefunctions, a large number of plane waves is needed. Since the use of many plane waves is computationally expensive it is not feasible to use plane waves to solve the Kohn-Sham equations without introducing other approximations. In order to deal with this issue, the fact that chemical properties of a compound are strongly dependent only on valence electrons are exploited. That allows one to divide the space in the vicinity of nuclei onto the core electron region and the valence electron region (frozen-core

approximation), where the second contains the smooth part of the wave function and can be easily described by a moderate-size set of plane waves.

1.11. Pseudopotential method:

The natural choice for basis functions for periodic solids are plane waves, but an extraordinary number of plane waves are required in the region near to the nuclei for a reasonable description of the wave function. One can overcome this problem by replacing the strong electron-ion potential by a much weaker pseudopotential. This makes the pseudo wave function smooth near to the nucleus for $r < r_c$ and matches the exact solution: $\psi^{PS}(\vec{r}) = \psi(\vec{r})$ at $r > r_c$, where r_c is a "cut-off" distance (core radius). As shown in Fig 1.5

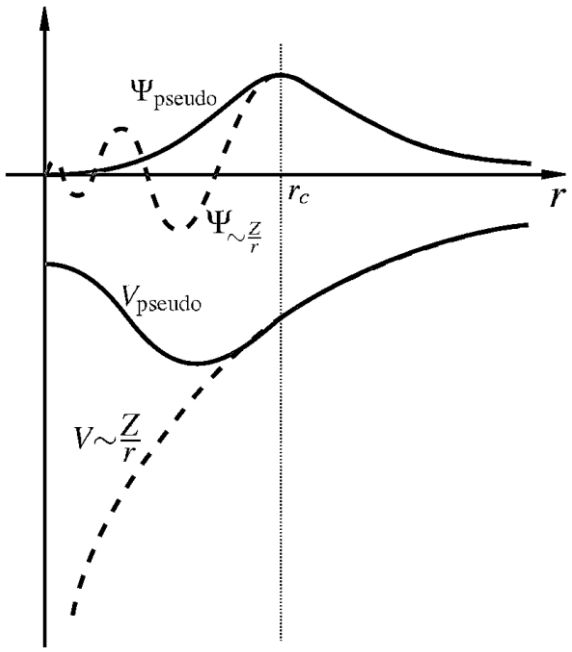

Fig. 1. 5 Schematic illustration of the replacement of the all-electron wavefunction and core potential (solid line) by a pseudo-wavefunction and pseudopotential (dashed line) [39].

There are pseudopotentials that require high cutoff energy (hard pseudopotentials), or low cutoff energy (soft pseudopotentials). The most common type of pseudopotentials was developed by Vanderbilt, this type requires the least cutoff energy among others, so it was named USPP (ultrasoft pseudopotential). One of the disadvantages of USPP is that in order to create a pseudo-potential for each element, several empirical parameters must be set. Another approach with a frozen core approximation that avoids some of the disadvantages of USPP is

called PAW (projector augmented-wave) [40]. It was originally developed by Bloch, and was later adapted for calculations with a plane wave basis by Kress and Joubert. They conducted a detailed comparison of calculations using USPP, PAW and calculations with all electrons. Their work shows that correctly compiled USPP and PAW methods give almost identical results in many cases, and that these results are in agreement with the results of calculations with all electrons.

1.12. Types of calculations in QUANTUM ESPRESSO

Quantum Espresso [41] is based on pseudopotential method, it can calculate many calculations such as:

· Scf (self-consistent field): the usual calculation of the electronic structure for a given fixed supercell with fixed positions of atoms according to the iterative algorithm of the density functional theory.

Relax (relaxation): structural optimization with a fixed supercell. The forces acting on the atoms in the supercell are minimized. At each iteration of the structural optimization algorithm, a "scf" calculation is performed. In all calculations in this paper the quasi-Newtonian BFGS algorithm (the Broiden-Fletcher-Goldfarb- Shanno algorithm) was used.

Vc-relax (variable-cell relaxation): is a structural optimization with a variable supercell. The same as "relax", but the tension in the supercell are also minimized.

Bands: calculation of the energies of Kohn-Sham states along a given path with a given density of points in the Brillouin zone, based on the results of the "scf" calculation. Allows you to obtain the zone structure of the crystal

1.13. Development of Full Potential Method Linearized Augmented Plane Wave Method (FP-LAPW)

1.13.1. Augmented Plane Wave Method (APW):

The APW method is an all-electron method, it actually treats both, valence and core electrons self-consistently, which is not possible with the very common pseudopotential-based methods. In 1937, J. C. Slater[42] established the augmented plane wave (APW) method, according to his works, the space in the unit cell into two regions, as shown in Fig 1.6: a set of

non-overlapping spheres cantered at each atom (often called muffin-tin spheres) (M) and an interstitial region (remaining space) (I). Inside each atomic sphere, the wave functions have nearly an atomic character, by taking only the spherical part of the potential inside this sphere. The wave functions are written as sum of radial functions u_l^α times spherical harmonics Y_{lm} labeled with the quantum numbers *l* and *m*. We use the muffin-tin approximation only for numerically solving the radial functions, which depend on the energies ϵ. In the interstitial region, where the potential varies only slowly, we can expand the wave functions in a set of plane waves (PWs).

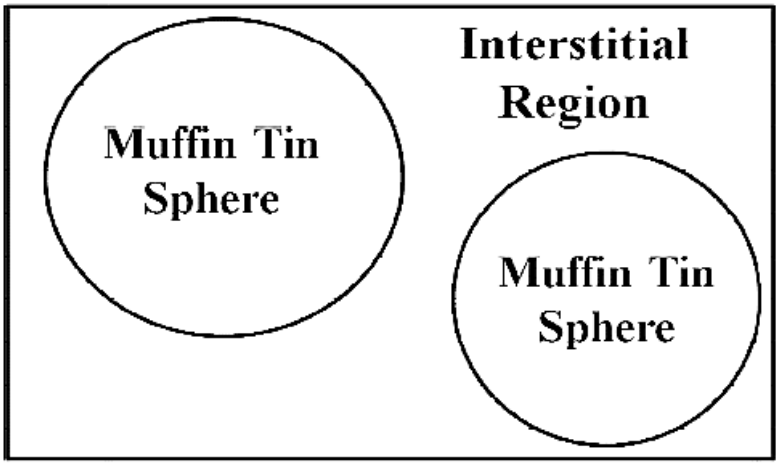

Fig. 1. 6 Division of a unit cell into muffin tin regions M and interstitial region I

The all-electron wave function adopts the following form:

$$\psi_{\vec{k}}(\vec{r}) = \begin{cases} \sum_{l,m} A_{lm}^{\alpha,\vec{k}+\vec{G}} u_l^\alpha(r,\epsilon) Y_{lm}(\hat{r}), & r \in MT \\ \Omega^{-1/2} \sum_{\vec{G}} c_{\vec{k}+\vec{G}} e^{i(\vec{k}+\vec{G})\vec{r}} & , \ r \in I \end{cases} \qquad 1.70$$

Where r the radial distance from the nucleus, $\vec{k}$ is the wave vector which lies in the first Brillouin zone and $\vec{G}$ is a reciprocal lattice vector. Ω is the unit cell volume, Y_{lm} are spherical harmonics and u_l^α are solutions to the atomic radial Schrödinger equation for some energy $\epsilon_l^{\vec{k}}$ while $A_{lm}^{\alpha,\vec{k}+\vec{G}}$ is $\vec{k}$ dependent parameter. This parameter can be determined from the requirement that plane waves outside muffin tin spheres should match with wave function inside those spheres over all muffin tin spheres surface. For that purpose, plane waves can be expanded in terms of spherical harmonics about the origin of the sphere:

$$c_{\vec{k}+\vec{G}}e^{i(\vec{k}+\vec{G})\vec{r}} = \frac{4\pi}{\sqrt{\Omega}}c_{\vec{k}+\vec{G}}e^{i(\vec{k}+\vec{G})\vec{r}_\alpha}\sum_{lm} i^l j_l(|\vec{k}+\vec{G}|R_\alpha)\left(Y_{l,m}(\vec{K}+\vec{G})\right)^* Y_{l,m}(\hat{r}) \qquad 1.71$$

where j_l is the Bessel function of order *l*. Then:

$$A_{\alpha,lm}^{\vec{k}+\vec{G}} = \frac{4\pi i^l c_{\vec{k}+\vec{G}}e^{i(\vec{k}+\vec{G})\vec{r}_\alpha}}{\sqrt{\Omega}u_l^\alpha(R_\alpha,\epsilon_{l,\vec{k}})} j_l(|\vec{k}+\vec{G}|R_\alpha)\left(Y_{l,m}(\vec{K}+\vec{G})\right)^* \qquad 1.72$$

the main problem with the APW method is the necessity to determine u_l^α for each energy $\epsilon_{l,\vec{k}}$ (u_l^α depends on the unknown energy ϵ) which in turn are the searched eigen energies of the problem, inside the MT sphere, the APWs are solutions of the Schrödinger equation only at the reference energy $\epsilon_l = \epsilon_n$. If the eigenenergy does not equal ϵ_l , another trial energy must be chosen until the eigenenergy equals ϵ_l .Mathematically, the problem becomes nonlinear and its solution much more computationally demanding for each k-point. This makes the APW method extremely inefficient.

Another shortcoming of the APW method, known as the asymptote problem, is related to the indetermination of the augmentation coefficients when the radial function has a node at the MT radius u_l^α in the denominator of Eq. (1.72). In the vicinity of this region, the relation between A_{lm} and C_G becomes numerically unstable.

1.13.2. LAPW method:

To overcome the energy dependence problem, the APW basis set has been linearized by Anderson and thus, the linearized augmented plane wave method was introduced[43], [44]. The trick is to make a first order Taylor expansion for $u_l^\alpha(r,\epsilon)$ around a fixed energy ϵ_l :

$$u_l^\alpha(r,\epsilon) = u_l^\alpha(r,\epsilon_l) + (\epsilon-\epsilon_l)\left.\frac{\partial u_l^\alpha(r,\epsilon)}{\partial \epsilon_{l,\vec{k}}}\right|_{\epsilon=\epsilon_l} + \mathcal{O}(\epsilon-\epsilon_l)^2 \qquad 1.73$$

By substituting the first two terms of this expansion in the APW wave-functions Eq. 1.70, we obtain the linear augmented plane wave (LAPW) basis set, which is defined by:

$$\psi_{\vec{k}}(\vec{r}) = \begin{cases} \sum_{l,m} (A_{lm}^{\alpha,\vec{k}+\vec{G}} u_l^{\alpha}(r,\epsilon) + B_{lm}^{\alpha,\vec{k}+\vec{G}} \dot{u}_l^{\alpha}(r,\epsilon_l)) Y_{lm}(\hat{r}), & r \in MT \\ \Omega^{-1/2} \sum_{\vec{G}} c_{\vec{k}+\vec{G}} e^{i(\vec{k}+\vec{G})\vec{r}} & , \ r \in I \end{cases} \quad 1.74$$

In the interstitial region, the basis set is the same as in the APW method, but in the MT spheres, the basis functions depend not only on u_l^{α}, but also on its energy derivative, $\dot{u}_l^{\alpha}$. The LAPW basis set is designed to be flexible in describing the wave functions in the vicinity of the reference energy, the modified basis functions (Eq. 1.74) provide the extra flexibility to cover a large energy region around this linearization energy. In order to determine both A_{lm} and B_{lm}, the functions in the MT spheres are required to match the plane wave function both in value and in slope at the sphere boundary. However, the requirement of continuous derivatives at the MT radius increases the number of plane waves needed to achieve a given level of convergence with respect to the APW method.

1.13.3. LAPW+LO method:

Based on whether or not electrons in an atom participate in the chemical bonding with other atoms, the electrons can be divided into two types. One type of electrons are core electrons, which are extremely bound to their nucleus and are thus entirely localized in the MT sphere. The corresponding states are called core states. The other type of electrons are valence electrons, who are leaking out of the MT sphere and bond with other atoms. However, for many elements, the electrons cannot be clearly distinguished like that. Some states are neither constrained in the core states, nor lie in the valence states and are correspondingly termed semi-core states. They have the same angular quantum number l as the valence states but with lower principal quantum number n. When applying LAPW on these states, it is thus hard to use one ϵ_l to determine the two same *l* in Eq. 1.74. The dilemma is solved by introducing local orbitals (LO), which are defined as:

$$\phi_{\alpha,\ell m}^{LO}(r) = \begin{cases} \sum_{l,m} (A_{lm}^{LO} u_l^{\alpha}(r,\epsilon_l) + B_{lm}^{LO} \dot{u}_l^{\alpha}(r,\epsilon_l) + C_{lm}^{LO} u_l^{\alpha}(r,\epsilon_l^2)) Y_{lm}(\hat{r}), & r \in MT \\ 0 & , \ r \in I \end{cases} \quad 1.75$$

Each local orbital is zero in the interstitial region and other atoms MT sphere. The three coefficients A_{lm}, B_{lm} and C_{lm} can be determined by requiring the LO to have both zero value and zero slope at the MT boundary and be normalized

1.13.4. APW+lo method:

It has been realized that the standard LAPW method is not the most efficient way to linearize APW method. However, the basis set of the APW+lo [45] method is energy independent and has the same basis size as the original APW method. In APW+lo the orbital (lo) is added, which is different from the LOs used to describe semi core states. A lo, which is nonzero only inside a MT sphere, is given by:

$$\phi_{\ell m}^{lo}(r) = \begin{cases} \left[(A_{lm}^{lo} u_l^{\alpha}(r,\epsilon_l) + B_{lm}^{lo} \dot{u}_l^{\alpha}(r,\epsilon_l)\right] Y_{l,m}(r) & r \in MT \\ 0 & r \in I \end{cases} \qquad 1.76$$

The two coefficients A_{lm} and B_{lm} are determined by normalization, and by requiring that the local orbital has zero value at the Muffin-tin boundary. The advantage of the APW+lo method is that it has the same small basis set size as the APW method, and has the same accuracy compared to the LAPW method.

As mentioned by Madsen et al, it is also possible to use a hybrid basis set. LAPW in combination with APW [(L)APW+lo], and treat the physically important orbitals by the APW+lo method, but the polarization l-quantum numbers with LAPW.

1.13.5. Full Potential (L)APW+lo Method

By supposing the potential is constant in the interstitial region and spherical in the MT region. The accuracy of (L)APW+lo method can be further improved by considering the full potential (FP), and expand it similar to the wave functions,

$$V(r) = \begin{cases} \sum_{l,m} V_{l,m}(r) Y_{l,m}(r) & r \in MT \\ \sum_{k} V_k e^{ikr} & r \in I \end{cases} \qquad 1.77$$

This is also called non-muffin-tin correction. In this case, the radial function u_l is not the exact solution inside the MT sphere. It should be evaluated for the true MT potential.

1.14. Two important basis set parameters: Energy Cutoff and K-mesh:

In all DFT codes for solid state calculations the energy cutoff (Ecut) and k-mesh (or k-points) are important basis set parameters to determine the accuracy of the computational results. Both parameters must be tested in DFT calculations in order to find the optimum compromise between accuracy and implied computational burden.

When we use plane waves to construct wave functions, in principle the more plane waves, the better the results are. However, it is not necessary to use infinitely many plane waves to construct the wave function. We can limit the energy cutoff, which describes the number of plane waves used, to an optimum value. The relationship between energy cutoff and plane wave coefficient is:

$$E_{cut} = \frac{\hbar^2}{2m_e} K_{max}^2 \qquad 1.78$$

In the FP-(L)APW+lo method this energy cutoff is employed in the interstitial region. Turning to the MT sphere, the spherical harmonics should also be terminated at a maximum *l m* for the same reason.

The evaluation of the Kohn-Sham equations in a periodic boundary calculation requires many system quantities like the charge density to be integrated over the Brillouin Zone (BZ). Exploring the symmetry of the system, it is more specifically only necessary to integrate over the irreducible part of the Brillouin Zone (IBZ). The integrals are dealt with numerically by summing over a finite number of k-points in the IBZ.

$$\int \frac{1}{\Omega_{IBZ}} dk \rightarrow \sum_k \omega_k \qquad 1.79$$

Therefore, the denser the k-mesh, the more accurate the integrand is. Similar to Ecut, we should also find an optimum k-mesh at which the quantities of interest are converged.

There are two common methods to get k-points: The tetrahedron method [46] and the special k-points method [47] (Monkhorst and Pack), which generates a uniform k-point grid in the full BZ, then uses the space group of the system to rotate the k-points into the IBZ, and determine the proper weights, ω_k, of each special k-point by dividing the number of equilibrium k-points of a special k-point in the BZ by the total number of points in the grid.

1.15. WIEN2k code:

The DFT calculations in this work were performed using the WIEN2k software package, which is based on the all-electron (L)APW+lo(+LO) method and includes relativistic effects and has many features. WIEN2k has been in the continuous process of development in the group of Prof. Peter Blaha and Prof. Schwarz for more than 35 years at the TU Wien[48]. More than 3200 groups have acquired the license, both in the field of academic and industrial research, and all over the world. This package allows to study many properties related to the electronic structure of a crystalline solid: optimized atomic structure, cohesive energy, electronic band structure, electron density, density of states (DOS), various types of spectra, magnetism (ferromagnetic, antiferromagnetic and non-magnetic configurations), Fermi surface, optical properties, electronic polarization, electric field gradients, NMR chemical, and other properties. Many different exchange-correlation potentials including the LDA, various GGAs (Perdew-Wang or PBE, Wu-Cohen), MGGA, the DFT+U method in various flavors for the double counting terms, as well as the so-called local modified Becke-Johnson potential, and hybrid functionals are implemented in this code.

WIEN2k is a collection of several Fortran90 programs that are linked together via C shell scripts. We can divide the whole process of calculation into two parts:

1. Initialization (preparation of the input files)
2. Self-consistent cycle (SCF)

The program flow of the WIEN2k code is shown in Fig 1.8

1.15.1. Initialization process:

To start a calculation using WIEN2k[48] a case.struct–file has to be created. In this file the crystal properties, like structure type, lattice constants, atomic positions and the radii of the muffin-tin spheres R_{MT} are given.

The program nn calculates distances to neighbouring atoms and checks for overlapping atomic spheres. It also verifies that equivalent atom positions are entered correctly in the case.struct–file.

The space group of the structure and the point group of the non-equivalent sites are calculated by sgroup.

symmetry generates all symmetry operations for the given structure. It also determines the point group of each atomic site and generates the respective symmetry operations. Furthermore, the expansion for the lattice harmonics is calculated.

The program lstart generates free atomic densities and potentials. It prints out a warning if density of the core states leaks out of the muffin-tin spheres. Also, whether different orbitals are treated as core-, semi-core-, or valence-states is determined. The program asks which method should be used for calculation of the exchange-correlation potential and at which energy core-states are separated from valence-states. In the input file case.inst the electron configuration of each atom, as well as the information which electrons should be treated as spin-up or spin-down electrons, is given.

kgen generates a k-mesh in the irreducible wedge of the Brillouin zone, which is used in a modified tetrahedron scheme for further calculations t takes the number of k-points as input parameter.

dstart generates the crystalline starting density for the SCF cycle by superposition of the atomic densities calculated in lstart.

1.15.2. Self-consistent cycle:

Each SCF iteration is started with lapw0 which uses an input density ρ (either from dstart or from the output of a previous iteration) to create the total potential as a sum of the Coulomb potential V_c and the exchange-correlation potential V_{xc} .The program also calculates the expansion of the Coulomb potential into multipole moments, while the exchange-correlation potential is calculated numerically using lattice harmonics inside the muffin-tin spheres and using a fast Fourier transformation outside.

The eigenvectors and eigenvalues of the valence bands are calculated by lapw1 by means of diagonalisation. Different calculation schemes are implemented. In this program the LAPW or APW+lo expansion is performed.

The program lapw2 calculates the Fermi energy and generates the expansion of the valence densities with respect to the crystal symmetry. The charges or partial charges (decomposed with respect to quantum number `) inside the muffin-tin spheres are calculated by integration over the Brillouin zone.

lcore computes the eigenvalues for core states and the corresponding densities. The program mixer calculates the overall density by summing up the core-, semi core- and valence densities. It then mixes this total density with the input density to generate a new output density. This is done in order to stabilize the SCF cycle. Several mixing schemes are implemented. The simplest one is $\rho_{i+1}^{in} = (1-\alpha)\rho_i^{in} + \alpha\rho_i^{out}$. Also, several multi-secant mixing schemes are implemented.

All the calculations of the SCF iteration are repeated until chosen convergence criteria, like convergence of the total energy or charge convergence, are met. When performing spin-polarized calculations dstart, lapw1, lapw2 and lcore are called separately for each spin direction.

For calculations using orbital potentials like LDA+U or when hybrid functionals are used, two other programs are invoked during each SCF iteration. The program orb calculates the orbital potential, which is non-zero inside the muffin-tin spheres only and depends on the quantum numbers l and m. lapwdm computes the density matrices, which are needed for this type of calculations.

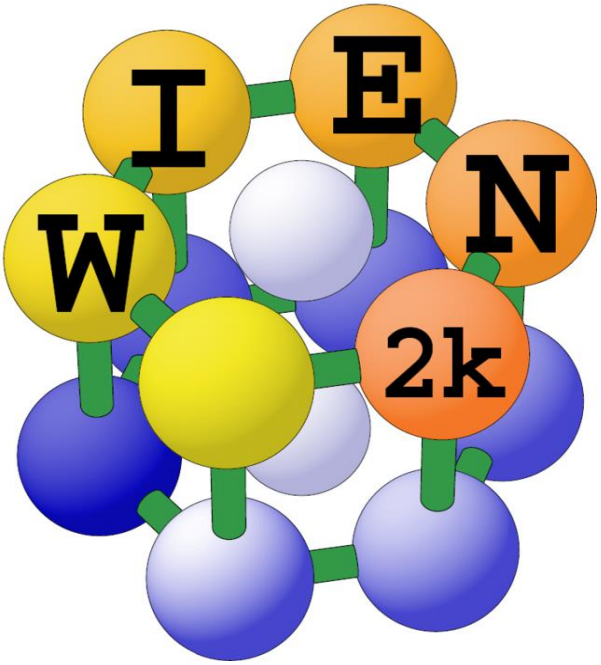

Fig. 1. 7 Wien2k logo [48]

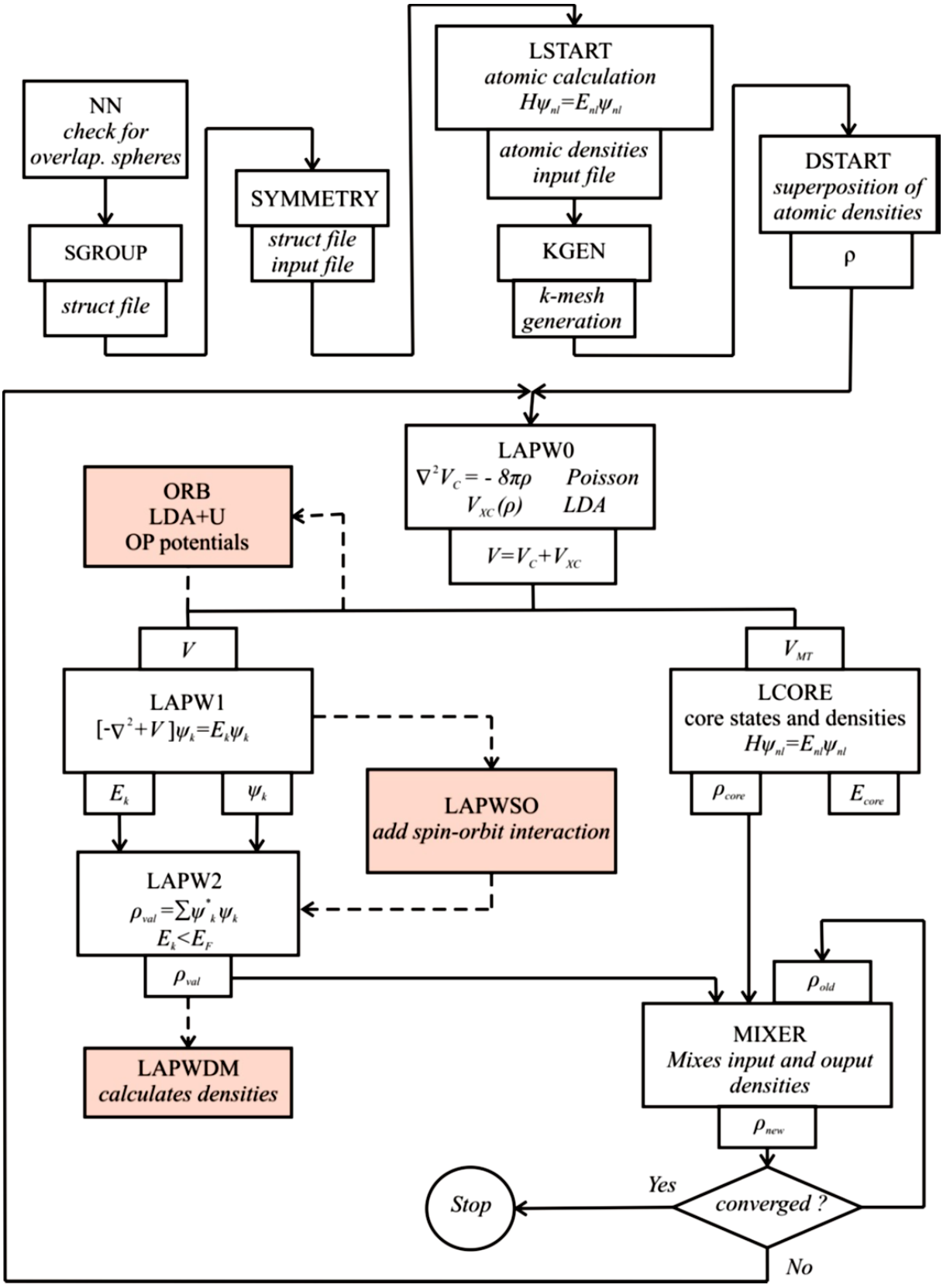

Fig. 1. 8 Step by step program flow in WIEN2k. In first part input files are processed and a self-consistent calculation is performed in second part [48].

1.16. References:

[1] R. O. Jones, "Density functional theory: Its origins, rise to prominence, and future," *Rev Mod Phys*, vol. 87, no. 3, p. 897, 2015.

[2] E. Schrödinger, "An undulatory theory of the mechanics of atoms and molecules," *Physical review*, vol. 28, no. 6, p. 1049, 1926.

[3] M. Born and W. Heisenberg, "Zur quantentheorie der molekeln," in *Original Scientific Papers Wissenschaftliche Originalarbeiten*, Springer, 1985, pp. 216–246.

[4] D. R. Hartree, "The wave mechanics of an atom with a non-Coulomb central field. Part I. Theory and methods," in *Mathematical Proceedings of the Cambridge Philosophical Society*, 1928, vol. 24, no. 1, pp. 89–110.

[5] D. R. Hartree, "The wave mechanics of an atom with a non-coulomb central field. Part II. Some results and discussion," in *Mathematical Proceedings of the Cambridge Philosophical Society*, 1928, vol. 24, no. 1, pp. 111–132.

[6] D. R. Hartree, "The wave mechanics of an atom with a non-coulomb central field. part iii. term values and intensities in series in optical spectra," in *Mathematical Proceedings of the Cambridge Philosophical Society*, 1928, vol. 24, no. 3, pp. 426–437.

[7] V. Fock, "„Selfconsistent field "mit Austausch für Natrium," *Zeitschrift für Physik*, vol. 62, no. 11, pp. 795–805, 1930.

[8] V. Fock, "Näherungsmethode zur Lösung des quantenmechanischen Mehrkörperproblems," *Zeitschrift für Physik*, vol. 61, no. 1, pp. 126–148, 1930.

[9] J. C. Slater, "Note on Hartree's method," *Physical Review*, vol. 35, no. 2, p. 210, 1930.

[10] J. C. Slater, "A simplification of the Hartree-Fock method," *Physical review*, vol. 81, no. 3, p. 385, 1951.

[11] P. Hohenberg and W. Kohn, "Inhomogeneous electron gas," *Physical review*, vol. 136, no. 3B, p. B864, 1964.

[12] R. O. Jones and O. Gunnarsson, "The density functional formalism, its applications and prospects," *Reviews of Modern Physics*, vol. 61, no. 3, p. 689, 1989.

[13] E. Fermi, "Eine statistische Methode zur Bestimmung einiger Eigenschaften des Atoms und ihre Anwendung auf die Theorie des periodischen Systems der Elemente," *Zeitschrift für Physik*, vol. 48, no. 1, pp. 73–79, 1928.

[14] L. H. Thomas, "The calculation of atomic fields," in *Mathematical proceedings of the Cambridge philosophical society*, 1927, vol. 23, no. 5, pp. 542–548.

[15] P. A. M. Dirac, "Note on exchange phenomena in the Thomas atom," in *Mathematical proceedings of the Cambridge philosophical society*, 1930, vol. 26, no. 3, pp. 376–385.

[16] W. Kohn and L. J. Sham, "Self-consistent equations including exchange and correlation effects," *Physical review*, vol. 140, no. 4A, p. A1133, 1965.
[17] W. Kohn, "Nobel Lecture: Electronic structure of matter—wave functions and density functionals," *Reviews of Modern Physics*, vol. 71, no. 5, p. 1253, 1999.
[18] P. A. M. Dirac, "Note on exchange phenomena in the Thomas atom," in *Mathematical proceedings of the Cambridge philosophical society*, 1930, vol. 26, no. 3, pp. 376–385.
[19] E. Wigner, "On the interaction of electrons in metals," *Physical Review*, vol. 46, no. 11, p. 1002, 1934.
[20] D. M. Ceperley and B. J. Alder, "Ground state of the electron gas by a stochastic method," *Phys Rev Lett*, vol. 45, no. 7, p. 566, 1980.
[21] J. P. Perdew and A. Zunger, "Self-interaction correction to density-functional approximations for many-electron systems," *Physical Review B*, vol. 23, no. 10, p. 5048, 1981.
[22] J. P. Perdew and Y. Wang, "Accurate and simple analytic representation of the electron-gas correlation energy," *Physical review B*, vol. 45, no. 23, p. 13244, 1992.
[23] S. H. Vosko, L. Wilk, and M. Nusair, "Accurate spin-dependent electron liquid correlation energies for local spin density calculations: a critical analysis," *Canadian Journal of physics*, vol. 58, no. 8, pp. 1200–1211, 1980.
[24] U. von Barth and L. Hedin, "A local exchange-correlation potential for the spin polarized case. i," *Journal of Physics C: Solid State Physics*, vol. 5, no. 13, p. 1629, 1972.
[25] O. Gunnarsson, B. I. Lundqvist, and J. W. Wilkins, "Contribution to the cohesive energy of simple metals: Spin-dependent effect," *Physical Review B*, vol. 10, no. 4, p. 1319, 1974.
[26] O. Gunnarsson and B. I. Lundqvist, "Exchange and correlation in atoms, molecules, and solids by the spin-density-functional formalism," *Physical Review B*, vol. 13, no. 10, p. 4274, 1976.
[27] J. P. Perdew *et al.*, "Atoms, molecules, solids, and surfaces: Applications of the generalized gradient approximation for exchange and correlation," *Physical review B*, vol. 46, no. 11, p. 6671, 1992.
[28] J. P. Perdew, K. Burke, and M. Ernzerhof, "Generalized gradient approximation made simple," *Phys Rev Lett*, vol. 77, no. 18, p. 3865, 1996.
[29] J. P. Perdew, K. Burke, and M. Ernzerhof, "Perdew, burke, and ernzerhof reply," *Physical Review Letters*, vol. 80, no. 4, p. 891, 1998.
[30] B. Hammer, L. B. Hansen, and J. K. Nørskov, "Improved adsorption energetics within density-functional theory using revised Perdew-Burke-Ernzerhof functionals," *Physical review B*, vol. 59, no. 11, p. 7413, 1999.

[31] J. P. Perdew *et al.*, "Restoring the density-gradient expansion for exchange in solids and surfaces," *Phys Rev Lett*, vol. 100, no. 13, p. 136406, 2008.
[32] J. Tao, J. P. Perdew, V. N. Staroverov, and G. E. Scuseria, "Climbing the density functional ladder: Nonempirical meta–generalized gradient approximation designed for molecules and solids," *Physical Review Letters*, vol. 91, no. 14, p. 146401, 2003.
[33] J. Heyd, G. E. Scuseria, and M. Ernzerhof, "Hybrid functionals based on a screened Coulomb potential," *J Chem Phys*, vol. 118, no. 18, pp. 8207–8215, 2003.
[34] J. Heyd, G. E. Scuseria, and M. Ernzerhof, "Hybrid functionals based on a screened Coulomb potential," *J Chem Phys*, vol. 118, no. 18, pp. 8207–8215, 2003.
[35] M. Ernzerhof and G. E. Scuseria, "Assessment of the Perdew–Burke–Ernzerhof exchange-correlation functional," *J Chem Phys*, vol. 110, no. 11, pp. 5029–5036, 1999.
[36] C. Adamo and V. Barone, "Toward reliable density functional methods without adjustable parameters: The PBE0 model," *J Chem Phys*, vol. 110, no. 13, pp. 6158–6170, 1999.
[37] D. G. Anderson, "Iterative procedures for nonlinear integral equations," *Journal of the ACM (JACM)*, vol. 12, no. 4, pp. 547–560, 1965.
[38] P. H. Dederichs and R. Zeller, "Self-consistency iterations in electronic-structure calculations," *Physical Review B*, vol. 28, no. 10, p. 5462, 1983.
[39] M. Roknuzzaman and A. Islam, "Ab Initio Investigation of Nitride in Comparison with Carbide Phase of Superconducting InX (X= C, N)," *Int Sch Res Notices*, vol. 2013, 2013.

[40] G. Kresse and D. Joubert, "From ultrasoft pseudopotentials to the projector augmented-wave method," *Phys Rev B*, vol. 59, no. 3, p. 1758, 1999.
[41] P. Giannozzi *et al.*, "Advanced capabilities for materials modelling with Quantum ESPRESSO," *Journal of physics: Condensed matter*, vol. 29, no. 46, p. 465901, 2017.

[42] J. C. Slater, "Wave functions in a periodic potential," *Physical Review*, vol. 51, no. 10, p. 846, 1937.
[43] D. J. Singh and L. Nordstrom, *Planewaves, Pseudopotentials, and the LAPW method*. Springer Science & Business Media, 2006.
[44] X.-Z. Li and E.-G. Wang, *Computer Simulations of Molecules and Condensed Matter: From Electronic Structures to Molecular Dynamics*. World Scientific, 2018.

[45] G. K. H. Madsen, P. Blaha, K. Schwarz, E. Sjöstedt, and L. Nordström, "Efficient linearization of the augmented plane-wave method," *Phys Rev B*, vol. 64, no. 19, p. 195134, 2001.

[46] D. J. Chadi and M. L. Cohen, "Special points in the Brillouin zone," *Phys Rev B*, vol. 8, no. 12, p. 5747, 1973.

[47] J. Rath and A. J. Freeman, "Generalized magnetic susceptibilities in metals: Application of the analytic tetrahedron linear energy method to Sc," *Phys Rev B*, vol. 11, no. 6, p. 2109, 1975.

[48] P. Blaha, K. Schwarz, G. K. H. Madsen, D. Kvasnicka, and J. Luitz, "wien2k," *An augmented plane wave+ local orbitals program for calculating crystal properties*, vol. 60, 2001.

Chapter 2

Overview of magnetic materials and problematic

2.1. Introduction:

Today, the challenge in conventional electronic devices (traditional devices). is to solve many problems such as power consumption, storage and loss of data. Those traditional devices use the charge of electrons and the spin is ignored.

Recently, there is a new technology appeared named spintronics or spin-electronics [1] .The basic concept of spintronics is the manipulation of the electron spin in addition to the charge in contrast to traditional electronics in which the spin of the electron is ignored. Adding the spin degree of freedom provides new, capabilities, and new functionalities. The first widely studied spintronics effect was giant magnetoresistance (GMR), discovered in in the 1980's., This spin-based approach offers a number of advantages over traditional electronics, including higher data storage and lower power consumption. The key success of spintronics is to find materials with strong spin polarization.

Half-metallic ferromagnets[2] (HMF's) are defined as magnetic materials with one spin channel possesses metallic conduction while the other spin channel is insulating or semiconducting. The concept of HM was first established from electronic structure calculations of half-Heusler NiMnSb alloy by De Groot et al (1983). These materials with strong spin polarization that can reach 100% are good candidates for spintronics.

In this chapter, we give an overview of magnetic materials and their classification, then we introduce the concept of half metallic ferromagnets (HMFs) and their characteristics , next we talk about spintronics and its basics GMR (Giant magnetoresistance) and TMR (Tunnelling magnetoresistance), furthermore, we present some important HMFs predicted in the last decade to be HMFs and we end up by introducing new types of materials that without having transitions metals elements were recently proved to be good HMFs and ,we present our compounds the ternary oxides XMg_3O_4(X=Li, Na, K, Rb) and their crystallographic structure that are predicted to half metallic ferromagnets.

2.2. Overview of magnetic materials:

2.2.1. Origin of Magnetism

The origin of magnetism lies in the orbital and spin motion of electrons and how the electrons interact with each other., the most important sources of magnetization are, specifically, the orbital motion of electrons caused by the electron's movement about the nucleus, it has an associated magnetic moment $\vec{\mu}_l = -g_l\mu_B\vec{l}$, and the intrinsic magnetic moment of electrons called spin that can be up or down, with its associated magmatic moment which is given by $\vec{\mu}_s = -g_s\mu_B\vec{S}$. Here $\mu_B = e\hbar/2m_e = 9.27 \times 10^{-24}$ JT^{-1} [3]is the Bohr magneton, m_e is the electron mass and charge respectively, $\hbar$ is the reduced Max-Planck constant, l is the orbital angular momentum and S is the spin angular momentum, the spin g-factor g_s ≈2 is a good approximation, and the orbital g-factor has the value g_l=1 for free electrons but this value changes with the electron effective mass in solids. The corresponding total magnetic moment is then given by:

$$\vec{\mu} = \vec{\mu}_l + \vec{\mu}_s \qquad 1.62$$

Sometimes, the orbital moment is said to be quenched $\vec{\mu}_l \approx 0$ by the crystal field. In fact, about 95% of the magnetization of iron originates from the spin of the electrons [4].It is instructive also to describe the nuclear magnetic moment which originates from the nuclear spin quantum number I, it can be written as $\mu_n = -g_n\mu_n I$, Here, I is a nuclear spin operator and g_n is a proportionality constant called the 'nuclear g value', analogous to Bohr magneton $\mu_n = e\hbar/2m_n = 5.05824 \times 10^{-27}$ JT^{-1}. The ratio of $|\mu_B/\mu_n|$ is in the order of 10^3[5], indicating the dominant contribution of the electron to the magnetic moments of materials, therefore the magnetism originating from the nuclei is usually neglected.

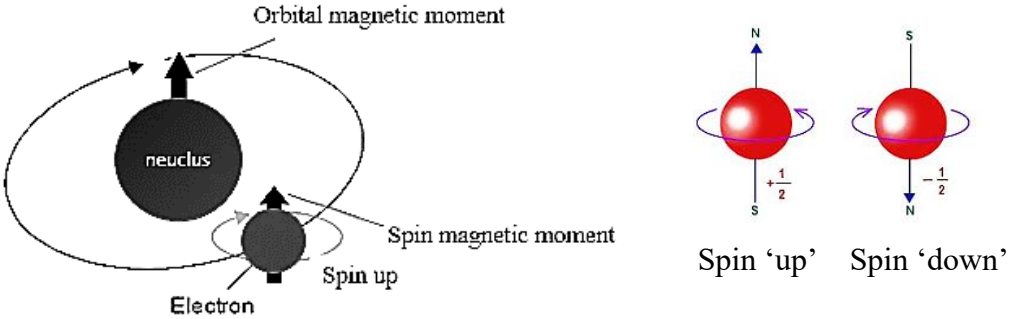

Fig. 2. 1 Representation of the spin magnetic moment and the orbital magnetic moment of the electron

2.3. Classification of Magnetic Materials

All materials can be classified in terms of their magnetic behaviour falling into one of five categories depending on their bulk magnetic susceptibility and magnetic moments orientations. The two most common types of magnetism are diamagnetism and paramagnetism, which account for most of the periodic table of elements at room temperature. These elements are usually referred to as non-magnetic, whereas those which are referred to as magnetic are actually classified as ferromagnetic. The only other type of magnetism observed in pure elements at room temperature is antiferromagnetism. Finally, magnetic materials can also be classified as ferrimagnetic although this is not observed in any pure element but can only be found in compounds, such as the mixed oxides, known as ferrites, from which ferrimagnetism derives its name.

The magnetic susceptibility indicates how responsive a material is to an external magnetic field. If H is the applied field and M is the material's magnetization in that field, they are related by:

$$\chi = \frac{M}{H} \qquad 2.01$$

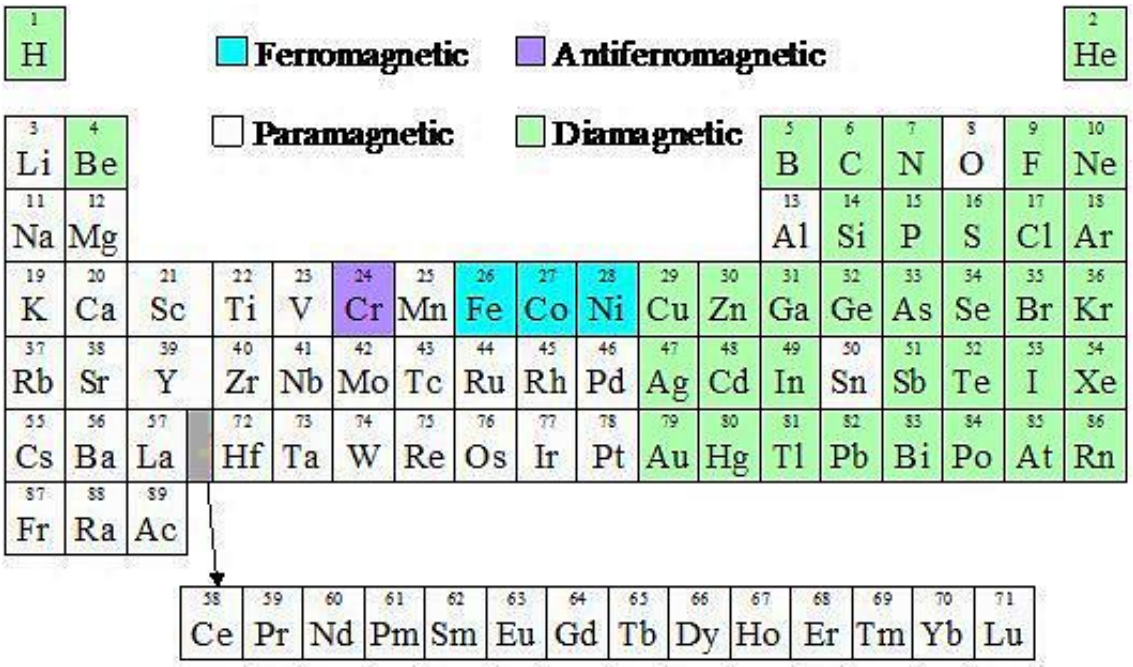

Fig. 2. 2 Diagram of a periodic table showing elements coloured according to the type of magnetism they show at room temperature (Magnetic Materials Group, University of Birmingham).

2.3.1. Diamagnetism:

Diamagnetic materials have no unpaired electrons, which means that all orbitals are filled with electrons. These materials have no magnetic moment Fig. 2.3., However, when exposed to a magnetic field, the alignment of the magnetic moments is in the opposite direction to the applied field (negative magnetization is produced Fig. 2.7). All materials have a diamagnetic effect; however, it is often masked by the larger paramagnetic or ferromagnetic effect. The other characteristic feature of diamagnetic materials is that the susceptibility is negative, small and independent of temperature.

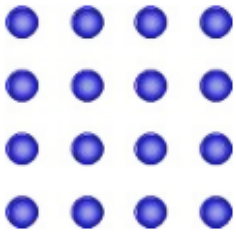

Fig. 2. 3 Schematic diagram of the no net magnetic moments in diamagnetic materials. Absence of external magnetic field H=0. (Magnetic Materials Group, University of Birmingham).

2.3.2. Paramagnetism:

Paramagnetic materials have partially filled orbital with electrons, which is why these materials have a net magnetic moment. each atom has a magnetic moment which is randomly oriented Fig 2.4 In the presence of an external magnetic field, the magnetic moments align up, a net positive magnetization is resulting as shown in. Fig. 2.7. As the temperature increases, the thermal agitation increases and it is become harder to align the atomic magnetic moments and hence the susceptibility decreases Fig.2.6, according to the Curie law $\chi = C/T$ (special case of the more general Curie-Weiss law $\theta = 0$ in Eq 2.02) where C is a material constant called the Curie constant

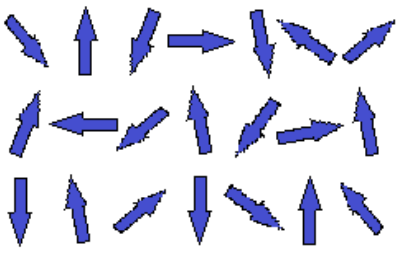

Fig. 2. 4 Schematic diagram of randomly oriented magnetic moments in diamagnetic materials H=0. (Magnetic Materials Group, University of Birmingham).

2.3.3. Ferromagnetism:

Ferromagnetic materials have unpaired electrons in their atoms, so each atom has a net magnetic moment. The atomic magnetic moments tend to align parallel with each other in a region called a domain Fig 2.5. Within the domain, the magnetization is intense, but in a bulk sample the material is usually demagnetized because the many domains are randomly oriented with respect to one another. An externally imposed magnetic field can cause the magnetic domains to line up with each other to get saturation magnetisation Ms (magnetisation when all domains are aligned) Fig 2.7. This effect is first explained by Weiss in 1907. In quantum mechanics, the Heisenberg model of ferromagnetism describes the parallel alignment of magnetic moments in terms of an exchange interaction between neighbouring moments.

One important property of ferromagnets is that at high temperature their magnetism is lost. In fact, when ferromagnetic materials are heated then the thermal agitation of the atoms means that the degree of alignment of the atomic magnetic moments decreases and hence the saturation magnetisation also decrease and for high temperature becomes paramagnetic and the transition temperature is called Curie temperature T_C. For the following systems (Fe: T_C=770°C, Co: T_C=1131°C and Ni: T_C=358°C). the susceptibility is time dependent, and given by Curie Weiss law Eq 2.02, if θ is positive then the material is ferromagnetic θ=Tc.

$$\chi = \frac{C}{T - \theta} \qquad 2.02$$

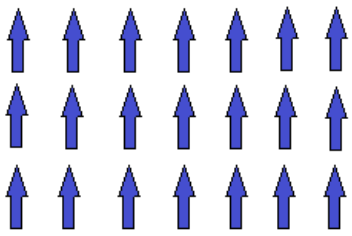

Fig. 2. 5 Schematic diagram of magnetic parallel aligned moments in ferromagnetic materials in one domain H=0. (Magnetic Materials Group, University of Birmingham).

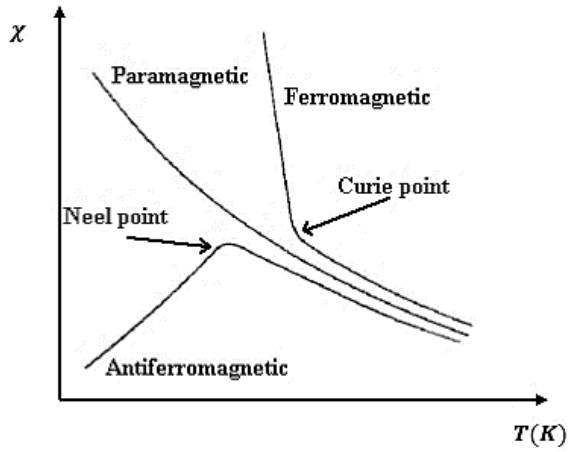

Fig. 2. 6 Schematic diagram of the magnetic susceptibility as a function of temperature [29]

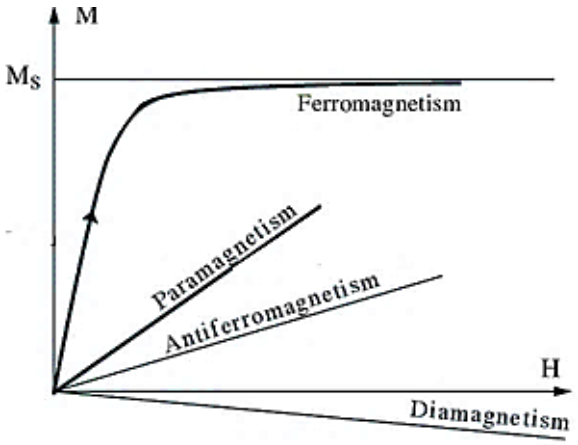

Fig. 2. 7 Schematic diagram of the Magnetization M with respect to the applied magnetic field H [30]

When a ferromagnetic material is magnetized in one direction, it is not relaxed back to zero magnetization when the imposed magnetizing field is removed. It must be driven back to zero by a field in the opposite direction, if an alternating magnetic field is applied to the material, its magnetization traces out a loop called a hysteresis loop (see Fig 2.8). The width of this hysteresis loop determines several applications of magnetic materials. For example, magnetic alloys with narrow hysteresis width, informally called soft magnets, are used in transformer cores and induction motors while magnetic alloys with wide hysteresis width, called hard magnets, are used in permanent magnets and some computer memories

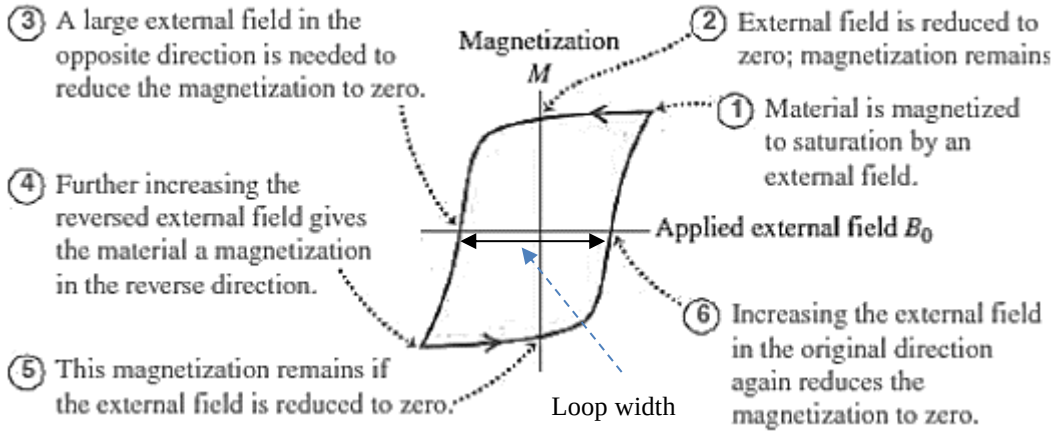

Fig. 2. 8 Hysteresis loop [31]

2.3.4. Antiferromagnetism:

In the periodic table the only element exhibiting antiferromagnetism at room temperature is chromium. Antiferromagnetic materials are very similar to ferromagnetic materials but the exchange interaction between neighbouring atoms leads to the anti-parallel alignment of the atomic magnetic moments Fig. 2.9, they are of the same magnitude and thus cancel each other out entirely and the sum of a material's parallel and anti-parallel magnetic moments is zero. Like ferromagnetic materials these materials become paramagnetic above a transition temperature, known as the Néel temperature T_N Fig. 2.6 (Cr: T_N=37ºC). Their response to an external magnetic field is similar to that of paramagnetic materials, with a small positive susceptibility Fig. 2.7.

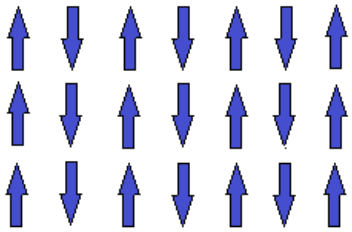

Fig. 2. 9 Schematic diagram of antiparallel aligned magnetic moments in antiferromagnetic material. (Magnetic Materials Group, University of Birmingham).

2.3.5. Ferrimagnetism:

The magnetic moments arrangement in Ferrimagnetic materials is somewhat similar to antiferromagnetic materials. However, unlike antiferromagnetic materials, the antiparallel moments in ferrimagnetic compounds do not cancel each other Fig 2.10, and there is a net magnetization The net magnetization occurs because the magnetic moment associated with one

direction is greater than that of the opposite magnetic moment. Ferrimagnetism also shows similar behavior like ferromagnetism, in that they exhibit a large susceptibility

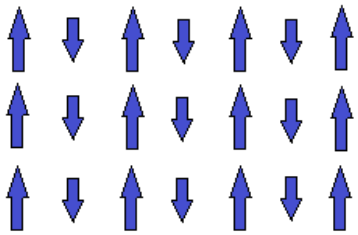

Fig. 2. 10 Schematic diagram of mixed parallel and antiparallel magnetic moments in ferrimagnetic materials. (Magnetic Materials Group, University of Birmingham).

2.4. Half-metals (new class of magnetic materials):

In 1983, de Groot et al.[6] discovered by using first principles calculations a new class of magnetic materials called half-metallic (HM) ferromagnets, they have the potential to play a key role in improving the performance of spintronic devices. Half metals are a class of ferromagnets that have a metallic density of states at the Fermi level in one spin channel and simultaneous semiconducting or insulating properties in the opposite one. they are predicted to be very good for spintronics applications.

Density of states (DOS) N(E) is a useful concept in solid state physics, it represents the number of electrons in the system having energy within the interval (E, E+dE). The Pauli exclusion principle requires that up and down spin electrons be counted separately. So, spin up bands and spin down bands can be formed and all the lowest energy levels are filled by electrons and the highest occupied energy level is called the Fermi energy E_F.

Fig. 2.11 shows density of states N(E) diagram for (a) nonmagnet (b) ferromagnet and (c) half-metal. $N_\uparrow$ and $N_\downarrow$ represent the spin-up and spin-down densities respectively. For a nonmagnetic compound like copper, silver and gold, Fig. 2.11. (a) shows equal occupancy of spin-up $N_\uparrow$ and spin-down $N_\downarrow$ (spin-up and spin-down electrons at the Fermi level are equal in number, and mobility), But for a ferromagnetic material like Fe, Co, and Ni, spin down density is shifted and $N_\uparrow(E_F) \neq N_\downarrow(E_F)$, From Fig 2.11 (b), (spin up electron density $N_\uparrow$ is larger than the spin down electron density $N_\downarrow$, at the Fermi level E_F), this shift results in an unequal filling of the bands which is the source of magnetic moment for the ferromagnetic materials and it also causes the spin-up and spin-down electrons at the Fermi level to be unequal in number, and

mobility. The so-called spin polarization can be defined in terms of electron densities at Fermi level as:

$$P = \frac{N_{\uparrow}(E_F) - N_{\downarrow}(E_F)}{N_{\uparrow}(E_F) + N_{\downarrow}(E_F)} \qquad 2.03$$

From the definition of spin polarization, it is clear that the non-magnetic material have zero spin polarization P=0% whereas ferromagnetic materials (such as Fe, Co, and Ni and their alloys) have polarization of 0% < P < 100%. These materials are known to be partially spin polarized. There exists a special class of materials which show 100% spin polarization and are known to be half metallic. In this case, one spin electron density is metallic and the other is insulating or semiconducting (Only one electron density exists at the Fermi level).as shown by Fig 2. 11 (c).

To obtain half metals, it is necessary to pass from a pure element to an alloy or compound; all half metals contain more than one element. Most known examples are oxides, or Heusler alloys. Even strong ferromagnets, are not half metals. Cobalt and nickel Fig. 2.12 have fully spin-polarized d-bands with a filled 3d↑ band and only 3d↓ electrons with empty states at the Fermi level E_F. However, the Fermi level crosses the unpolarized 4s band (both 4s↓ and 4s↑ are crossing the Fermi level).

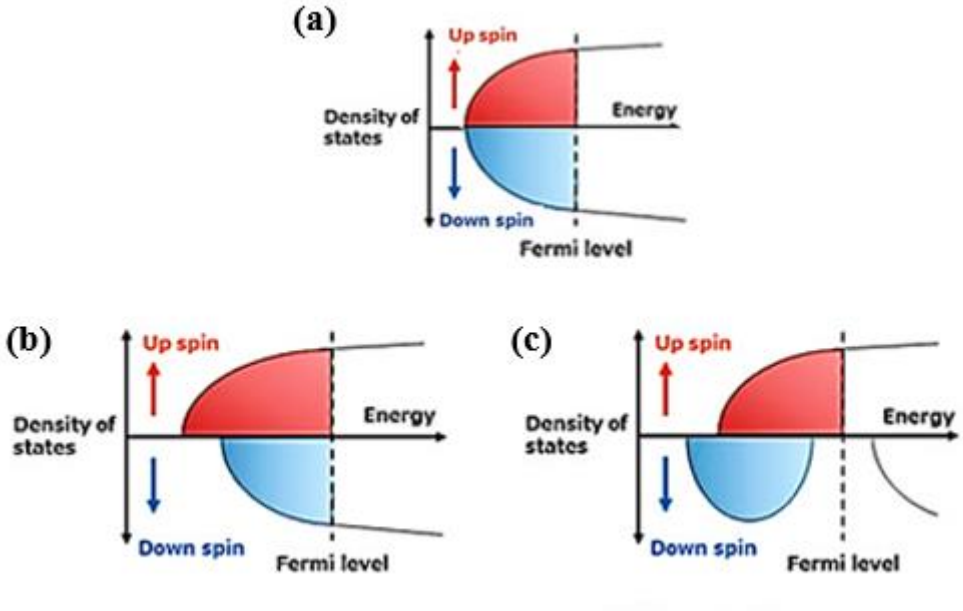

Fig. 2. 11 Schematic diagram of density of states N(E) as a function of energy. (a) Non-magnetic metals (zero spin polarization). (b) Ferromagnetic metals (partial spin polarization). (c) Half metals (full spin polarization)[32]

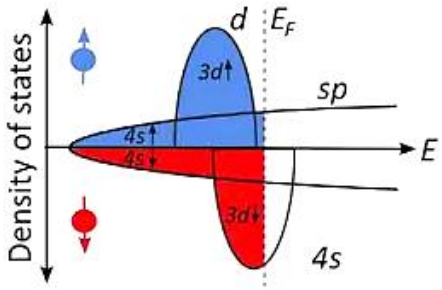

Fig. 2. 12 Schematic diagram of density of states N(E) as a function of energy for strong pure ferromagnet[33]

2.5. Spintronics:

Spin-based electronics (spintronics) is a new type of electronics that utilizes both the spin and the electric charge of electrons to create new devices. Spintronics technology began with the discovery of giant magnetoresistance (GMR) in 1988 independently by Peter Grunberg in Fe/Cr/Fe trilayer[7] and Albert Fert's team in multilayers (*e.g.*, Fe/Cr or Co/Cu)[8], large resistance in multilayers (up to 50% change in resistance) that led to its naming, Albert Fert and Peter Grünberg were awarded the Nobel Prize in 2007 for their discovery of GMR[9]. This discovery of GMR is considered as the birth of Spintronics. In 1991, such GMR effects were also highlighted in more sophisticated multilayers such as spin valves., and in 1995 tunneling magnetoresistance (TMR) effects were observed in another device, called a magnetic tunnel junction (MTJ). This device is made up of two ferromagnetic metal layers separated by a non-magnetic tunnel barrier. These discoveries, led to the research and growth of materials for spintronics devices.

One present challenge is to find materials with a stronger spin polarization than that of common ferromagnetic metals (iron, nickel, etc.). with high curie temperature Tc

2.6. Origin of GMR:

The origin of GMR lies in the band structure of ferromagnets. In 1936, Nevill Mott[10] remarked that transition metals such as nickel, palladium, and platinum are worse electrical conductors than their neighbors in the periodic table copper, silver, and gold. He suggested that the conductivity was mainly determined by the 4s electrons, 3d electrons are more tightly bound and contribute far less to conduction.

For Copper (Cu), all the 3d states are situated below the Fermi level and therefore not available for scattering processes. (3d orbitals are completely full) Fig. 2.12**.** However, for Nickel 3d band has empty states. Those empty states, Mott realized that they serve as traps: If a conduction electron scatters off an impurity, defect, or phonon, or drop into the 3d band resistance is increased. Mott also realized that spin would influence conduction. As figure 2.12 shows, spin down end up with fewer unoccupied states in the 3d↓ sub-band. However, spin up 3d↑ sub-bands are not available at E_F (completely filled 3d↑ orbital). There are two currents flow through the ferromagnet: a larger one of spin up and a smaller one of spin down.

GMR effect in magnetic multilayer can also be understood from the band structure and Mott explanation. Fig. 2.13 (c) shows a band structure of each layer in trilayer FM/NM/FM. In case of parallel configuration (presence of an external magnetic field H), spin down are strongly scattered by 3d↓ empty states available in FM layers when they are transported from one layer to the other, but 3d↑ don't exist at Fermi level for all layers the spin-up. Thus, up electrons are weakly scattered when they are transported from one layer to the other leading to low resistance R_P of the multilayer. For the antiparallel case (absence of external magnetic field H=0), both spin up and spin down electrons will alternately experience high and low resistance when they are transported from one layer to the other (scattered alternately to 3d↑ and 3d↓ empty states available at Fermi level in FM layers), and the resultant global resistance R_{AP} is high compared to R_P [11].

Let us note *r* the resistance of low resistance and R when electrons strongly scattered in FM layers. Here the resistance of the NM separating layer is neglected. As illustrated in Fig.2,13 (b) and (a), in the (AP) configuration and (P) configuration the multilayer resistances have the following expressions respectively[11]

$$R_{AP} = \frac{R + r}{2}, \quad R_P = \frac{2Rr}{R + r} \qquad 2.04$$

Following this model, the amplitude of the GMR ratio can be simply deduced:

$$\frac{\Delta R}{R} = \frac{R_{AP} - R_P}{R_P} = \frac{(R - r)^2}{4Rr} \qquad 2.05$$

Thus, the larger the difference between R and r , the larger magnetoresistance is reached. This expression clearly shows that the magnetoresistance effect arises from the difference between the resistance behaviour of the spin up and down electrons.

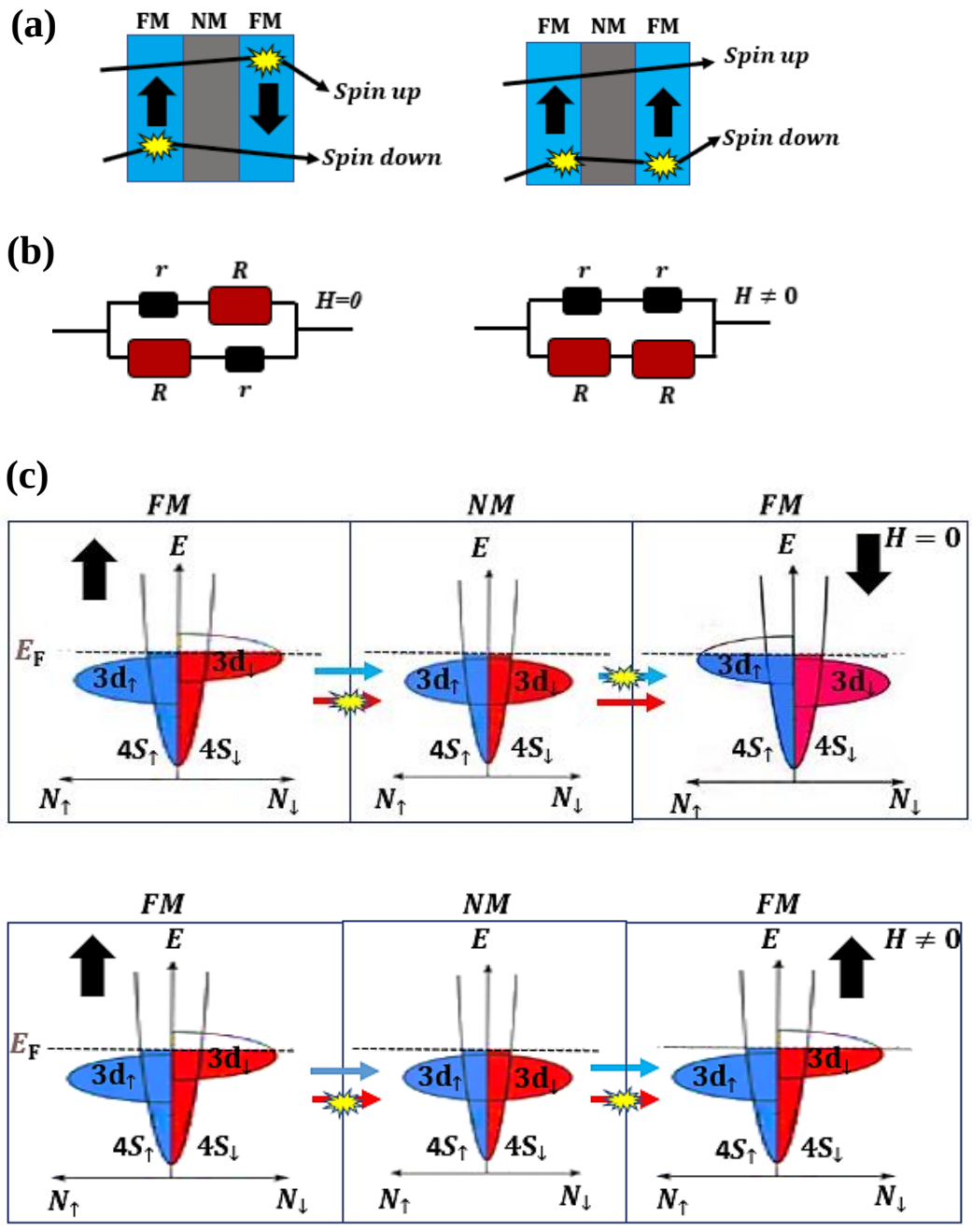

Fig. 2. 13 GMR (a) parallel and anti-parallel trilayer (b) resistance interpretation in trilayer (c) band structure of each layer for parallel layers (existence of magnetic field) and anti-parallel (absence of magnetic field)

2.6.1. GMR effect for a half-metal:

The following figure 2.14 represents a trilayer of two ferromagnetic half metals with one non-magnetic metallic layer between them[9]. When a magnetic field is applied $H \neq 0$, the two half-metals are parallel Fig 2.14 (a) and there will be a current made up exclusively of spin down electrons (because only red bands exist at Fermi level). However, in absence of a magnetic field Fig 2.14 (b), $H = 0$, the spin down channel is totally blocked for conduction of electricity. Hence, there is a large change in resistance between these two configurations that gives rise to a strong magnetoresistance behaviour.

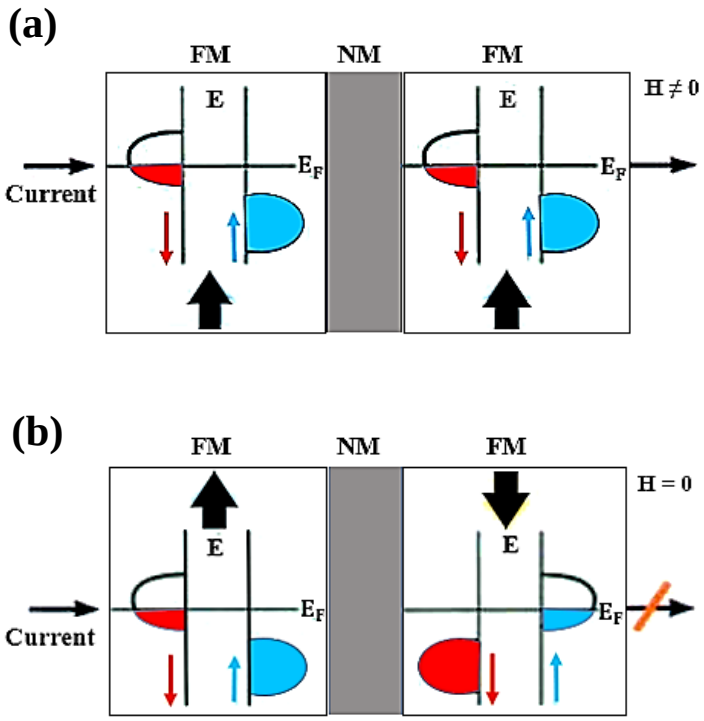

Fig. 2. 14 Trilayer in case of using half-metals (a) parallel layers (existence of magnetic field) and (b) anti-parallel (absence of magnetic field) [9]

2.7. Tunneling magnetoresistance (TMR):

The tunneling magnetoresistance (TMR) is a quantum mechanical phenomenon and it occurs in magnetic tunnel junctions (MTJ) [12]which are structures consisting of two ferromagnetic layers separated by a very thin insulating layer (see Fig 2. 15). In short, if the insulating barrier, which is between the two ferromagnetic electrodes, is thin enough (in the order of a few nanometres), the electrons can tunnel quantum mechanically through the insulating barrier; a tunnel current flows between the ferromagnetic layers.

In the case of parallel magnetizations (ferromagnetic coupling), the electrons tunnel through the insulating layer; since spin is conserved in the tunneling process, the current is larger for parallel than for antiparallel magnetizations, because in antiferromagnetic coupling there is a low tunneling probability. As a result, an MTJ can operate as a switch between a low state and a high state of electrical resistance.

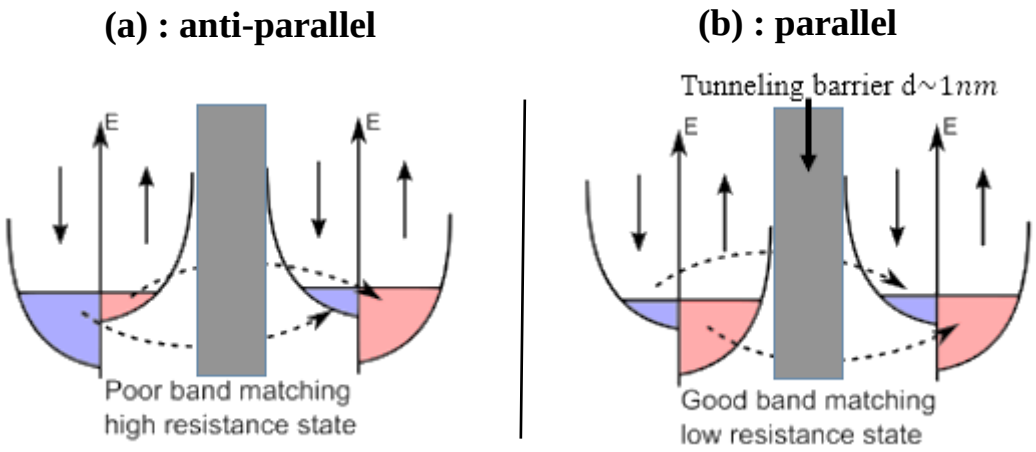

Fig. 2. 15 TMR effect in its simplest interpretation. [34]

Due to the better performance of the magnetic tunnel junctions, TMR are expected to become the material of choice when it comes to technical applications. One expects that TMR based technologies will become dominant over the GMR sensors. However, the discovery of the GMR effect paved the way for the TMR technology.

2.8. Theoretical design of spintronics materials:

In the last decade, half-metallic ferromagnets (HMF's) have attracted huge attention of scientists because of their novel applications in the field of spintronics

Spintronics materials are the basis of spintronics. Although lots of spintronics materials have been proposed previously, most of them are far from practical applications due to a number of problems, such as the destruction of half-metallicity by spin-flip transitions, low magnetic ordering temperature, difficulty in synthesis, and bad controllability. The of design spintronics materials that work at room temperature and that can be easily manipulated in experiment is the key to bring spintronics to real life.

In this aspect, first-principles calculations provide us with a powerful and cheap tool. compared to experimental materials design, which is a trial-and-error job, consuming much time and energy and inevitably causing a waste of experimental resources, first-principles calculations do not need any real sample and can be performed even for materials that have not been synthesized yet. By first-principles calculations, the properties of materials can be routinely predicted, based on which one selects those with required properties, and confirms them by a followed experiment. Such a procedure can largely reduce the period of materials design. Moreover, thanks to the development of computer technology and theoretical chemistry, the speed and accuracy of first-principles calculations have both been significantly improved.

2.9. Recent advances in half metals:

In the following, we present spintronics materials including half metals with or without transition metals, designed by experiments or by first-principles calculations and our compounds XMg_3O_4 (X = Li, Na, K, Rb)**.**

2.9.1. Half-metals with transition metal elements:

Heusler alloys:

Since 1903, year of the discovery of these alloys by the German engineer Heusler[13], these alloys have attracted the attention of the scientific community.

Heusler alloys can be classified into ternary Heusler alloys and quaternary Heusler alloys. Ternary Heusler alloys can be subdivided into half Heusler alloys with the chemical formula XYZ, where X and Y are transition-metal atoms and Z is a main-group element, and full Heusler alloys with the chemical formula X_2YZ. In half Heusler alloys, the energetically most stable occupation sequence along the diagonal is $X-Y-Z$, while in full Heusler alloys, the sequence is $X-Y-X-Z$, when the valence of X is larger than Y, or $X-X-Y-Z$ when the valence of Y is the largest. The latter is also called inverse Heusler alloys. For quaternary Heusler alloys, the chemical formula is identified by XX' YZ, where the valence of X is larger than X', and X' is larger than Y. The preferred occupation sequence along the diagonal is $X-Y-X'-Z$. Examples of Heusler alloys that exhibit half metallicity: NiMnSb[14] the first half Heuser alloy that was proposed to be an HMF by De Groot, Heusler compounds have been

intensively studied such as: half Heusler alloys NiYSb and CoYSb[15] , full Heusler alloys Co_2MnX (X = Al, Ga, Si, Ge, Sn)[16] and inverse Heusler alloys Sc_2CrAl, Ti_2NiAl, Mn_2ZnSi [17] …

Transition-metal oxides:

Transition-metal oxides such as CrO_2 [18]and Fe_3O_4[19] are the oldest HMFs. Although they were widely used for their magnetic properties, the half-metallicity in these oxides remained unknown until it was revealed by first-principles calculations.

perovskites:

ABO_3, where A is mostly an s-block element, B is a transition element or can rarely be an sp element, and O is oxygen. Bouadjemi et al.[20] found that perovskite $PrMnO_3$ is a HM ferromagnet.

Double perovskites:

Double perovskite with the general formula $A_2MM'O_6$ is based on the perovskite structure ABO_3, with the transition-metal sites B being occupied alternately by different cations M and M′. First-principles calculations revealed that Sr_2FeMoO_6[21] (most widely studied double perovskite) is HMF with a ferromagnetic transition temperature Tc≈ 420K which is well above room temperature, double perovskites Sr_2CrReO_6[22] and Sr_2FeReO_6[23] also potential HMFs.

2.9.2. HM ferromagnets without transition metals:

Magnetism in the above-mentioned compounds is due to the presence of localized d or f electrons. The magnetic moment in these materials results mainly from transition metals and hence, they are known as HM-3d compounds. However, recently, an unusual class of ferromagnetic materials, which do not contain transition-metal or rare-earth atoms have been found and analyzed theoretically by ab-initio calculations.

Gao and Yao studied MC (M= Mg, Ca, Sr, and Ba) [24] compounds in ZB structure and SrC and BaC in rocksalt (RS) structure. They observed that CaC, SrC, and BaC compounds in ZB structure and SrC and BaC in RS structure are HMF's and the calculated T_C's are higher than the room temperature. Moreover, Zhang [25] has reported that ZB of LiC, NaC, and KC

compounds are HMF's ferromagnets, but these compounds in RS structure show nearly HM ferromagnetic properties.

In 2011, Gao et al [26] have carried out theoretical investigation of alkali-metal compounds MS (M = Li, Na, and K) and found that all the compounds in ZB and RS-type structure (except RS-LiS) are HMF with an integer magnetic moment of 1 μ_B.

From the discussions of HM-3d compounds, it is observed that the magnetic moment of these compounds is usually 3 μ_B or 4 μ_B by Galanakis and Mavropoulos[27], which is larger than 1 μ_B or 2 μ_B of ZB-HM sp ferromagnets. In real-time applications, HM sp ferromagnets are more meaningful due to their smaller values of magnetic moment. The explanation for the presence of non-vanishing spin-polarization for these sp compounds HM compounds is due to the effect of strong spin-polarization of energy states near the Fermi level in which a strong Hund's coupling take place.

Recently, ternary oxides without transition metals were reported to be half metals ferromagnets (HMFs) such as perovskites $KMgO_3$[28], $LiBeO_4$. Those works motivate us to search for new types or ternary oxides namely XMg_3O_4(X=Li, Na, K, Rb) compounds with space group N^0 221, the compounds crystallize in simple cubic lattice Fig. 2.17. They were derived from the conventional unit cell of the rocksalt MgO Fig 2.16 by substituting one Mg atom by X atom.

The purpose of this work is to study structural, electronic, elastic properties and its magnetic properties of XMg_3O_4 (X = Li, Na, K, Rb) compounds.

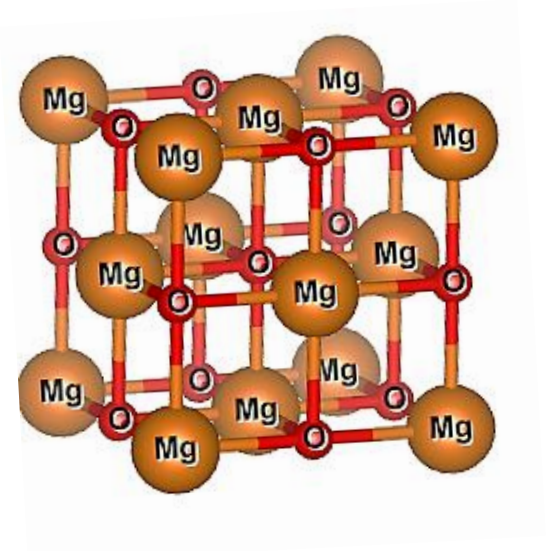

Fig. 2. 16 Conventional unit cell of magnesium oxide MgO plotted with Vesta [35]

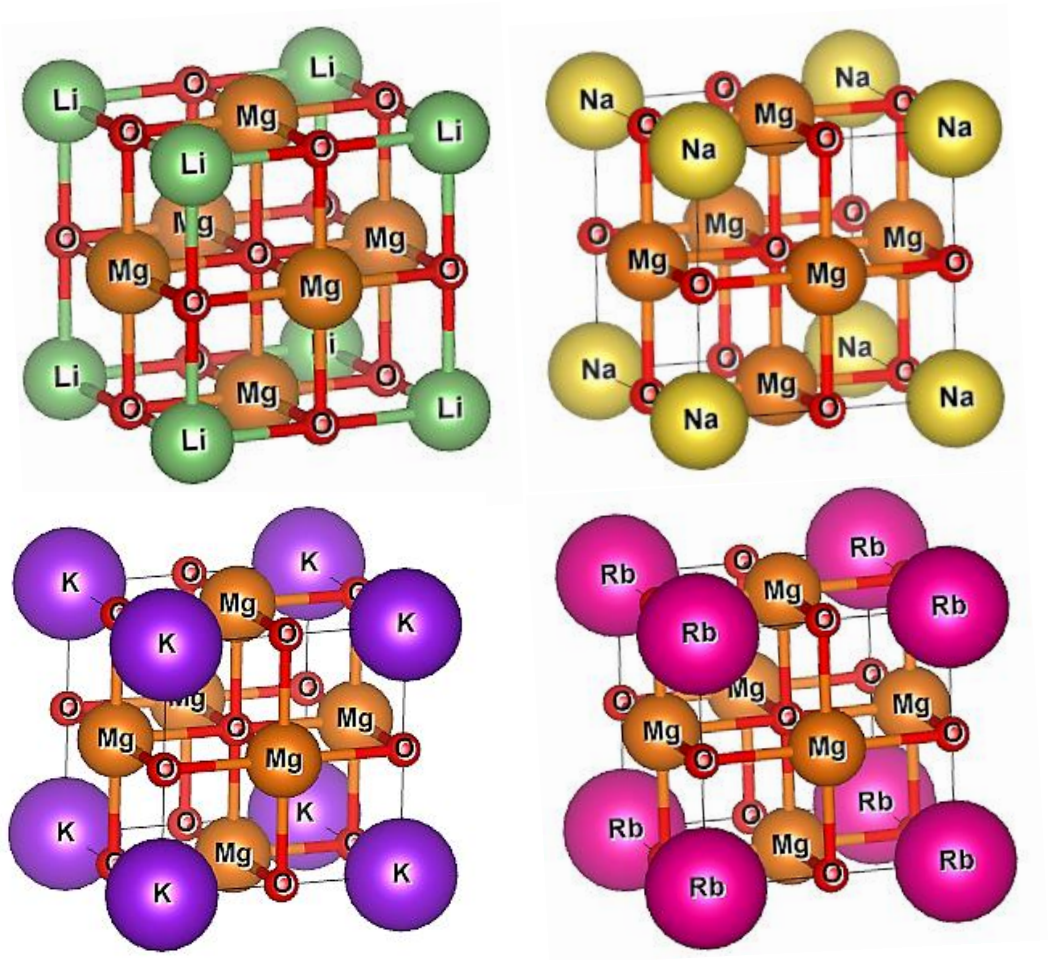

Fig. 2. 17 Unit cell of our four compounds XMg_3O_4 (X = Li, Na, K, Rb) plotted with Vesta [35]

2.10. References:

[1] I. Žutić, J. Fabian, and S. das Sarma, "Spintronics: Fundamentals and applications," *Rev Mod Phys*, vol. 76, no. 2, p. 323, 2004.

[2] R. Umamaheswari, M. Yogeswari, and G. Kalpana, "Ab-initio investigation of half-metallic ferromagnetism in half-Heusler compounds XYZ (X= Li, Na, K and Rb; Y= Mg, Ca, Sr and Ba; Z= B, Al and Ga)," *J Magn Magn Mater*, vol. 350, pp. 167–173, 2014.

[3] C. Kittel, P. McEuen, and P. McEuen, *Introduction to solid state physics*, vol. 8. Wiley New York, 1996.

[4] R. Skomski, *Simple models of magnetism*. Oxford University Press on Demand, 2008.

[5] J. Yamauchi, "Fundamentals of magnetism," *Nitroxides: applications in chemistry, biomedicine, and materials science*, pp. 1–45, 2008.

[6] R. A. de Groot, F. M. Mueller, P. G. van Engen, and K. H. J. Buschow, "New class of materials: half-metallic ferromagnets," *Phys Rev Lett*, vol. 50, no. 25, p. 2024, 1983.

[7] G. Binasch, P. Grünberg, F. Saurenbach, and W. Zinn, "Enhanced magnetoresistance in layered magnetic structures with antiferromagnetic interlayer exchange," *Phys Rev B*, vol. 39, no. 7, p. 4828, 1989.

[8] M. N. Baibich *et al.*, "Giant magnetoresistance of (001) Fe/(001) Cr magnetic superlattices," *Phys Rev Lett*, vol. 61, no. 21, p. 2472, 1988.

[9] C. Day, "Discoverers of giant magnetoresistance win this year's physics Nobel," *Phys Today*, vol. 60, no. 12, p. 12, 2007.

[10] N. F. Mott, "The electrical conductivity of transition metals," *Proceedings of the Royal Society of London. Series A-Mathematical and Physical Sciences*, vol. 153, no. 880, pp. 699–717, 1936.

[11] D. Samal and P. S. Anil Kumar, "Giant magnetoresistance," *Resonance*, vol. 13, no. 4, pp. 343–354, 2008.

[12] S. Yuasa and D. D. Djayaprawira, "Giant tunnel magnetoresistance in magnetic tunnel junctions with a crystalline MgO (0 0 1) barrier," *J Phys D Appl Phys*, vol. 40, no. 21, p. R337, 2007.

[13] C. Felser and A. Hirohata, *Heusler alloys*. Springer, 2015.

[14] C. M. Fang, G. A. de Wijs, and R. A. de Groot, "Spin-polarization in half-metals," *J Appl Phys*, vol. 91, no. 10, pp. 8340–8344, 2002.

[15] I. Galanakis, P. H. Dederichs, and N. Papanikolaou, "Origin and properties of the gap in the half-ferromagnetic Heusler alloys," *Phys Rev B*, vol. 66, no. 13, p. 134428, 2002.

[16] I. Galanakis, P. H. Dederichs, and N. Papanikolaou, "Slater-Pauling behavior and origin of the half-metallicity of the full-Heusler alloys," *Phys Rev B*, vol. 66, no. 17, p. 174429, 2002.

[17] S. Skaftouros, K. Özdoğan, E. Şaşıoğlu, and I. Galanakis, "Generalized Slater-Pauling rule for the inverse Heusler compounds," *Phys Rev B*, vol. 87, no. 2, p. 024420, 2013.

[18] K. Schwarz, "CrO2 predicted as a half-metallic ferromagnet," *Journal of Physics F: Metal Physics*, vol. 16, no. 9, p. L211, 1986.

[19] Z. Zhang and S. Satpathy, "Electron states, magnetism, and the Verwey transition in magnetite," *Phys Rev B*, vol. 44, no. 24, p. 13319, 1991.

[20] B. Bouadjemi, S. Bentata, A. Abbad, W. Benstaali, and B. Bouhafs, "Half-metallic ferromagnetism in PrMnO3 perovskite from first principles calculations," *Solid State Commun*, vol. 168, pp. 6–10, 2013.

[21] B. Garcıa-Landa *et al.*, "Magnetic and magnetotransport properties of the ordered perovskite Sr2FeMoO6," *Solid State Commun*, vol. 110, no. 8, pp. 435–438, 1999.

[22] H. Kato *et al.*, "Metallic ordered double-perovskite Sr 2 CrReO 6 with maximal Curie temperature of 635 K," *Appl Phys Lett*, vol. 81, no. 2, pp. 328–330, 2002.

[23] K.-I. Kobayashi, T. Kimura, Y. Tomioka, H. Sawada, K. Terakura, and Y. Tokura, "Intergrain tunneling magnetoresistance in polycrystals of the ordered double perovskite Sr 2 FeReO 6," *Phys Rev B*, vol. 59, no. 17, p. 11159, 1999.

[24] G. Y. Gao, K. L. Yao, E. Şaşıoğlu, L. M. Sandratskii, Z. L. Liu, and J. L. Jiang, "Half-metallic ferromagnetism in zinc-blende CaC, SrC, and BaC from first principles," *Phys Rev B*, vol. 75, no. 17, p. 174442, 2007.

[25] C.-W. Zhang, "Half-metallic ferromagnetism in the zinc-blende MC (M= Li, Na and K)," *J Phys D Appl Phys*, vol. 41, no. 8, p. 085006, 2008.

[26] G. Y. Gao, K. L. Yao, M. H. Song, and Z. L. Liu, "Half-metallic ferromagnetism in rocksalt and zinc-blende MS (M= Li, Na and K): a first-principles study," *J Magn Magn Mater*, vol. 323, no. 21, pp. 2652–2657, 2011.

[27] I. Galanakis and P. Mavropoulos, "Zinc-blende compounds of transition elements with N, P, As, Sb, S, Se, and Te as half-metallic systems," *Phys Rev B*, vol. 67, no. 10, p. 104417, 2003.

[28] M. Hamlat, K. Boudia, K. Amara, F. Khelfaoui, and N. Marbouh, "Half-metallic stability of the cubic perovskite KMgO3," *Computational Condensed Matter*, vol. 23, p. e00456, 2020.

[29] Vahideh Abdolazimi, "Inversse perovskites EU3TO(T=Si, Ge, Sn, Pb) Magnetism and Transport," Stuttgart University, 2014.

[30] J. L. Bouchez, "Granite is never isotropic: an introduction to AMS studies of granitic rocks," in *Granite: from segregation of melt to emplacement fabrics*, Springer, 1997, pp. 95–112.

[31] H. D. Young, R. A. Freedman, and A. L. Ford, *University Physics with Modern Physics Technology Update*. Pearson Education, 2013.

[32] S. Semboshi, R. Y. Umetsu, Y. Kawahito, and H. Akai, "A new type of half-metallic fully compensated ferrimagnet," *Sci Rep*, vol. 12, no. 1, pp. 1–9, 2022.

[33] R. Mattana, N. Locatelli, and V. Cros, "Spintronics and Synchrotron Radiation," in *Magnetism and Accelerator-Based Light Sources*, Springer, Cham, 2021, pp. 131–163.

[34] A. Makarov, "Modeling of emerging resistive switching based memory cells," *Institute for Microelectronics, TU Wien, Vienna*, 2014.

[35] K. Momma and F. Izumi, "VESTA: a three-dimensional visualization system for electronic and structural analysis," *J Appl Crystallogr*, vol. 41, no. 3, pp. 653–658, 2008.

Chapter 3

Results and discussions

In this chapter, we present the structural, mechanical and magneto-electronic properties of these compounds of XMg_3O_4 (X=Li, Na, K and Rb) compounds. Useful findings and conclusive discussion of these materials along with the possible applications has been mentioned in this part.

3.1. Computational method

In this work, first principles studies of XMg_3O_4 (X = Li, Na, K and Rb) compounds were performed using the full potential linearized augmented plane wave method (FP-LAPW) [1]as implemented in wien2k[2]within the framework of the density functional theory. The generalized gradient approximation (GGA) of Perdew-Burke-Ernzerhof (PBE)[3], [4] was taken for evaluating the exchange-correlation energy. In this method, the space was divided into non-overlapping muffin-tin (MT) spheres separated by an interstitial region, the chosen muffin-tin radii (MT) for Li, Na, K, Rb, Mg and O atoms were 1.66,1.90,1.98,2.03,1.85 and 1.81 (a.u.), respectively. In the calculations reported here, we set the parameter of the plane wave cut-off $R_{MT}.K_{max}=8.0$, where R_{MT} is the smallest muffin-tin sphere radius and K_{max} is the largest reciprocal lattice vector radius. The K-point sampling scheme of 14×14×14 grid in the first Brillouin zone. We used 10^{-5} eV and 10^{-4} e as convergence criteria for the energy and charge respectively. The maximum angular quantum number for the expansion of wave functions inside the atomic spheres was $L_{max}=10$. In the interstitial region, the charge density and potential were expanding as a Fourier series with wave vectors up to $G_{max}=12(a.u.)^{-1}$: the Li $2s^1$, Na $3s^1$, K $4s^1$, Rb $5s^1$, Mg $3s^2$ and O $2s^22p^4$were treated as valence electrons.

3.2. Results and discussions:

3.3. Structural properties:

XMg_3O_4 (X = Li, Na, K and Rb) have a simple cubic lattice with space group N°221, where atoms are sited as X(0, 0, 0), Mg $(0,\frac{1}{2},\frac{1}{2})$, $(\frac{1}{2}, 0,\frac{1}{2})$, $(\frac{1}{2}, \frac{1}{2}, 0)$ and O $(\frac{1}{2}, 0, 0)$, $(0, \frac{1}{2},0)$, $(0, 0,\frac{1}{2})$ and $(\frac{1}{2},\frac{1}{2},\frac{1}{2})$ positions. In order to explain the physical properties of XMg_3O_4 (with X = Li, Na, K and Rb), the structural properties were firstly investigated by using energy minimization procedure with the aim to obtain the ground state properties. In fact, the total energies were calculated as a function of unit-cell volume for the three magnetic phases (non-magnetic-NM, ferromagnetic-FM and antiferromagnetic-AFM). Energy versus volume data were adjusted to the Birch–Murnaghan equation of state (EOS)[5], [6], and the results are shown in Fig.3.1,

Fig.3.2, Fig.3.3 and Fig.3.4. Then, the structural parameters, such as lattice parameters (Bohr), bulk modulii (GPa), and their derivative pressures were calculated and given in table 3.1. One can clearly observe that among the three phases, FM phase with the lowest energy is the most stable one. From the comparison of the equilibrium energies for FM phase, the observed order as:

$$E_{min}(RbMg_3O_4) < E_{min}(KMg_3O_4) < E_{min}(NaMg_3O_4) < E_{min}(LiMg_3O_4) \quad 3.1$$

can be explained by the decrease of the number of electrons per formula unit:

$$Z(Li) < Z(Na) < Z(K) < Z(Rb). \quad 3.2$$

The bulk modulus increases as following sequence:

$$B(LiMg_3O_4) < B(NaMg_3O_4) < B(KMg_3O_4) < B(RbMg_3O_4) \quad 3.3$$

proportionally to the reverse of the lattice parameters (table 1) $B \propto a_0^{-1}$and thus verifying the relationship between the bulk and the lattice volume $B \propto V_0^{-1}$ where V_0 is the volume of the unit cell. Unfortunately, no previous experimental or theoretical data available for XMg_3O_4 (with X = Li, Na, K and Rb) to compare with our work.

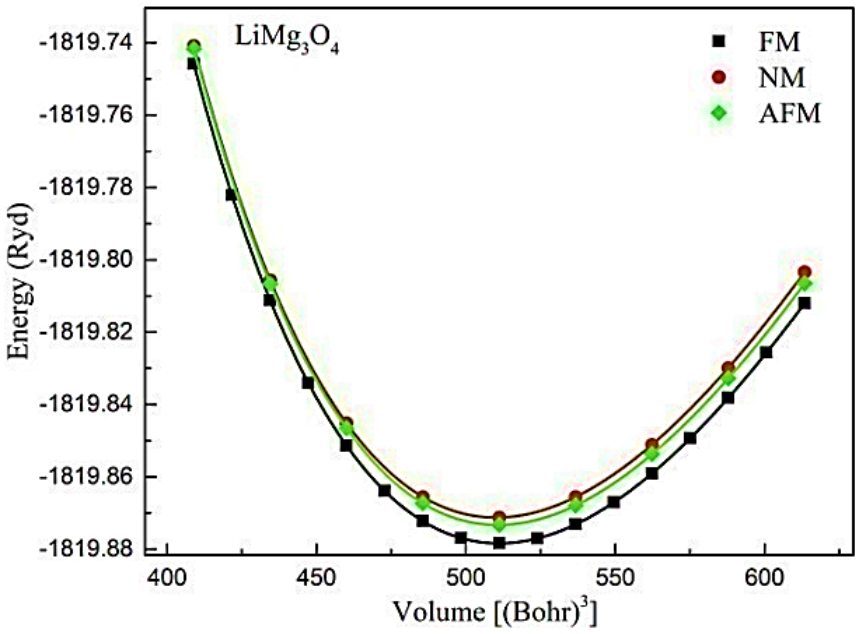

Fig. 3. 1 Total energy versus volume for $LiMg_3O_4$

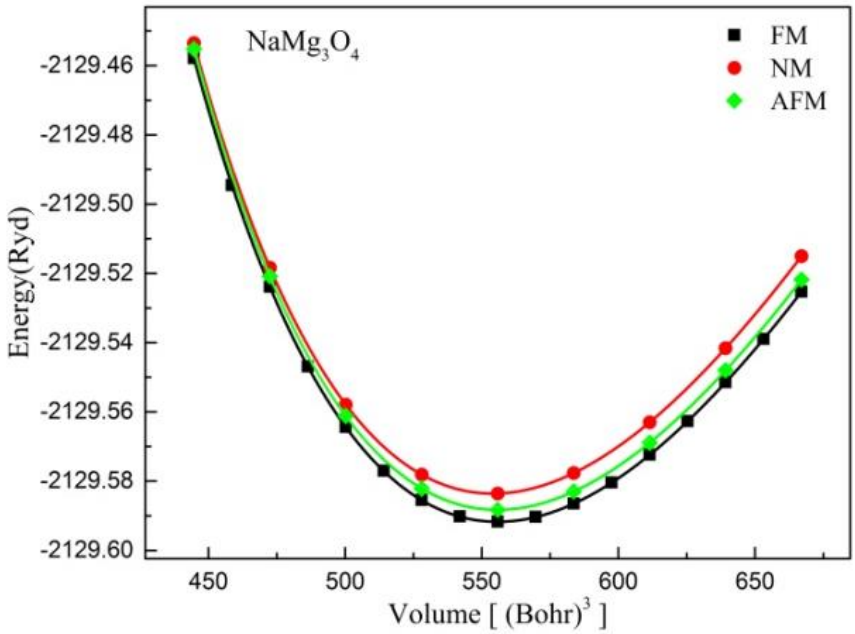

Fig. 3. 2 Total energy versus volume for $NaMg_3O_4$

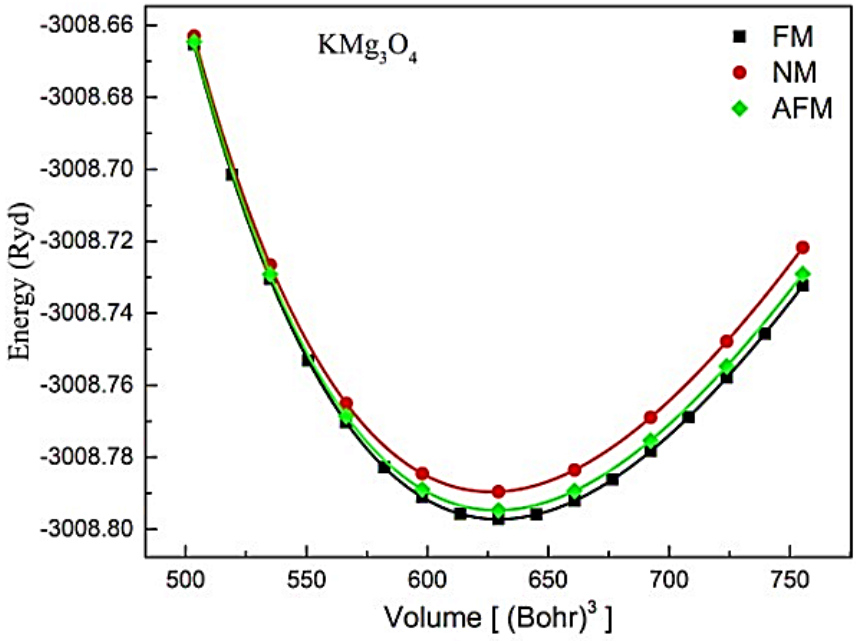

Fig. 3. 3 Total energy versus volume for KMg_3O_4

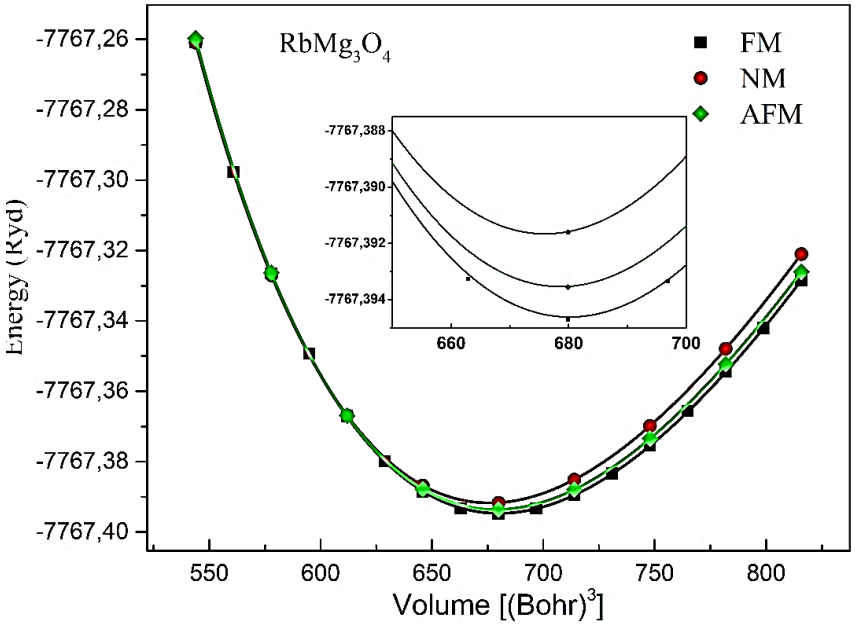

Fig. 3. 4 Total energy versus volume for $RbMg_3O_4$

X	a_0	*a*	*B*	*B'*	E_{coh}	E_{for}
Li	7.9951	7.99165178	130.3748	4.1504	-38.82	-2.78
Na	8.2219	---	120.5110	4.1895	-36.86	-2.07
K	8.5699	8.579357	104.3289	4.2445	-34.19	-1.77
Rb	8.7941	----	98.3352	4.1462	-32.50	-1.58

Table. 3. 1 Calculated lattice parameters a_0, lattice parameters *a* from materials project [7] (in Bohr), bulk modulii (in GPa), their derivative pressures, formation (E_{for}) and cohesive (E_{coh}) energies (in eV) of the structural and magnetic ground phase (FM) for XMg_3O_4.

From table 3.1, the calculated lattice parameters a_0 for $LiMg_3O_4$ and KMg_3O_4 are in agreement with the data *a* (obtained from Materials project). The formation (E_{for}) and cohesive (E_{coh}) energies, that show thermodynamic and chemical stabilities, are defined for our considered materials, as [8]–[9]:

$$E_{\text{for}} = E^{tot}_{XMg_3O_4} - \left(E^{bulk}_{X} + 3E^{bulk}_{Mg} + 2E^{O_2}\right) \qquad 3.4$$

$$E_{coh} = E^{tot}_{XMg_3O_4} - \left(E^{iso}_{X} + 3E^{iso}_{Mg} + 4E^{iso}_{O}\right) \; ; \quad X = Li, \quad Na, \quad K, \quad Rb \qquad 3.5$$

Where $E^{tot}_{XMg_3O_4}$is the total energy per formula unit for each compounds at the equilibrium state and E^{bulk}_{Li}, E^{bulk}_{Na}, E^{bulk}_{K},E^{bulk}_{Rb}, E^{bulk}_{Mg} $and E^{O_2}$correspond to the energy per atom of Li , Na, K, Rb, Mg atoms and O_2 molecular energy at ground state.E^{iso}_{Li}, E^{iso}_{Na}, E^{iso}_{K}, E^{iso}_{Rb},E^{iso}_{Mg} and $E^{iso}_{O}$are the energy of isolated Li, Na, K, Rb, Mg and O atoms, respectively. As can be seen from Table 3.1, the calculated values of formation energy E_{for} and cohesive energy E_{coh} confirm that these compounds are energetically stable in the FM phase and can be experimentally fabricated.

3.4. Elastic properties:

In order to confirm the stability of our materials, we calculated their elastic constants which provide us with information such as brittleness/ductility, stiffness and hardness, and understanding other solid state phenomena like (interatomic potential, bonding characteristics and anisotropy.). The elastic constants are the physical quantities that reflect the resistance of a material to the external forces. Because of the cubic symmetry, the total number of independent elastic constants are reduced to only three independent elastic constants, namely C_{11},C_{12} and C_{44}, necessary to investigate the elastic properties. Once the elastic constants are determined, other elastic parameters can be easily calculated, such as the bulk (B), shear (G), Young modulii (E) and anisotropy parameter (Bohr), using the assumed Voigt-Reuss-Hill approximations for the cubic structures[10]–[13]:

$$G = \frac{G_V + G_R}{2};\ G_V = \frac{C_{11} - C_{12} + 3C_{44}}{5};\ G_R = \frac{5C_{44}(C_{11} - C_{12})}{4C_{44} + 3(C_{11} - C_{12})} \quad 3.6$$

$$A = \frac{2C_{44}}{C_{11} - C_{12}} \quad 3.7$$

$$B = \frac{C_{11} + 2C_{12}}{3} \quad 3.8$$

$$E = \frac{9BG}{3B + G} \quad 3.9$$

$$\upsilon = \frac{3B - 2G}{2(3B + G)} \quad 3.10$$

The results for XMg_3O_4 (X=Li, Na, K, Rb) are reported in Table 3.2. The mechanical stability of a cubic system requires that its independent elastic constants C_{11},C_{12} and C_{44}should satisfy the following Born's stability criteria[13], [14]:

$$C_{11} > 0;\ C_{12} > 0; C_{44} > 0; C_{11} > C_{12};\ \ C_{11} + 2C_{12} > 0; C_{11} > B > C_{12} \qquad 3.11$$

As shown in Table 3.2, the values of the cubic elastic constants are positive and satisfy the stability conditions, so these materials are mechanically stable. There are two well-known modulii used to investigate the mechanical properties such as hardness, brittleness or ductility of a material. The bulk B value indicates the hardness of a material or represents the resistance to fracture. The shear modulus G represents the resistance to a plastic deformation. Pugh reported that if the ratio $\mathrm{B/G} > 1.75$, the material behaves in a ductile nature otherwise, the material is brittle. According to the presented results in Table 3.2, the B/G ratios of $NaMg_3O_4$ and $RbMg_3O_4$ at equilibrium lattice constant are higher than 1.75, indicating that they are ductile, but for $LiMg_3O_4$ and KMg_3O_4 the ratio B/G is less than 1.75 showing their brittle nature. Another index to distinguish brittleness and ductility of a material is the rule suggested by Frantsevich[15] , A material behaves in a brittle manner, when the Poisson's ratio is less than $1/3$,otherwise it should be ductile.

X	C_{11}	C_{12}	C_{44}	C_P	*B*	*E*	*G*	*B/G*	*A*	υ
Li	236.82	75.00	76.52	-1.75	128.94	195.242	78.245	1.65	0.95	0.247
Na	230.76	70.96	60.74	10.22	124.22	172.084	67.797	1.83	0.76	0.269
K	169.55	72.28	79.96	-7.68	104.71	162.601	65.503	1.60	1.64	0.241
Rb	150.55	74.12	71.27	2.85	99.59	140.419	55.501	1.79	1.86	0.265

Table. 3. 2 Elastic constants C_{11}, C_{12}, C_{44} (GPa), Cauchy pressure C_p (GPa), bulk B, Young E(GPa), Shear G moduli (in GPa), B/G, and Poisson's coefficients υ of XMg_3O_4.

According to Frantsevich, our materials are all brittle and that's a contradiction between the pugh's relation and Frantsevich rule. However, we can easily show that:

$$\upsilon = \frac{1}{2}\frac{3\frac{B}{G} - 2}{3\frac{B}{G} + 1} \qquad 3.12$$

From which it follows that the corresponding Pugh's critical υvalue is 0.26 , so that the two empirical rules only differ on the exact border between the two types of behavior. For $LiMg_3O_4$ and KMg_3O_4 $\upsilon \approx 0.25$, but $\upsilon \approx 0.27$ for $NaMg_3O_4$ and $RbMg_3O_4$ therefore we consider them a borderline case between the classes of ductile and brittle materials[16]. A third way suggested by Pettifor[17] to check ductility/brittleness is the Cauchy pressure given by the equation $C_p = C_{12} - C_{44}$. From Table 2, the Cauchy pressure values for $NaMg_3O_4$ and $RbMg_3O_4$ are positive, indicating their ductility. On the other hand, they are negative for $LiMg_3O_4$ and KMg_3O_4, demonstrating their brittleness. Thus, these results confirm the Pugh's suggestion.

The Poisson's ratio υ is also used to describe the bonding nature of materials. As reported, If the Poisson's ratio is around 0.1, the material has dominantly covalent bonding, while if it is around 0.25, it has dominantly ionic bonding[18]. From table 2, the Poisson's ratios are higher than 0.25 for $NaMg_3O_4$ and $RbMg_3O_4$. Thus, these compounds have dominantly ionic bonding. However, the Poisson's ratio is around 0.25 for both KMg_3O_4 $LiMg_3O_4$ which indicates also an important ionic bonding.

The lower and the upper limits for the value of central force solids are 0.25 and 0.5, respectively [19]. The calculated Poisson's ratio ν values are small than 0.25 which indicates that interatomic forces for KMg_3O_4 are noncentral. However, ν is higher than 0.25 for $NaMg_3O_4$ and $RbMg_3O_4$ and approximately 0.25 for $LiMg_3O_4$ which demonstrates that interatomic forces for these compounds are central.

The young modulus E, defined as the ratio of stress and strain, characterizes the stiffness of a material. From the calculated values of E, the stiffness relationship among the four compounds is: $E_{LiMg_3O_4} > E_{NaMg_3O_4} > E_{KMg_3O_4} > E_{RbMg_3O_4}$. Therefore, $LiMg_3O_4$ is the stiffest material among the studied compounds. In addition, with increasing the value E, the material will exhibit covalent properties which have impact on the ductility[18] .The anisotropy factor(A) is used to indicate the degree of anisotropy of a material[20]. In Table 3.2, we also present the calculated anisotropy factors of XMg_3O_4(X=Li, Na, K, Rb). For an isotropic material, the value of A is unity otherwise. Any value of *A* differs from 1 indicates the anisotropy. For $LiMg_3O_4$ and $NaMg_3O_4$, Table 3.2 shows that their anisotropy factors are less than 1, while for KMg_3O_4 and $RbMg_3O_4$, A is found to be greater than unity.

3.5. Electronic and magnetic properties:

3.5.1. Band structure:

The electronic band structures with the spin-up and spin-down channels along the high symmetry directions of the Brillouin zone (BZ) were computed for XMg_3O_4 compounds and plotted in Fig. 3.5, Fig. 3.6, Fig. 3.7 and Fig. 3.8.

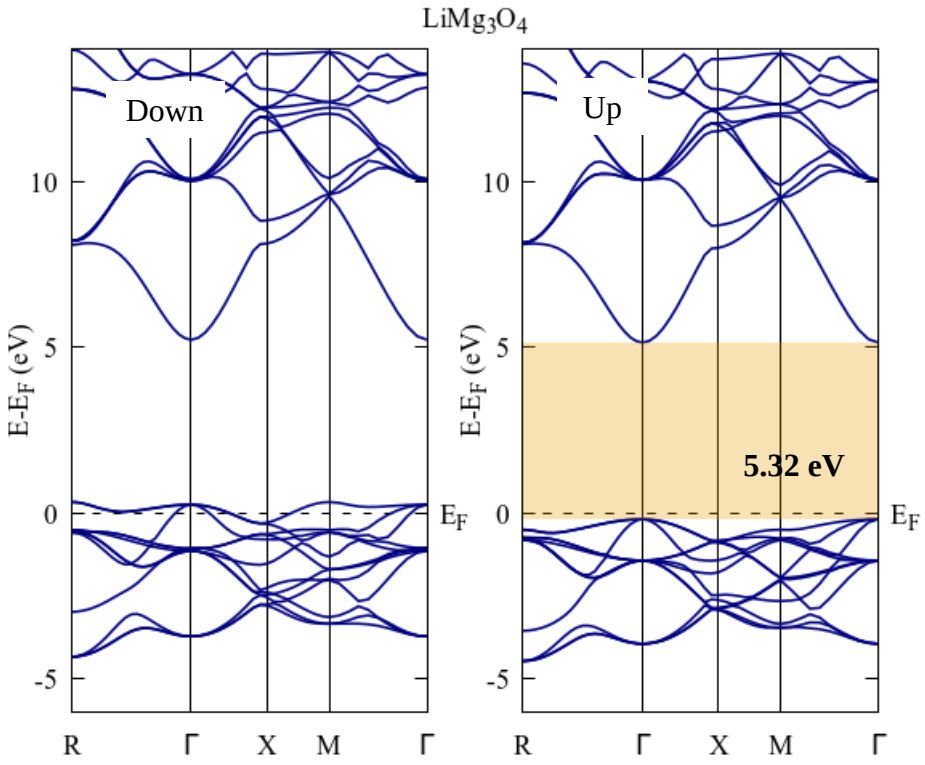

Fig. 3. 5. Spin-polarized band structures of $LiMg_3O_4$. Down (Left) and up (Right) spin channels

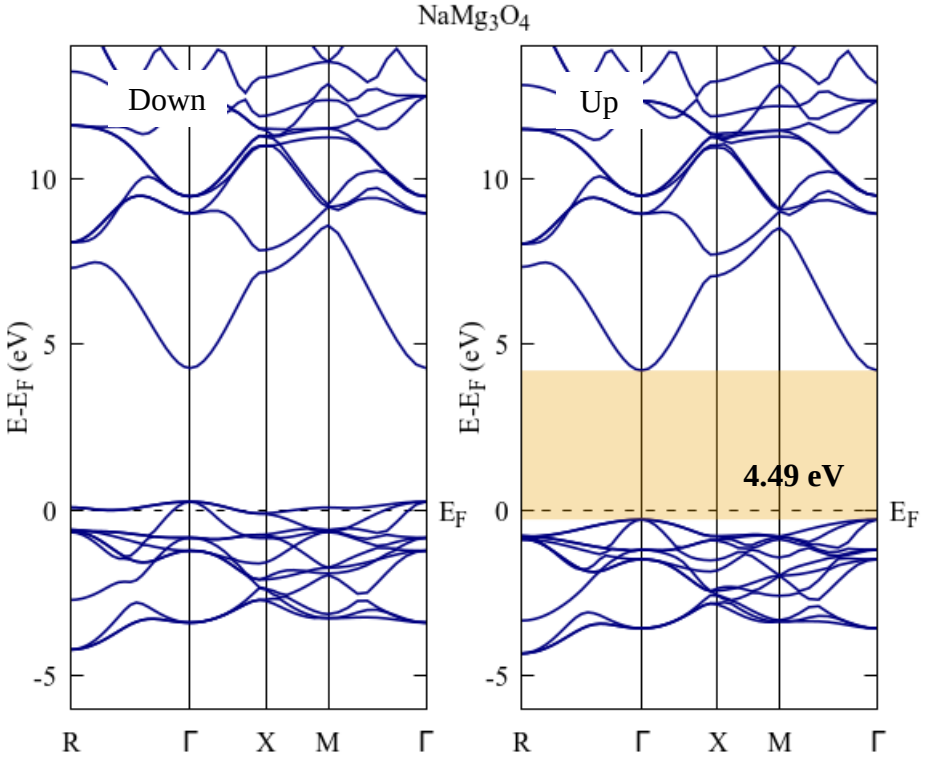

Fig. 3. 6 Spin-polarized band structures of $NaMg_3O_4$. Down (Left) and up (Right) spin channels

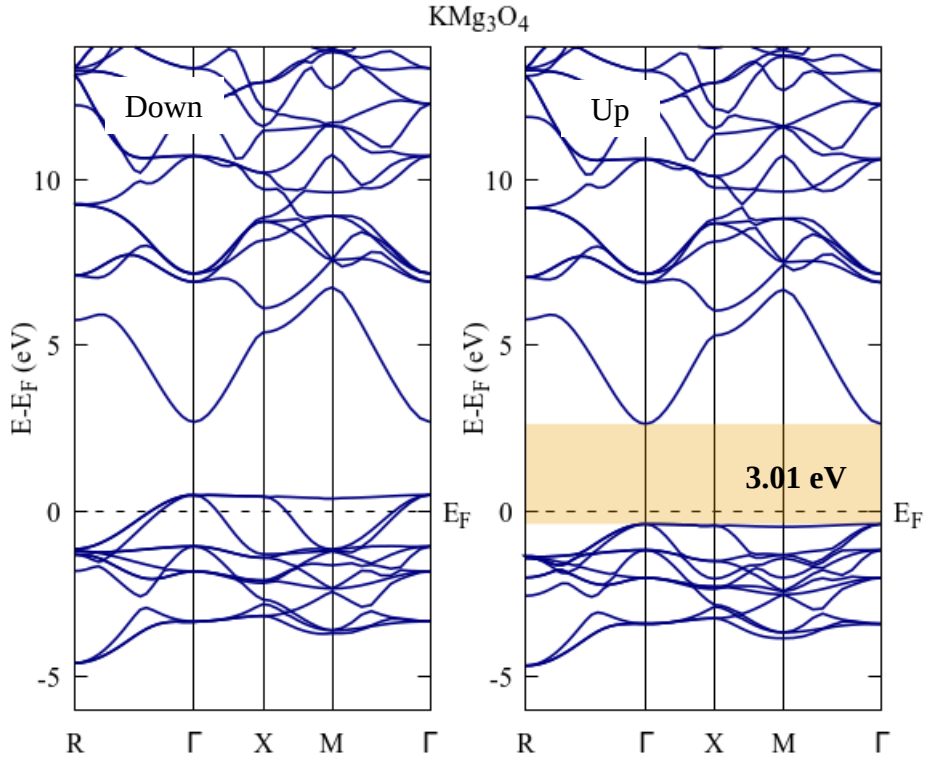

Fig. 3. 7 Spin-polarized band structures of KMg_3O_4. Down (Left) and up (Right) spin channels.

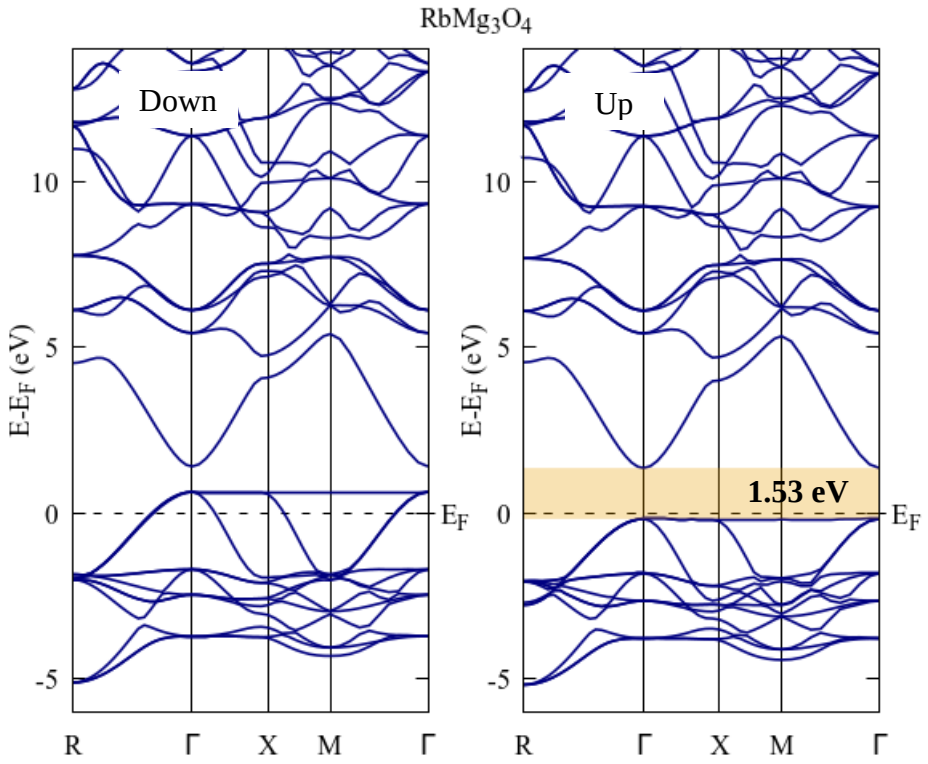

Fig. 3. 8 Spin-polarized band structures of $RbMg_3O_4$. Down (Left) and up (Right) spin channels.

The Fermi level is set to 0.0 eV. In the spin-up channel, for all compounds, we can observe that no band crosses the Fermi level and the corresponding band gap values are 1.53 eV, 3.01 eV, 4.49 eV and 5.32 eV for $RbMg_3O_4$, KMg_3O_4, $NaMg_3O_4$ and $LiMg_3O_4$, respectively. However, a metallic behavior can be seen in spin-down channels. In fact, the Fermi level intersects few valence bands. Therefore, we can conclude that the four compounds exhibit half-metallic (HM) nature.

3.5.2. Density of states:

To further understand the electronic properties, total (TDOS) and partial (PDOS) densities of states of our studied compounds are also calculated and shown in Fig 3.9, Fig 3.10, Fig 3.11 and Fig 3.12. The spin-up and spin-down states are represented as upper and lower panels, respectively in this figure. From TDOS of these compounds, it is observed that the spin-down states show metallic behavior while, in the spin-up, the Fermi level just locates in the energy band gap, confirming the HM behavior, obtained by the previously presented band structures. Also, the TDOS for each compound show that the spin-up and spin-down states are somewhat identical to each other. From Fig 3.9 and Fig 3.10, TDOSs for $LiMg_3O_4$ and

$NaMg_3O_4$ have very similar shapes and they are distributed into two main energy regions from -4.5 eV to 0.5 eV and from 4 eV to 14 eV and that's also remarkable for $RbMg_3O_4$ and KMg_3O_4 with TDOS that can be separated into two energy regions from -5 eV to 0.8 eV and from 2 eV to 14 eV. For each compound the contribution to the TDOS come mainly from p states of O atoms in the first region which contains the Fermi level and the second region is made up from p states of O and Mg atoms.

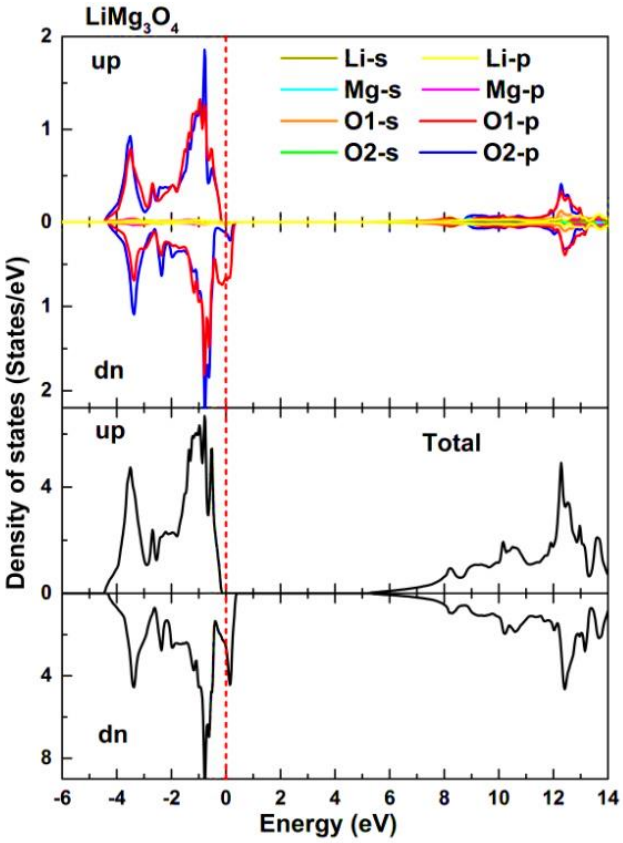

Fig. 3. 9 Density of states of $LiMg_3O_4$

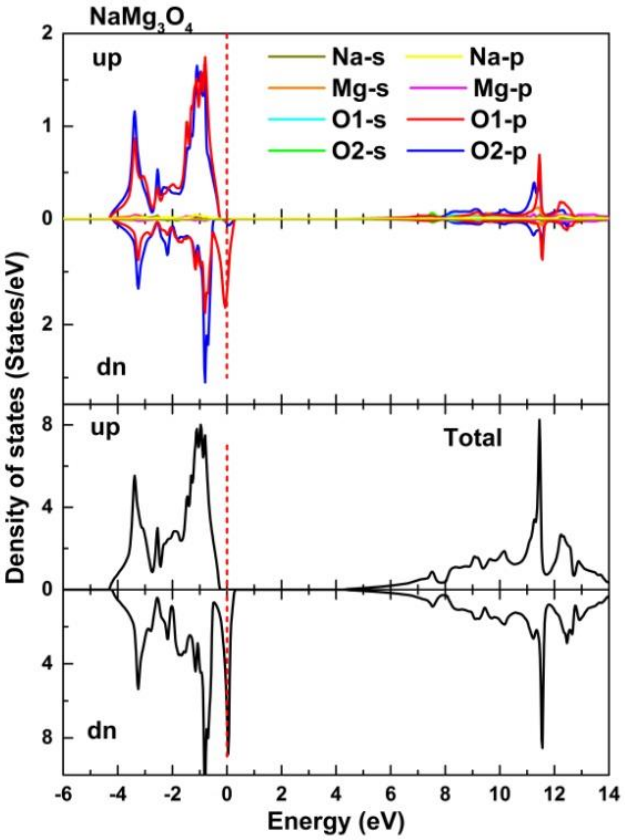

Fig. 3. 10 Density of states of $NaMg_3O_4$

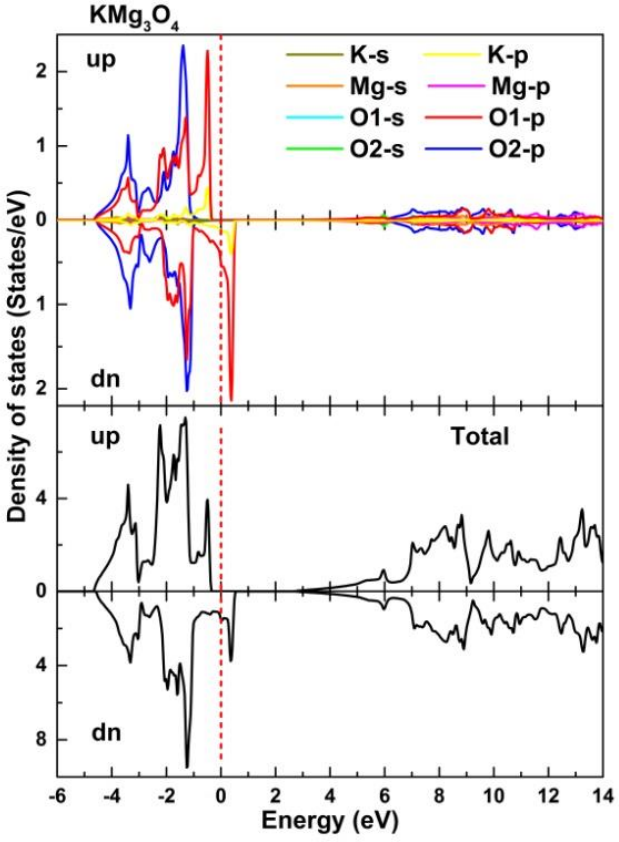

Fig. 3. 11 Density of states of KMg_3O_4

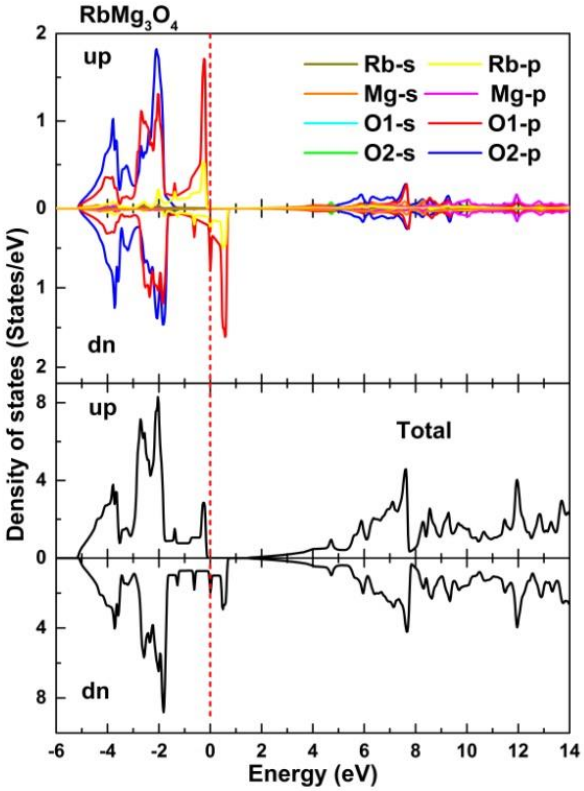

Fig. 3. 12 Density of states of $RbMg_3O_4$

In addition, the magnetism of our investigated systems is induced by O atoms whence the density of states of each compound reveals that the p states of the O1 atom have a large exchange division between the states of the spin up and -down channels around the Fermi level, as shown in figures of density of states It can be also observed that there are no Li and Na contributions around the Fermi level. A small contribution originates from Mg around E_F.

From Figs. 3.9–3.12, we see that the lowest bands with energy between −4.5/−4.4/−4.7/−5.2 eV and 0.34/0.26/0.46/0.66 eV, including both spin channels, are mainly originate from the O-p states, However, around the Fermi level, O1-p contribution is greater than that of O2-p, with strong K(p)-O1(p) and Rb(p)-O1(p) hybridizations which are the main cause of the flat bands above and below the Fermi level for KMg_3O_4 and $RbMg_3O_4$. These lowest bands can accommodate 24 electrons. Because of the spin splitting, the spin-up O1-p or O1(p)-K/Rb(p) bands lie lower in energy than the spin-down corresponding bands. Therefore, the spin-up p bands are fulfilled by 12 electrons, while the spin-down p bands are partly filled with 11 electrons, which appeared in the spin-down valence states. Thus, the above-mentioned spin-splitting gives rise to a half-metallic ferromagnetic character with an integer total magnetic

moment of 1.0 μ_B. The spin splitting mainly originates from O1-p states and is situated close to Fermi level, which provides the main magnetic moment, and the K/Rb(p)-O1(p) hybridization leads to the non-negligible magnetic moment of the K/Rb atom.

X	M_X	M_{Mg}	M_{O1}	M_{O2}	M_{Inter}	M_{tot}
Li	0.00138	-0.00223	0.29828	0.04457	0.06589	0.99998
Na	0.00806	-0.00269	0.30269	0.02183	0.07008	0.99998
K	0.10012	-0.00250	0.28801	-0.00513	0.04848	1.00000
Rb	0.17040	-0.00233	0.27280	-0.00447	0.02266	0.99999

Table. 3. 3 Atomic (M_X, M_{Mg}, M_{O1}, M_{O2}) Interstitial (M_{Inter}) and total magnetic (M_{tot}) moments (in μ_B) of XMg_3O_4.

The accumulation of spin around the atoms can be visualized and analyzed by plotting spin density which represents the difference between the spin-up and spin-down charge densities. It can help us to investigate the spin magnetic moments. Fig.3.13 and Fig.3.14 and show the plotted spin density of XMg_3O_4 compounds. One can see for each compound that the oxygen atoms O1 situated in the middle of the cube edge and K/Rb atoms are surrounded by (yellow) isosurfaces, showing that the spin density is accumulated around them. Therefore, the magnetic moment of O1, K and Rb are important, but for the Li, Na, Mg and O2 (located in the center of the cube) atoms, there is no accumulation of spin which means that their magnetic moment is negligible. These results are in accordance with the computed atomic magnetic moments, as seen in table 3.3.

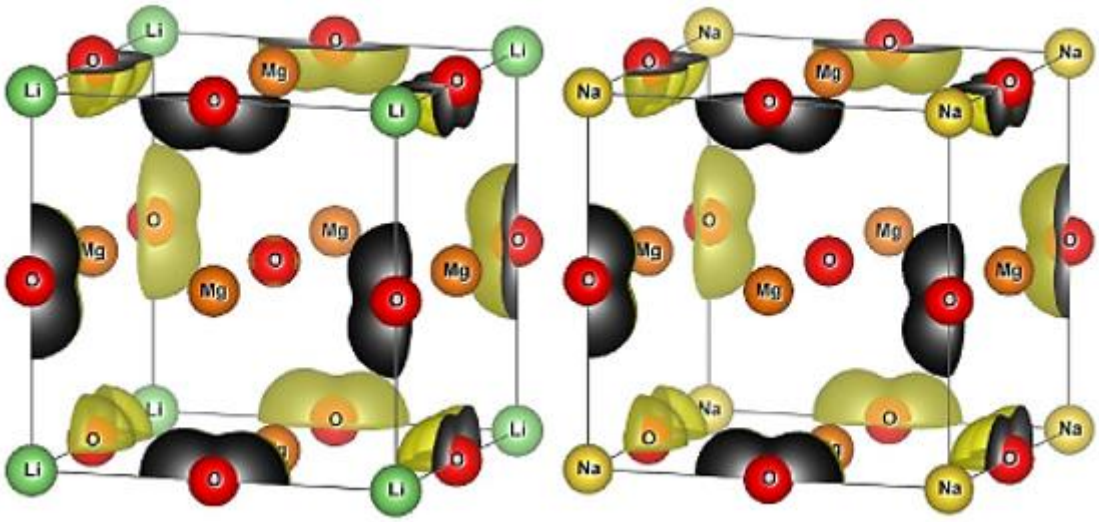

Fig. 3. 13 Spin density of XMg_3O_4 (X=Li, Na) with an isosurface of 0.01 /Å^3

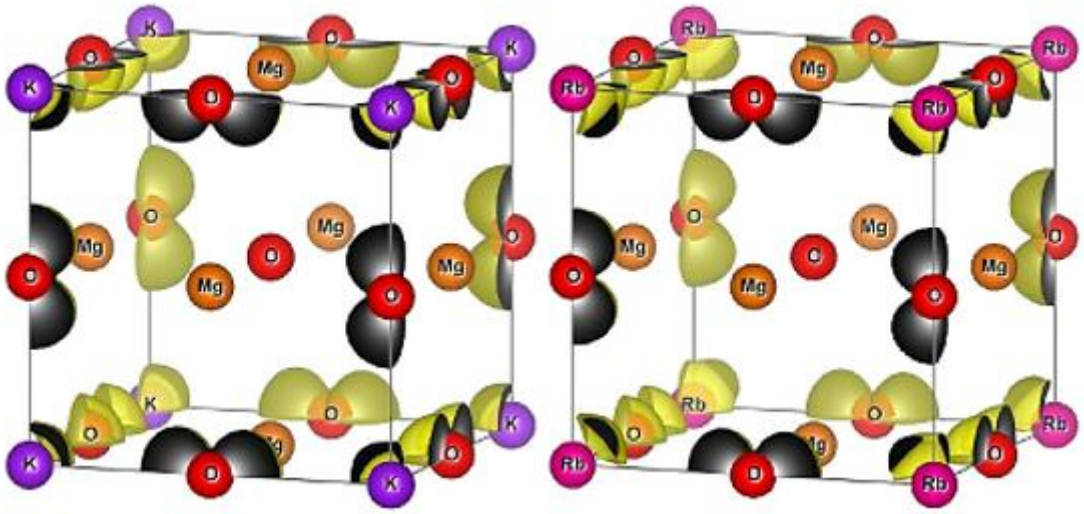

Fig. 3. 4 Spin density of XMg_3O_4 (X= K, Rb) with an isosurface of 0.01 /Å^3

3.5.3. Curie temperature and HM gap:

The HM gap shows the robustness of the half-metallicity with respect to the thermal fluctuations. It is expressed by**:**

$$HM_{Gap} = min\left(|E_F - E_{VBM}|, |E_F - E_{CBM}|\right) \quad \text{with} \quad E_F = 0\ eV \qquad 3.13$$

Where E_F, E_{VBM} and E_{CBM}, are the Fermi energy, valence band maximum (VBM), and conduction band minimum (CBM), respectively. As listed in Table 3.4, the HM gap values are 0.17, 0.18, 0.28, 0.38 for $RbMg_3O_4$, $LiMg_3O_4$, $NaMg_3O_4$ and KMg_3O_4, respectively.

X	*Gap*	*HMGap*	T_c
Li	5.32	0.18	537
Na	4.49	0.28	365
K	3.01	0.38	260
Rb	1.53	0.17	113

Table. 3. 4 Gap, Half-metallic gap (in eV) and Curie temperature T_c(in K)of XMg_3O_4.

The Curie temperature $T_c$in the mean field approximation (MFA) can be evaluated by the following formula[21]:

$$T_c = \frac{2(E_{AFM} - E_{FM})}{3k_B} \quad 3.14$$

Where E_{AFM} and E_{FM} are the total energies per formula unit in AFM and FM phases and k_B is the Boltzmann constant. Table 4 shows that the Curie temperatures $T_c$are 537 K, 365 K, 260 K, 113 K for XMg_3O_4 (X = Li, Na, K and Rb), respectively. One can see that the estimated Curie temperatures for $LiMg_3O_4$, $NaMg_3O_4$ are higher than room temperature, which is not the case for KMg_3O_4 and $RbMg_3O_4$. It should be noted that the estimated Curie temperature from the mean-field theory is often overestimated. The HM gap of 0.28 eV for $NaMg_3O_4$ is larger than the HMgap (0.18 eV) of $LiMg_3O_4$ showing that $NaMg_3O_4$is more efficient than $LiMg_3O_4$ to prevent the spin-flip transition of carriers due to thermal excitation, whereas $LiMg_3O_4$ has the highest Curie temperature. Consequently, both compounds can be potential candidates for spintronic applications.

3.6. References:

[1] P. Blaha, K. Schwarz, P. Sorantin, and S. B. Trickey, "Full-potential, linearized augmented plane wave programs for crystalline systems," *Comput Phys Commun*, vol. 59, no. 2, pp. 399–415, 1990.

[2] P. Blaha, K. Schwarz, G. K. H. Madsen, D. Kvasnicka, and J. Luitz, "wien2k," *An augmented plane wave+ local orbitals program for calculating crystal properties*, vol. 60, 2001.

[3] J. P. Perdew, K. Burke, and Y. Wang, "Generalized gradient approximation for the exchange-correlation hole of a many-electron system," *Physical review B*, vol. 54, no. 23, p. 16533, 1996.

[4] J. P. Perdew, K. Burke, and M. Ernzerhof, "Generalized gradient approximation made simple," *Phys Rev Lett*, vol. 77, no. 18, p. 3865, 1996.

[5] F. Birch, "Finite elastic strain of cubic crystals," *Physical review*, vol. 71, no. 11, p. 809, 1947.

[6] F. D. Murnaghan, "The compressibility of media under extreme pressures," *Proceedings of the National Academy of Sciences*, vol. 30, no. 9, pp. 244–247, 1944.

[7] A. Jain *et al.*, "Commentary: The Materials Project: A materials genome approach to accelerating materials innovation," *APL Mater*, vol. 1, no. 1, p. 011002, 2013.

[8] N. Karimian and F. Ahmadian, "Electronic structure and half-metallicity of new quaternary Heusler alloys NiFeTiZ (Z= Si, P, Ge, and As)," *Solid State Communications*, vol. 223, pp. 60–66, 2015.

[9] X.-H. Kang and J.-M. Zhang, "The structural, electronic and magnetic properties of a novel quaternary Heusler alloy TiZrCoSn," *Journal of Physics and Chemistry of Solids*, vol. 105, pp. 9–15, 2017.

[10] W. Voigt, "Lehrbuch der Kristallphysik (Teubner, Leipzig, 1928)," *There is no corresponding record for this reference*, 1908.

[11] A. Reuss, "Calculation of the flow limits of mixed crystals on the basis of the plasticity of monocrystals," *Z. Angew. Math. Mech*, vol. 9, pp. 49–58, 1929.

[12] R. Hill, "The elastic behaviour of a crystalline aggregate," *Proceedings of the Physical Society. Section A*, vol. 65, no. 5, p. 349, 1952.

[13] R. Hill, "On the elasticity and stability of perfect crystals at finite strain," in *Mathematical Proceedings of the Cambridge Philosophical Society*, 1975, vol. 77, no. 1, pp. 225–240.

[14] G. A. Alers and J. R. Neighbours, "Crystal stability and elastic constants," *Journal of Applied Physics*, vol. 28, no. 12, p. 1514, 1957.

[15] I. N. Frantsevich, "Elastic constants and elastic moduli of metals and insulators," *Reference book*, 1982.

[16] G. Vaitheeswaran, V. Kanchana, A. Svane, and A. Delin, "Elastic properties of MgCNi3—a superconducting perovskite," *Journal of Physics: Condensed Matter*, vol. 19, no. 32, p. 326214, 2007.

[17] D. G. Pettifor, "Theoretical predictions of structure and related properties of intermetallics," *Materials science and technology*, vol. 8, no. 4, pp. 345–349, 1992.

[18] H. Fu, D. Li, F. Peng, T. Gao, and X. Cheng, "Ab initio calculations of elastic constants and thermodynamic properties of NiAl under high pressures," *Computational Materials Science*, vol. 44, no. 2, pp. 774–778, 2008.

[19] J. Haines, J. M. Leger, and G. Bocquillon, "Synthesis and design of superhard materials," *Annual Review of Materials Research*, vol. 31, p. 1, 2001.

[20] H.-C. Cheng, C.-F. Yu, and W.-H. Chen, "First-principles density functional calculation of mechanical, thermodynamic and electronic properties of CuIn and Cu2In crystals," *J Alloys Compd*, vol. 546, pp. 286–295, 2013.

[21] N. Kervan, S. Kervan, O. Canko, M. Atiş, and F. Taşkın, "Half-metallic ferrimagnetism in the Mn2NbAl full-Heusler compound: a first-principles study," *Journal of Superconductivity and Novel Magnetism*, vol. 29, no. 1, pp. 187–192, 2016.

General conclusion and perspectives:

In this work, we have studied the structural, elastic electronic and magnetic properties of XMg_3O_4 (X = Li, Na, K and Rb) compounds, the calculations were carried out using first-principles calculations based on full-potential linearized augmented plane wave (FP-LAPW) method as implemented in the Wien2k package. GGA approximation was used for the exchange and correlation energy.

From structural properties. Our compounds are stable in the FM phase, these results are obtained for these compounds by fitting data for energy as a function of volume to the Birch–Murnaghan equation of state (EOS). The elastic constants indicate that our compounds are mechanically stable. Also, elastic properties indicate that $LiMg_3O_4$ and KMg_3O_4 are brittle and $NaMg_3O_4$ and $RbMg_3O_4$ are ductile.

In addition, electronic properties show that all XMg_3O_4 compounds are HM ferromagnets. In fact, from energy band structures, no band crosses the Fermi level for spin-up channels, However, a metallic behavior can be seen in spin-down channels for all compounds. This result is also confirmed by density of states (DOS). The half-metallic-ferromagnetic character is mainly originated from O1-p situated in the middle of the cube edge.

Furthermore, from magnetic properties calculation, the integer total magnetic moment of 1.0 μ_B in agreement with the half-metallic character of these compounds.

Moreover, the estimated Curie temperatures T_c and the HM gap values indicate that $LiMg_3O_4$, $NaMg_3O_4$ are both potential candidates for spintronics technology.

As perspectives, to confirm the mechanical stability, dynamical stability can be studied by performing phonon calculations. In addition, other properties can be calculated for these compounds such as thermoelectric properties. Since there no previous work, it is possible to use other codes such as Quantum espresso or experiments to confirm our results. Furthermore, the investigation of new compounds can be extended to similar ternary oxides.

Finally, we hope that our results could provide baseline information for future investigations of other properties for ternary oxides.

Abstract:

First principles calculations, based on the density functional theory (DFT), were used in this work to predict structural, elastic, electronic and magnetic properties of XMg_3O_4 (X = Li, Na, K and Rb) compounds. These calculations were performed by employing the full-potential linearized augmented plane wave method (FP-LAPW) as implemented in Wien2k code. It was found that all compounds were ferromagnetic by energy minimization procedure. The computations of elastic constants show that our compounds are mechanically stable. The electronic properties including the density of states and band structures indicate that these compounds exhibit half-metallic nature, and the spin up band gaps (HM gaps) were found to be 5.32(0.18) eV, 4.49(0.28) eV, 3.01(0.38) eV and 1.53(0.17) eV for, $LiMg_3O_4$, $NaMg_3O_4$, KMg_3O_4 and $RbMg_3O_4$ respectively. In addition, the calculated total magnetic moment is 1.0 μ_B, which approves the half-metallic behavior of these compounds and the calculated Curie temperatures T_c are 537, 365, 260 and 113 K for, $LiMg_3O_4$, $NaMg_3O_4$, KMg_3O_4 and $RbMg_3O_4$, respectively.

Keywords: FP-LAPW, Half-metallic, Spin-polarized calculation, Ternary oxides, Spintronics.

Résumé :

Des calculs de premiers principes, basés sur la théorie de la fonctionnelle de la densité (DFT), ont été utilisés dans ce travail pour prédire les propriétés structurelles, élastiques, électroniques et magnétiques des composés XMg_3O_4 (X = Li, Na, K et Rb). Ces calculs ont été effectués en utilisant la méthode des ondes planes augmentées linéarisées à plein potentiel (FP-LAPW) qui est implémentée dans le code Wien2k. Il a été constaté que tous les composés étaient ferromagnétiques par la procédure de minimisation de l'énergie. Les calculs de constantes élastiques montrent que nos composés sont mécaniquement stables. Les propriétés électroniques, y compris la densité d'états et les structures de bande, indiquent que ces composés présentent une nature demi-métallique, et les valeurs des bandes interdites de spin up (HM gap) se sont 5,32 (0,18) eV, 4,49 (0,28) eV, 3,01 (0,38) eV et 1,53(0,17) eV pour $LiMg_3O_4$, $NaMg_3O_4$, KMg_3O_4 et $RbMg_3O_4$ respectivement. De plus, le moments magnétique total calculé est de 1,0 μ_B, ce qui approuve le comportement demi-métallique de ces composés et les températures de Curie calculées Tc sont de 537, 365, 260 et 113 K pour $LiMg_3O_4$, $NaMg_3O_4$, KMg_3O_4 et $RbMg_3O_4$, respectivement.

Mots-clés : FP-LAPW, Semi-métalliques, Calcul polarisés en spin, Oxydes ternaires, Spintronique.

ملخص:

تم استخدام حسابات المبادئ الأولى ، بناءً على نظرية الكثافة الوظيفية (DFT) في هذا العمل للتنبؤ بالخصائص الهيكلية والمرونية والإلكترونية والمغناطيسية لمركبات XMg_3O_4 (X = Li و Na و K و Rb). تم إجراء هذه الحسابات من خلال استخدام طريقة الموجة المستوية المعززة ذات الإمكانات الكاملة (FP-LAPW) كما تم تنفيذها ببرنامج Wien2k. وجد أن جميع المركبات كانت مغنطيسية حديدية عن طريق إجراء تقليل الطاقة. تظهر حسابات الثوابت المرنة أن مركباتنا مستقرة ميكانيكيًا. تشير الخصائص الإلكترونية بما في ذلك كثافة الحالات وهياكل النطاق إلى أن هذه المركبات تظهر طبيعة نصف معدنية ، وتم العثور على فجوات (فجوات HM) لتكون 5.32 (0.18) eV، 4.49 eV (0.28)، 3.01 ((0.38) eV و 1.53 (0.17) eV لـ ، $LiMg_3O_4$، $NaMg_3O_4$، KMg_3O_4 و $RbMg_3O_4$ على التوالي. بالإضافة إلى ذلك ، فإن العزوم المغناطيسية المحسوبة هي 1.0 μ_B ، والتي توافق على السلوك نصف المعدني لهذه المركبات ودرجات حرارة Curie المحسوبة Tc هي 537 و 365 و 260 و 113 K للمركبات ، $LiMg_3O_4$، $NaMg_3O_4$، KMg_3O_4 و $RbMg_3O_4$ ، على التوالي.

الكلمات المفتاحية :FP-LAPW ، نصف معدني، حسابات مستقطبة ، الأكاسيد الثلاثية ، Spintronic.